

**MECHANICAL AND THERMO-  
MECHANICAL PROPERTIES OF  
WOVEN SISAL FIBER REINFORCED  
BIODEGRADABLE COMPOSITES**

Thesis

Submitted in partial fulfillment of the requirements for the degree of

**DOCTOR OF PHILOSOPHY**

by

**NAGAMADHU M.**



DEPARTMENT OF MECHANICAL ENGINEERING  
NATIONAL INSTITUTE OF TECHNOLOGY KARNATAKA,  
SURATHKAL, MANGALORE – 575025, INDIA.

DECEMBER, 2019

## DECLARATION

I hereby *declare* that the Research Thesis entitled “**Mechanical and Thermo-Mechanical Properties of Woven Sisal Fiber Reinforced Biodegradable Composites**” which is being submitted to the **National Institute of Technology Karnataka, Surathkal** in partial fulfillment of the requirements for the award of the Degree of **Doctor of Philosophy** in **Department of Mechanical Engineering** is a *bonafide report of the research work carried out by me*. The material contained in this Research Thesis has not been submitted to any University or Institution for the award of any degree.

Register Number : **123033ME12P09**

Name of the Research Scholar : **NAGAMADHU M.**

Signature of the Research Scholar :

Department of Mechanical Engineering

**Place: NITK-Surathkal**

**Date :**

## CERTIFICATE

This is to *certify* that the Research Thesis entitled “**MECHANICAL AND THERMO-MECHANICAL PROPERTIES OF WOVEN SISAL FIBER REINFORCED BIODEGRADABLE COMPOSITES**” submitted by **Mr. NAGAMADHU M. (Register Number: 123033ME12P09)** as the record of the research work carried out by him, is *accepted as the Research Thesis submission* in partial fulfillment of the requirements for the award of degree of **Doctor of Philosophy**.

### Research Guide(s)

**Dr. G. C. Mohan Kumar**

Professor

Department of Mechanical Engineering

NITK, Surathkal

**Dr. P. Jeyaraj**

Associate Professor

Department of Mechanical Engineering

NITK, Surathkal

Chairman-DRPC

Date:

## DEDICATION



ವಿದ್ಯೆ ಕಡಿಮೆಯಾದರೂ ನಡತೆ ಶುದ್ಧವಾಗಿರಬೇಕು  
Dr Sri Sri Shivakumara Swamiji

## ACKNOWLEDGEMENTS

With a deep sense of gratitude, I wish to express my sincere thanks to my supervisors **Prof. G. C. Mohan Kumar and Dr. P. Jeyaraj**, Department of Mechanical Engineering, National Institute of Technology Karnataka (N.I.T.K), Surathkal, for there excellent guidance and support throughout the work. I received very useful, encouraging and excellent academic feedback from them, which has stood in good stead while writing this thesis. There constant encouragement, help and review of the entire work during the course of the investigation were invaluable. I profoundly thank them.

I am also grateful to my Research Progress Assessment Committee (RPAC) members **Dr. Srikanth Bontha**, Associate Professor, Department of Mechanical Engineering, and **Dr. Arun Kumar Thalla**, Associate Professor, Department of Civil Engineering, National Institute of Technology Karnataka, Surathkal for their insightful suggestions, advices and patience.

I take this opportunity to thank **Prof. Shrikantha S. Rao**, Professor and Head, Department of Mechanical Engineering, NITK for his continuous and timely suggestions.

I sincerely thanks **Prof. Prabhukumar G.P.**, Former Principal, University U B T College of Engineering, Davanagere, **Prof. Chandrashekar R.**, Department of Mechanical Engineering, Acharya Institute of Technology, Bengaluru, **Prof. Krupashankara M.S.**, Principal, Goa College of Engineering, Goa, and **Prof. H. N. Narasimha Murthy**, Department of Mechanical Engineering, R. V. College of Engineering, Bengaluru for their support and encouragement in carrying out research activities.

A special thanks to my family. Words cannot express how grateful I am to **my mother, father, mother-in-law, father-in-law and brothers** for all of the sacrifices that you've made on my behalf. Your prayer for me was what sustained me thus far. I would also like to thank all of my **friends and relatives** who supported me and incented me to strive towards my goal. At the end, I would like to express

appreciation to my beloved wife **Shruthi M.C.** who spent sleepless nights with and was always my support in the moments when there was no one to answer my queries.

I wish to express my sincere gratitude to all the faculty members of the Department of Mechanical Engineering, N.I.T.K Surathkal and Acharya Institute of Technology, Bengaluru for their help, encouragement and support all through this research work.

**(Nagamadhu M.)**

## ABSTRACT

Natural fiber reinforced composites have extensively used in non-structural components, mainly in the automotive industry. The use of short and random fibers in those composites leads to discontinuity. These create a non-uniform stress distribution in the matrix during loading. Due to this non-uniform stress distribution, the composite fails early with a lower strain rate. This limitation can be overcome by using fabric reinforced composites. However, most of the textile properties influence the performance of the composites.

This study mainly focuses on mechanical (tensile and flexural) and dynamic mechanical characterization of fabric reinforced polymer composites. The thesis work is discussed in three phases: matrix, reinforcement, and composites. In the first phase, Polyvinyl Alcohol (PVA) is cross-linked with Glutaraldehyde (GA) for various volume fractions using a conventional vacuum-assisted pressure compression method. The mechanical and dynamic mechanical properties are carried out to optimize the volume fraction and is found at 20%. In the second phase, three types of woven fabrics prepared to study the effect of textile properties and woven patterns. Two plain woven fabrics (Plain 1 and Plain 2) are prepared with different grams per square meter (GSM). Also, another type of weft rib woven is prepared by keeping the same GSM as Plain 2 to analyze the effect of the woven pattern. The mechanical properties of these three fabrics are investigated and found that weft direction of weft rib fabric exhibits better mechanical properties. In the third phase, the composites are prepared using Plain 1, Plain 2 and Weft rib fabrics as reinforcement in 20% GA cross-linked PVA as matrix material and mechanical and dynamic mechanical properties are analyzed. The mechanical and dynamic mechanical properties of Plain 1 based composites exhibit better at room temperature, while based composites exhibit better dynamic mechanical properties at a higher temperature. It is shown that woven pattern of the fabric influenced significantly on composite properties. Similarly, weft direction of the composite exhibits better mechanical properties than warp direction, and it indicates loading direction also influenced.

**Keywords:** *Polyvinyl Alcohol; Glutaraldehyde; Sisal fabric; Mechanical properties; Dynamic Mechanical Analysis; Gram per unit area; Woven pattern.*

## CONTENTS

Declaration	i
Certificate	ii
Acknowledgements	iv
Abstract	vi
Contents	vii
List of figures	x
List of tables	xiii
Abbreviations	xiv
<b>1 INTRODUCTION</b>	<b>1</b>
1.1 Overview	1
1.2 Biodegradable Natural Fibre Woven Composites	2
1.3 Bio-Degradable Polymers	6
1.4 Textile Properties	8
1.4.1 Yarn linear density	9
1.4.2 Yarn crimp	9
1.4.3 Fabric count	12
1.4.4 Cover factor	12
1.5 Organization of the Thesis	12
<b>2 LITERATURE SURVEY</b>	<b>15</b>
2.1 Polymer Matrix Materials	15
2.2 Short and Long Sisal Fiber Composites	23
2.3 Mechanical and Dynamic Mechanical Properties	29
2.4 Natural Fiber Fabric Reinforced Bio-Degradable Composites	31
2.5 Applications	35
2.6 Motivation	38
2.7 Objectives	38
<b>3 MATERIALS AND METHODS</b>	<b>39</b>
3.1 Materials Selection	40
3.1.1 Matrix material	40



3.1.2	Sisal fiber and its processing	40
3.2	Processing of Matrix and Composite	42
3.3	Fourier Transform Infrared Spectroscopy	43
3.4	Methods Used for Fabric Physical Properties	45
3.5	Fabric Mechanical Properties	46
3.6	Mechanical Properties of Matrix and Composites	49
3.7	Dynamic Mechanical Analyzer	50
3.7.1	Temperature sweep	51
3.7.1	Multi frequency sweep	52
3.8	Hardness and Microstructure Studies	53
<b>4</b>	<b>CHARACTERIZATION OF PVA WITH GA</b>	<b>55</b>
4.1	Cross-linking of PVA with GA	55
4.2	Mechanical Properties	55
4.3	Dynamic Mechanical Properties Under Tensile Mode	59
4.4	Dynamic Mechanical Properties Under Three Point Bending Mode	63
4.5	Activation Energy	73
4.6	Estimation of the Operating Life of PVA-GA Polymer	75
4.7	Cross-linking Density	76
4.8	Effectiveness	77
4.9	Hardness	78
4.10	Summary and Conclusion	79
<b>5</b>	<b>CHARACTERIZATION OF SISAL FABRICS</b>	<b>81</b>
5.1	Sisal Yarn Characterization	81
5.2	Basic Physical Properties of Sisal Fabric	83
5.3	Mechanical Characterization of Fabrics	85
5.4	Summary and Conclusion	102
<b>6</b>	<b>CHARACTERIZATION OF COMPOSITES</b>	<b>105</b>
6.1	Structural Components of Composites	105
6.2	Mechanical Properties of Composites	107
6.2.1	Effect of GSM on mechanical properties	107

6.2.2 Effect of woven structure on mechanical properties	111
6.3 Fractured Surface Analysis	113
6.4 Dynamic Mechanical Analysis	116
6.4.1 Effect of GSM on dynamic mechanical properties	117
6.4.2 Effect of a woven pattern on dynamic mechanical properties	122
6.5 Effectiveness	126
6.6 Summary and Conclusion	128
<b>7 SUMMARY AND CONCLUSION</b>	<b>129</b>
7.1 Contribution to the Body of Knowledge	129
7.2 Effect of GA Cross-linking on PVA	130
7.3 Influence Sisal Fabric Properties on Mechanical and Dynamic Mechanical Properties of Composites	130
7.4 Scope for Future Work	131
<b>REFERENCES</b>	<b>133</b>
<b>PUBLICATIONS</b>	<b>153</b>

## LIST OF FIGURES

<b>Figure No.</b>	<b>Description</b>	<b>Page No.</b>
Figure 1.1	World consumption of biodegradable polymer by region – 2018	2
Figure 1.2	Terminology used in textile industries and its details	11
Figure 3.1	Schematic diagram of (a) Plain and (b) Weft rib woven fabrics and cross-section	41
Figure 3.2	The photographic view of plain and weft rib woven sisal fabrics used	42
Figure 3.3	Schematic representation preparation steps of woven sisal fabric composite	44
Figure 3.4	Schematic to determine flexural rigidity of fabric	47
Figure 3.5	Impact tearing tester (a) Elmendorf tear tester (b) Fabric mounted by fixing both the ends of fabric (c) Tearing testing template which is placed on P1 types of sisal fabric	49
Figure 3.6	Single rip tear method and its details	49
Figure 3.7	Dynamic mechanical analyzer under three point bending mode	51
Figure 3.8	Dynamic mechanical analyzer tensile mode setup	52
Figure 4.1	Tensile stress-strain plot for various percentage of GA in PVA	56
Figure 4.2	Flexural stress-strain plot for a various percentage of GA in PVA	57
Figure 4.3	Tensile fractured images (a) 15% GA in PVA, (b) 20% GA in PVA (c) 30% GA in PVA and (d) 40% GA in PVA	58
Figure 4.4	Flexural fractured images (a) 15% GA in PVA, (b) 20% GA in PVA (c) 30% GA in PVA and (d) 40% GA in PVA	58
Figure 4.5	Tensile storage modulus for GA cross linked PVA	60
Figure 4.6	Tensile loss modulus for GA cross-linked PVA	61
Figure 4.7	Tensile $\tan \delta$ for GA cross-linked PVA	62
Figure 4.8	Influence of GA volume fraction on storage modulus	65
Figure 4.9	Influence of GA volume fraction on loss modulus	67
Figure 4.10	Influence of GA cross-linking on $\tan \delta$	68
Figure 4.11	Effect of deflection with temperature of extent GA cross-linking	70

Figure 4.12	Cole-cole plot used to understand the effect of cross-linking of GA in PVA	71
Figure 4.13	SEM image after DMA analysis (a) Pure PVA, (b) 20% GA in PVA (c) 30% GA in PVA and (d) 40% GA in PVA	71
Figure 4.14	Influence of cross-linking percentage of GA on adhesion factor	73
Figure 4.15	Log frequency plot for pure PVA and various percentage of GA	74
Figure 4.16	Shift factor for time-temperature superposition analysis	75
Figure 4.17	Test duration in days for Pure and PVA-GA at different temperature	76
Figure 4.18	Cross-linking density of PVA-GA.	77
Figure 5.1	(a) Cross section of sisal fibers (b) Structure of sisal fiber	82
Figure 5.2	(a) Schematic load- elongation plot for fabric and its phases, (b) P1, (c) P2 and (d) WR fabrics load- elongation plot for in weft and warp directions	86
Figure 5.3	The fractured fabrics after tensile test, (a) P1, (b) Magnified fracture area of P2, (c) Magnified fracture area of P2, and (d) Magnified fracture area of WR.	87
Figure 5.4	Tearing failure of fabric under single rip tear test method	94
Figure 5.5	Tearing of P1 fabric in weft direction	95
Figure 5.6	Tearing of P1 fabric in warp direction	95
Figure 5.7	Tearing of P2 fabric in warp direction	96
Figure 5.8	Tearing of P2 fabric in weft direction	97
Figure 5.9	Tearing of WR fabric in warp direction	98
Figure 5.10	Tearing of WR fabric in weft direction	98
Figure 6.1	FTIR spectra of PVA, sisal fiber and their composites	106
Figure 6.2	Chemical structure of PVA, GA and its composites and reactions	107
Figure 6.3	Tensile stress-strain curves of (a) P1 and (b) P2 composites for various weight fractions in both warp and weft directions	108
Figure 6.4	Flexural stress-strain curves of (a) P1 and (b) P2 composites	110
Figure 6.5	Stress-strain diagram of weft rib composites for (a) Tensile and (b) Flexural loading.	111

Figure 6.6	SEM image of fractured surface (a) P1 under tensile loading, (b) P1 under flexural loading, (c) P2 under tensile loading, and (d) P2 under flexural loading.	114
Figure 6.7	(e) WR under tensile loading, (f) WR under flexural loading, (g) P1 under impact loading, and (h) P2 under impact loading.	115
Figure 6.8	Storage modulus of P1 and P2 fabric based composite (a) Linear scale (b) Log scale	119
Figure 6.9	Micro-finite element model of P1 and P2 fabric-based composites	119
Figure 6.10	Loss modulus of P1 and P2 fabric-based composites (a) Linear scale (b) Log scale	121
Figure 6.11	(a) $\tan \delta$ (b) Deflection of P1 and P2 fabric based composite linear scale	121
Figure 6.12	Storage modulus of P2 & WR fabric based composite (a) Linear scale (b) Log scale	123
Figure 6.13	Micro-finite element model of P2 and WR fabric-based composite	123
Figure 6.14	Loss modulus of P2 & WR fabric based composite (a) Linear scale (b) Log scale	125
Figure 6.15	(a) $\tan \delta$ (b) deflection of P2 and WR fabric based composite	126
Figure 6.16	Effectiveness of sisal woven composite at various temperatures	127

## LIST OF TABLES

<b>Table No.</b>	<b>Description</b>	<b>Page No.</b>
Table 3.1	Representation of different woven fabric of sisal textile fabric analyzed and their basic properties given by manufacturer	42
Table 3.2	Different standards used for characterization of textile properties of fabrics	43
Table 4.1	Dynamic mechanical properties of PVA cross-linked with GA	79
Table 4.2	Slope data from Figure 4.8	74
Table 4.3	Effectiveness of cross-linking agent	78
Table 4.4	Shore D hardness for a various percentage of GA	79
Table 4.5	Summery of mechanical property of PVA for various percentage of GA	80
Table 5.1	Physical properties of three fabrics	84
Table 5.2	Fabrics weight in warp and weft directions	84
Table 5.3	Tensile properties of fabrics	87
Table 5.4	ANOVA results for sisal fabrics for ultimate point elongation	88
Table 5.5	ANOVA results for sisal fabrics for ultimate point load	89
Table 5.6	Flexural strength, stretch and growth of fabrics	90
Table 5.7	Impact tearing strength (gram force) of three fabrics	92
Table 5.8	Variance for impact testing of fabric	93
Table 5.9	ANOVA for impact testing of fabric	93
Table 5.10	The variance of P1 fabric between warp and weft groups on static tearing for various crosshead speeds	100
Table 5.11	ANOVA for P1 fabric	100
Table 5.12	The variance of P2 fabric in warp and weft groups on tearing for various crosshead speeds	101
Table 5.13	ANOVA for P2 fabric	101
Table 5.14	The variance of WR fabric between warp and weft groups on static tearing for various crosshead speeds	102
Table 5.15	ANOVA for WR fabric	102

Table 6.1	Impact strength in $J/m^2$ by various fiber loading of P1, P2 and WR fabric in warp and weft directions	110
Table 6.2	Mechanical Properties of various types of composites and its weight fractions	128

## ABBREVIATIONS

ASTM	: American Society for Testing and Materials
DMA	: Dynamic Mechanical Analysis
DSC	: Differential Scanning Calorimetry
FTIR	: Fourier Transform Infrared Spectroscopy
PVA	: Polyvinyl Alcohol
GPa	: Giga Pascal
hr	: Hour
ISO	: International Standard Organization
mg	: Milligram
Hz	: Hertz
MPa	: Mega Pascal
Mw	: Molecular weight
mm	: Millimeter
Pa	: Pascal
PLA	: Polylactic Acid
s	: Second
Wt%	: Weight Percentage
°C	: Degree Celsius
T <sub>g</sub>	: Glass transition temperature
GSM	: Gram per square meter
SS	: Sum of Squares
MS	: Mean of Square
F	: F-test
Sig	: Significance level
df	: Degrees of freedom



# CHAPTER-1

## INTRODUCTION

### 1.1 Overview

The consumption of polymers and polymer based materials is ever increasing with a growing range of applications in diverse fields. Fiber-reinforced composites are very attractive in polymer industries, and offer many advantages. The advantages include but not limited to high strength-to-weight ratio, good corrosion resistance as well as structural and manufacturing flexibilities compared to metals and their composites. Composite materials are in use in a wide range of industrial applications for several decades. Air, land, and sea transportation areas cover large scale applications while sports equipment and biomedical devices cover small scale applications. About 35-40% of the annually produced fiber-reinforced polymeric composites are of thermoplastics (Marosi *et al.* 2016). Other composites are reinforced with glass, carbon, or natural fibers, while the rest is made of high-strength carbon or glass fiber reinforced thermosets. The number of fire risk scenarios are drastically increased with the expansion of plastic usage endangering our everyday life. Moreover, most commercial composites are fossil fuel-based synthetic materials that harm the environment during its disposal at the end of the product life cycle. Furthermore, with the growth in environmental awareness and a series of new regulations, the industries are being forced to search for eco-friendly materials to replace the existing fossil fuel-based polymer materials (Shankar Adhikari *et al.* 2018). Therefore, the introduction of eco-friendly composites made of biodegradable or sustainable materials such as natural fibers or man-made cellulose fibers reinforced biodegradable polymer composites have attracted growing interest in recent years (Huda *et al.* 2008).

During the year 2018, As per the IHS (Information Handling Services), global level demand biodegradable class of polymers was 3,60,000 metric tons, but the overall consumption of biodegradable polymers may be expected to increase up to 5,50,000

metric tons by the end of 2023. This represents an average annual growth rate of up to 9% in the duration of five years, almost equivalent to a volume increase of more than 50 percent from 2018 to 2023 reported by Bio-plastics market data 2018.

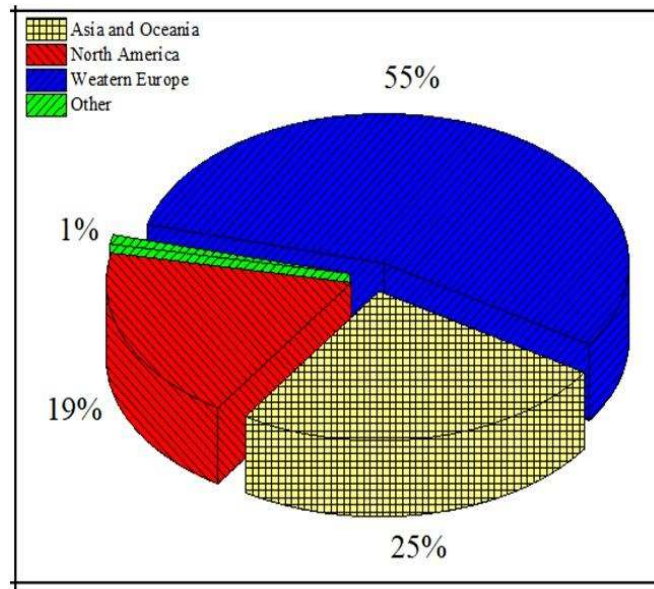


Figure 1.1: World consumption of biodegradable polymer by region – 2018

As per the IHS (Information Handling Services), Market Chemical Economics Handbook and Biodegradable Polymers Report, the ongoing market value of biodegradable plastics is greater than \$1.1 billion in 2018 but may reach up to \$1.7 billion by 2023. Figure 1.1 shows the percentage of bio-degradable polymer consumption throughout the world.

Biodegradable or compostable polymers are the bio-based or fossil-fuel-based polymers (plastics) that undergo microbial decomposition (Zheng *et al.* 2014). Some of these classes of polymers get decomposed in backyard compost bins or soil, freshwater or saltwater are discussed in next section.

## 1.2 Biodegradable Natural Fibre Woven Composites

Biodegradable products manufactured using natural fiber reinforced polymer composites are expected to grow exponentially. The reduction in the number of petroleum resources along with the global environmental problem leads to the

necessity of finding an alternative completely biodegradable green material. Green materials are highly compatible with the environment, and route of processing the green materials is independent of petroleum-based resources. The development of biodegradable polymer composites, which are reinforced with natural fiber, promotes the usage of environmentally friendly materials (Gurunathan *et al.* 2015). Also, the usage of green materials provides the solution for the disposal of agricultural residue problems. Agricultural crop residues such as palm oil, sisal, jute, hemp, pineapple leaf, banana, and sugar palm are produced in billions of tons throughout the world (Sunil *et al.* 2015). Out of this large amount of residues, only a small amount is used in the form of household fuel or fertilizer, the rest are burnt within the field. This creates a negative effect on the environment in the form of air pollution. These residues can be used effectively as a reinforcement in polymer composites that find applications in a variety of fields.

The research on natural fiber composites is increased because they are bio-based materials, renewable, and can replace synthetic fiber reinforced plastics (Mishra *et al.* 2002; Misnon *et al.* 2014; Nishino *et al.* 2003). The deployment of plant-based natural fibers for reinforcements in polymer composite materials results in meeting the above objectives.

Biodegradable materials have many applications in the automotive and building industry, largely for non-load bearing components (Chilton *et al.* 2005; Netravali *et al.* 2007). However, short fiber composites can be processed easily as compared to long fiber composites. The difficulty in maintaining the alignment of reinforcement material during the processing of composites can be overcome by using non-woven and woven fabric/textile materials. In woven fabric, the fibers are converted into yarn and these yarns are used to prepare fabric with different woven structures. The mechanical strength of a fabric reinforced composites depends on fabric material properties and weaving pattern of the fabric. In recent years, researchers are making use of advancements in textile engineering to prepare different kinds of natural fiber fabric reinforced polymer composites. This includes apparel, safety belts, and nets, airbags, seat covers, concrete reinforced with textiles, protection systems against erosion and landslide, dikes reinforced with textiles and some water management

systems (Canavan, 2015). Similarly, it can be used in applications like durable piping for canalization, in balloons and parachutes, in aircraft wing and body structures, boat rumps reinforced with textile-based composites, air-filled components of satellites and spacecraft ((Horrocks and Anand, 2016), (Caravan, 2015) (Bridgens and Birchall, 2012) and Jou and Hsu, 2014)).

Conventional textile-based composites are produced by using the combination of various types of synthetic fibers and resins. On the other hand, materials which are manufactured by combining the natural fibers and natural resources based resin may be called as textile bio-composites (Koichi Goda, YEAR). Since cellulose-based natural fibers are available with limited length, in the textile industry, the fibers are pinwheeled into a continuous yarn, called a spun yarn. Spun yarns are usually twisted to obtain a much stronger yarn, called as twisted or plied yarn, which is in correspondence with the filament yarn of synthetic fibers. Even though there is no chemical bonding between fibers, each fiber in spun yarn can exhibit its intrinsic strength and stiffness through inter-fiber friction. Natural fiber twisted yarns can furthermore be controlled in mechanical and other properties by changing the twist number per unit length, for example, twist per inch, and/or the number of spun yarns. Such a kind of structural changes in twisted yarns will be deeply related to the texture, suppleness, and contraction in textile products, and thus have a considerable amount of importance in terms of practical usage (Hearle, 2012).

On the other hand, natural fiber twisted yarns can be embedded in resin and can be applied as reinforcement for composite materials. One of such a practical natural fiber yarn composite is the tire cords for automobile tires, which were manufactured using cotton fibers in the past, but currently, synthetic fibers such as nylon and polyester are often used. For the purpose of reducing the environmental impact, natural fiber twisted yarns should be positively applied as reinforcement in a thermoset/thermoplastic resin composite, in place of synthetic yarns. The important advantage of the twisted yarns is in the continuous fibrous structure, that brings higher strength and stiffness to the resultant composite when compared with short natural fiber composites. The amount of strength and stiffness usually depends on the

twist per unit length as mentioned above. Young's modulus of the twisted yarn composites is closely related to the twist number (Nakamura, 2015).

For all these applications, performance characteristics of the fabrics like, smooth, rough, stiff or limp, wear, thermal studies, draping, etc. are important. These fabric properties are linked with many end-user applications and also many composites are used in textile applications. Many researchers also worked on yarn and textile properties and their influence on composites. Textile composites are composed of textile reinforcements combined with a binding matrix (polymeric matrix). This describes a large family of materials used for load-bearing applications within a number of industrial sectors. The term textile is used here to describe an interlaced structure consisting of yarns, although it also applies to fibers, filaments, and yarns, and most developed over hundreds or even thousands of years. Modern machinery for processes such as weaving, knitting, and braiding operates under automated control, and it is capable of delivering high-quality materials at the rate of up to several hundreds of kilograms per hour. Some of these processes (notably braiding) can produce reinforcements directly in the shape of the final component. Hence, such materials can provide an extremely attractive reinforcement medium for polymer composites.

Nowadays textile composites are attracting growing interests from the academic community and industry. This family of materials, at the center of the cost and performance spectra, offers significant opportunities for new applications of polymer composites. Although the reason for adopting a particular material can be various, the primary driver for the use of textile reinforcement is undoubtedly cost. Textiles can be produced in large quantities at a reasonable cost using modern and automated manufacturing techniques. While the direct use of fibers or yarns might be cheaper in terms of materials costs, such materials are difficult to handle and to form into complex components shapes. Textile-based materials offer a good balance in terms of the cost of raw materials and ease of manufacturing, attractive due to yarn interlacing, which improves structural stability and damage tolerance (Graham-Jones, 2014). As mechanical properties of the fabric are good in multi-directions, fabric reinforced in polymer material possesses very good stability in more than one direction due to the

yarn orientation and interlacing of warp and weft yarns. The target application areas for textile composites are primarily within the aerospace, marine, defense, land transportation, construction and power generation sectors. This clearly shows the need for finding alternative materials in the field of textile and its compatibility.

### **1.3 Bio-Degradable Polymers**

Most of the polymers used as matrix materials in polymer composites are derived from fossil fuel, a non-sustainable resource. These materials at the end of their useful life cannot be easily consumed and simply pile up as waste and cause significant damage to the environment. Biodegradable resins are capable of playing a key role in developing sustainable plastic production. The biodegradable issue can nevertheless be an important tactic in reducing pollution and waste in some instances.

The ability to compost single-use and other disposable items ensures that plastic waste will not remain on the planet for hundreds of years, reduces the amount of methane gas emitted from landfills and could help to prevent humans from needing to designate ever-larger parcels of land for trash disposal. According to the United Nations Environmental Programme (UNEP), between 22 and 43 percent of plastic consumed globally finds its way into landfills. Biodegradable resins could help to bring this number down, reducing one of the longest-lasting impacts of our plastic use.

Since plastic waste has a tendency to end up in parks, waterways and other sensitive ecosystems, it is important to verify when shopping for biodegradable resins that “biodegradable” does not simply mean the capability to disintegrate into pieces invisible to the naked eye. True biodegradability means the ability to be broken down by bacteria or other organisms. Since the rise of green consumer preferences has many companies trying to cash in on environmental benefits, it is important to verify that a material meets common industry criteria for actual biodegradability.

At the end of their life, the majority of the conventional plastics are traditionally disposed of in landfills where they may stay as it is for several decades without

degrading making that land unusable for any other applications. About 6-7% of the petroleum produced today is used for making polymers, fibers and other chemicals.

It is estimated that the world currently consuming petroleum at an 'unsustainable' rate, 100,000 times faster than nature can create it. At the current rate of consumption, it is estimated that the current petroleum reserves will last for only 50-60 years. These concerns have forced the development of environmentally friendly biobased and biodegradable polymers and their composites in recent years. Biobased and biodegradable polymers are generally defined as those polymers that can decompose in natural aerobic (composting) and anaerobic (landfill) environments.

Biobased polymers are those that are derived from renewable plant-based raw materials and tend to be inherently biodegradable. They always have oxygen or nitrogen atoms in their polymer backbones which is the feature that is mainly responsible for their biodegradability. Biobased polymers can be further subdivided into two categories, natural biopolymers, and synthetic biopolymers. Natural biopolymers often refer to those biobased polymers found directly in nature, including carbohydrates (starch, cellulose, chitin, agar, carrageenan, etc.), lignin, proteins, and bacterial produced polyesters. Synthetic biopolymers are polymers that are not found in nature but are made commercially from monomers that are found abundantly in nature. Polylactic acid (PLA) and polyamine acids (PAA) are examples of important synthetic biopolymers.

Biodegradable polymers normally refer to petroleum-based biodegradable synthetic polymers, such as polyvinyl alcohol (PVA), polyglycolic acid (PGA), polycaprolactone (PCL), polyethylene oxide (PEO), etc. Biodegradation of biobased and biodegradable polymers can be achieved by enabling microorganisms in the environment to metabolize the polymer to produce an inert humus-like material that is less harmful to the environment and can get easily blended with the natural soil. Although polymers are being employed more and more as structural materials, their use often is limited by their relatively low levels of stiffness and strength compared, for example, with metals. Because of the need to be lightweight and high stiffness as well as to possess other functionalities (wear resistance, thermal stability, electrical

property, low-cost and high volume, etc.) for materials to be used in diverse applications, advanced polymer composites have been developed over recent years with extremely high properties. Polymer composites consist of two or more distinct phases, normally including a polymer matrix (continuous) phase and fibrous or particulate material dispersed phase. Based on the nature of reinforcement, polymer composites can be categorized into three main classifications: particulate composites, continuous fiber composites, and discontinuous fiber composites. The polymers most commonly used as matrix materials at present are thermosetting network polymers such as unsaturated polyesters and epoxy resins. There have been developments in the field of thermoplastic polymer matrix composites using nylon or polypropylene as a matrix. For dispersed phase, silicate-based minerals, glass, carbon, and other high-modulus polymeric fibers are universally used as reinforcements in polymer composites, based on the properties desired. The dispersed phase size has become smaller to a few nanometers where significant benefits may be derived due to their small size. Recently, polymer composites using biobased and biodegradable polymers and natural fibers have been widely studied and developed due to the increasing environmental and energy concerns.

These biodegradable resins are extruded, injection-molded, compression molding, etc.. in much the same way as traditional plastics. These biodegradable composites having many applications example automobile, marine, aeronautical, other household items, disposable cutlery, and other single-use items are crying out for a material solution. In some cases, biodegradability lends a product a distinct functional advantage. This is often true in gardening and agricultural applications where a product may need to lend short-term support or to act as a temporary barrier. Mulch films and plant pots are examples of such products, packaging for food and other products, organic waste containers, gardening, and other agricultural applications.

#### **1.4 Textile Properties**

The above section clearly describes the need for woven fabric in composite applications. However, many of the physical properties of a fabric influence the mechanical properties of the fabric-reinforced composites significantly. So, it is



necessary to understand the main textile physical properties such as gram per unit area (GSM), woven pattern of a woven fabric, yarn diameter, number of yarn, yarn linear density, crimp of yarn, thickness of fabrics, and cover factor both in warp and weft directions. Some of the important physical properties associated with a piece of fabric are explained below.

#### **1.4.1 Yarn linear density**

Among the other parameters of yarn, yarn's diameter is a significant factor. But determining the diameter is impossible by any means due to the fact that it varies significantly as the yarn is squeezed. Besides the optical technique, all other methods involve compressing the yarn during testing.

Optical techniques for determining diameter have the difficulty of specifying the location of the peripheral edge of the yarn as its surface can be unclear or rough due to hairiness on it. That is why the determination of the yarn's edges is subject to the operator's understanding. Due to these problems, a system must be designed to ascertain the delicacy of yarn by weighing its predefined length. This quantity is called as linear density or yarn count. As the diameter of the yarn increases the yarn linear density also increases. However, the weight of the fabric depends on the number of yarns and its linear density.

#### **1.4.2 Yarn crimp**

Terminology associated with fabric along warp and weft directions are shown in Figure 1.2. The warp and weft yarns are interlacing at an angle of  $90^\circ$ , due to which yarns follow a wavy path. So, it is necessary to understand and determine the yarn length in the fabric and unraveled the yarn length from the fabric. The ratio of change in length ( $\Delta L$ ) to the original length of yarn ( $L$ ) is called as crimp. Crimp percentage is defined as the mean difference between the straightened thread length and the distance between the ends of the thread while in cloth which is expressed as a percentage. The crimp amplitude is defined as the amount of thread deflection from the central place of the fabric.

### **Influence of crimp-on fabric properties:**

Warp and weft crimp percentage are two factors which have an influence on the following fabric properties:

**Resistance to abrasion:** The abrasion resistance of fabric will be more if the yarn crimp is more. The yarns with high crimp take the brunt of abrasion action. This is because of crowns that are formed as the yarn bends around a transverse thread. This will be produced from the surface of the fabric and meet the destructive abrasion agent first. The other set of yarns lying in the center of the fabric will only play their part in resisting abrasion when the high crimped threads are nearly worn through.

**Shrinkage:** When the yarns are wet, they swell and consequently the warp thread takes longer bending path to align with the swollen weft thread. The warp thread must be either longer in length or alternatively the weft threads must move closer together. An increase in length of warp requires the application of tension is absent, equilibrium conditions will be attained by the weft threads moving closer together.

**Fabric behaviour during strength testing:** When a strip of fabric is extended in one direction, the crimp is removed and the threads are straightened. This causes the threads at right angles to the loading direction to be crimped further. When the load is applied along the warp threads, the crimp in the warp is removed and that in the weft threads is increased which is known as crimp interchange. The sample loses its original rectangular shape the middle position to the strip contracts which is known as wasting. Due to the removal of crimp, the load-elongation curve will show relatively high extension per unit increase in load in the early stages of strength testing of a strip of fabric.

**Faults of fabric:** Variation in crimp can give rise to faults in fabric such as a reduction in strength, bright picks, diamond bars in rayon, stripes in yarn-dyed cloth, etc. The crimp variation is mainly due to the improper tension on the yarn during the preparation of the fabric.

**Fabric design:** Control of crimp percentage is necessary when a fabric is designed to give a desired degree of extensibility. Some fabrics require control of crimp in the

finishing process to give the correct crimp balance between warp and weft so that the finished appearance is satisfactory. Therefore, the tension applied must be carefully controlled.

**Fabric costing:** Since crimp is related to length, it follows that the quantity of yarn required to produce a given length of fabric is affected by the warp, weft and crimp percentage. Therefore, in calculating the cost and the yarn requirements, the value of crimp play an important role.

**Measurement of crimp percentage:** From the definition of crimp, two parameters such as cloth length and straightened length can be obtained. Just applying tension is sufficient to remove all the crimp without stretching the yarn in order to straighten the thread.

The principle of yarn crimp determination is very simple. With a fine pen and rule, lines are drawn on a piece of cloth at a known distance. Some of the threads are removed out, the yarns are straightened without stretching and the stretched length is noted and from that, the crimp is calculated. The difficulty lies in the straightening of the yarn without stretching it.

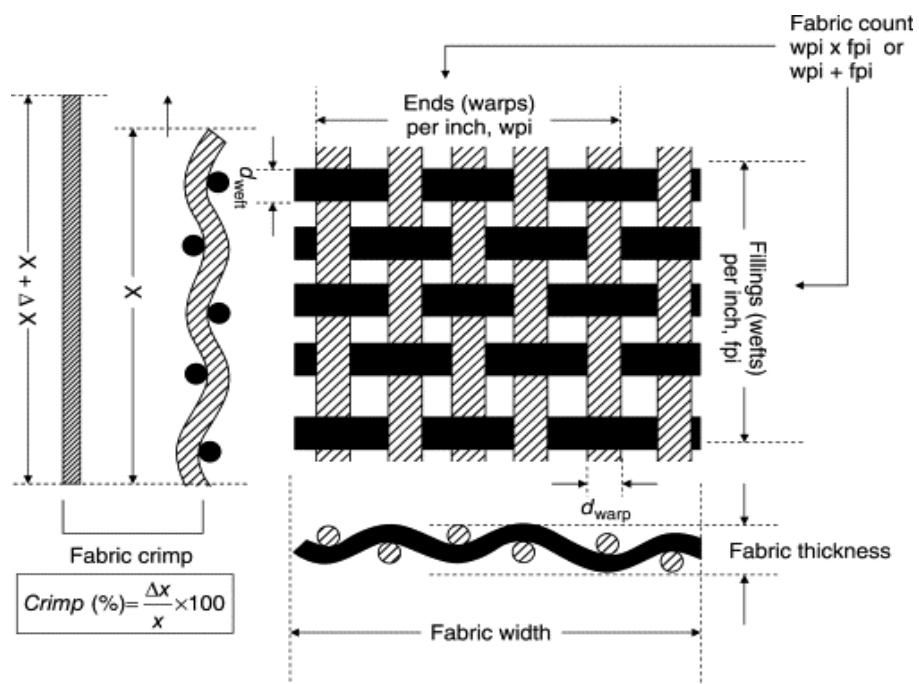


Figure 1.2: Terminology used in textile industries and its details

### **1.4.3 Fabric count**

Fabric count is also known as Thread count (TC) and it is the heart of a fabric bed linen. One can observe it as mentioned in duvet covers, sheets, and pillowcases. Ends per inch (EPI or e.p.i.) is the number of warp threads per inch of a woven fabric. In general, higher the ends per inch finer is the fabric. In weaving, the weft (sometimes called as woof) is the thread or yarn which is drawn through, inserted over-and-under, the lengthwise warp yarns that are held in tension on a frame or loom to create cloth. Warp is the lengthwise or longitudinal thread in a roll, while the weft is the transverse thread. A single thread of the weft, crossing the warp, is called a pick. Each individual warp thread in a fabric is called a warp end or end.

### **1.4.4 Cover factor**

A cover factor is a number that indicates the extent to which the area of fabric is covered by one set of threads. For any woven fabric, there are two cover factors: warp cover factor and weft cover factor.

## **1.5 Organization of the Thesis**

The thesis comprises of six chapters, each paragraph will give a brief note on each chapter.

Chapter 1 introduces the natural fiber reinforced biodegradable polymer composites, biodegradable textile composites, and significance of textile physical properties. This chapter also brings out a brief introduction about textile properties and the outline of the thesis can also be seen.

Chapter 2 presents a detailed literature review on biodegradable polymer and reinforcement materials, textile-based composite, influence of textile properties on composite. It also defines the motivation of the present study, objectives, and scope of the research work.

Chapter 3 presents the material selection and its processing, experimental methods, and standards. The detailed explanation about the preparation of raw materials and its processing methods used to evaluate the matrix and reinforcement materials.

Chapter 4 reveals the mechanical characterization of polymer matrix materials under tensile and flexural mode. Further, the dynamic mechanical analysis of polymer and its cross-linking effect are discussed.

Chapter 5 describes the physical characterization reinforcement material and analyze the influence of these physical properties on mechanical properties of fabric materials are discussed.

Chapter 6 reveals the results and discussion about composite by considering the influence of grams per unit area and woven pattern. Detailed study is carried out to analyze the influence of different important parameters of fabric on the mechanical and dynamic mechanical behaviors of the composites are presented in this chapter.

Chapter 7 concludes the findings from the research work, presents the future scope of the study and provides the key contributions from the study.

References used in the thesis and the list of publications made out of the research work follow this section.



## CHAPTER-2

### LITERATURE SURVEY

The purpose of this literature review is to provide background information on the issues concerned with this thesis work and to emphasize the relevance of the present study. This treatise embraces various aspects of textile fiber reinforced polymer composites with a special reference to their mechanical and dynamic mechanical characteristics. Initially, the detailed literature on the mechanical properties of polymer, fabric and its reinforced composites are discussed. Further, it includes review reports of natural fiber reinforced composites based on dynamic mechanical properties.

#### 2.1 Polymer Matrix Materials

Polymers are generally classified into different categories such as thermoplastics, thermosets, and elastomers based on the nature of behavior. Elastomers are rubbery materials having both viscous and elastic behavior. Some of the important elastomers are natural polyisoprene, polybutadiene, chloroprene, etc., Thermoset polymers are interlinked by covalent bonds and acquire a three dimensional network structure. Thermoset polymer cannot be remoulded and recycled. On the other hand, thermoplastic polymers possess linear and branched molecular chains with weak intermolecular bonding such as Van der Waals force or hydrogen bonding. Thermoplastic polymers form when repeating units called monomers link into chains or branches. As their bonds are weak, thermoplastic polymers readily soften when heated, allowing manufacturers to mould them into a wide range of shapes, then resoften them and mould them again. This ability to reuse thermoplastic polymers indefinitely means they are highly recyclable.

Biodegradable polymers are one group of polymeric materials. The molecular chains of these kinds of polymers can be broken down either through hydrolytic degradation or by enzymatic means. The usage of biodegradable polymers in biomedical

applications has increased and current trends show that in the future the biodegradable polymers may replace the use of conventional non-biodegradable materials, gradually (Zheng *et al.* 2014).

Biodegradable polymers cover a vast area of high molecular weight compounds. Usually, it is valuable to distinguish between biodegradable polymers of native and of synthetic origin. Native biodegradable polymers are the result of a synthesis developed during millions of years of evolution, leading to tailor-made materials for different applications in nature. These biopolymers include proteins, polysaccharides, nucleic acids or lipids which show completely different characteristics depending on the situation in which they are used. On the other hand, synthetic polymers are the result of many centuries of research and development. Synthetic polymers susceptible to biodegradation can be of different types, *e.g.*, polymers containing hydrolyzable backbone polyesters. Recent research activity on biodegradable synthetic polymers has often been focused on the simulation of different biopolymers or polymers with degradable backbones, *e.g.* polyanhydrides, polycarbonates, polylactones, etc (Karak *et al.* 2012) . In addition to that growing ecological and environmental consciousness has driven efforts for development of new innovative materials for various end-use applications. Polymers synthesized from natural resources have gained considerable research interest in recent years. By considering above points the usage eco-friendly materials like soy oil-based resin, cellulose fiber, Polylactic Acid (PLA), Polyvinyl Alcohol (PVA) based fiber and their blended materials find applications in roof structure, automobile parts, civil and construction industries (Dweib *et al.* 2006, Koronis *et al.* 2013 and Gurunathan *et al.* 2015). In addition, the applications of PVA also having a prominent role in biomedical devices like interference screws, tacks for ligament attachment, meniscal repair, suture anchors, rods and pins (Middleton and Tipton 2000).

Many researchers studied different biodegradable polymers like Agro polymers (Stéphane *et al.* 2005), Polyhydroxy Alkanoates (PHA) (Zulfiqar *et al.* 2018), Polylactides (PLA) (Hagen *et al.* 2016), Polycaprolactones (PCA) (Debasish *et al.* 2016), Polyesteramides (PEA) (Yujiang *et al.* 2016), Aliphatic Copolyesters (Bajaj *et*



*al.* 1979), Aromatic Copolyesters (Witt *et al.* 2001), Polyvinyl Alcohol (PVA) (Xiaohong *et al.* 2019), etc.

Many researchers studied the effect of fiber and filler reinforcement on mechanical behavior of PLA based bio-degradable composites. Maya and Thomas (2008) made a survey in 2008 and reported that the bio-materials play a vital role in reducing environmental hazards. They also reported that cellulosic fiber reinforced polymeric composites are finding applications in many fields ranging from construction industry to automotive industry. Among green composites, hybrid biocomposites and textile bio-composites are having better mechanical properties.

Imre *et al.* (2013) observed that use of blended biopolymers increased drastically in 2010 onwards, and they have better performance when compared to base materials. The modification of polymer is an approach to get better properties and attain property combinations essential for specific applications. Blending allows significant enhancement in the impact resistance of brittle polymers. They also reported that biopolymers and blended materials attracting and replacing non-biopolymers in several areas such as agriculture, consumer goods, packaging and automotive.

Shuai *et al.* (2014) fabricated the PVA/calcium silicate ( $\text{CaSiO}_3$ ) composite using selective laser sintering method. They found that effect of  $\text{CaSiO}_3$  reinforcement on compressive strength of PVA composite is better for 15 wt%.

Amir *et al.* (2015) examined influence of PVA content, screw speed, and clay content on the performance of starch/PVA clay nanocomposite films prepared by twin-screw extruder. In order to obtain better compatibility among starch and silicate layers, Montmorillonite (MMT) modification is accomplished using citric acid. Tensile strength of the composite is (17.7 MPa) found better at 3 wt% MMT, 5 wt% of PVA, 24 r/min screw speed, and 90–100–110–120°C of extruder four stage temperature profile.

Elena *et al.* (2016) worked on Polyvinyl Alcohol/Chitosan (CS)/ montmorillonite (C30B) nanocomposites for food packaging applications. These materials are processed using a noninvasive and low-cost freeze/thawing method by varying weight

fraction of nanoclay from 0 to 5. From the X-ray diffraction analysis, they observed an increase in basal spacing for 5 wt% of C30B, which indicates intercalation of CS into interlayers of C30B nanoclay.

Shamima *et al.* (2016) studied thermal and mechanical properties of potato starch-filled PVA and PLA composites for biomedical applications. The potato starch extracted from potato by acid hydrolysis, these particles range from 10-100  $\mu\text{m}$  are used as a reinforcement in PVA and PLA to prepare composite by solvent casting and hot press moulding methods, respectively. The tensile strength, elongation at break and tensile modulus are found better at 6% starch PVA composites. Results of tensile studies revealed that starch PVA composites have better mechanical properties than pure PVA (16.7 MPa) and starch-filled PLA.

Yuansen *et al.* (2016) worked on leather shaving reinforced PVA composite prepared by two techniques, which are Solid-State Shear Milling ( $\text{S}^3\text{M}$ ) combined with thermal processing. They found that  $\text{S}^3\text{M}$  processing exhibits very strong shearing and compressing forces, promoting the formation of more hydrogen bonds and the chelation in the interfaces between PVA and leather shavings. Their result also revealed that 5% weight fraction of 15 milling cycle processed composite exhibits a better tensile strength of 60 MPa with an excellent elongation response of 340 % at break.

Nor *et al.* (2017) studied mechanical properties of  $\gamma\text{-Fe}_2\text{O}_3$  nanoparticles filled polyvinyl alcohol nanofiber composite prepared using the electrospinning process. The five input electrospinning process parameter used as variable factors, namely nanoparticles content, voltage, flow rate, spinning distance, and rotating speed to understand the tensile properties. Their results revealed that 7% volume fraction of nanoparticle content, 35kV of voltage, 2 mL/h volume flow rate, and 8 cm spinning distance, and 3026 r/min of rotating speed gives the maximum Young's modulus.

Bhasha *et al.* (2019) investigated effect of processing conditions on fabrication Graphite (xGnP) and Graphene Oxide (GO) nanofiller PVA nanocomposite. The samples are prepared by varying xGnP and GO in PVA for 0 to 1.5% using Modified

Hummer's method. They observed that 1% GO content in PVA enhanced the tensile strength from 33 to 57.79 MPa and which could be attributed to the existence of hydroxyl and carboxylic groups in PVA and GO nanoparticles, respectively.

Subhakanta *et al.* (2019) worked on short areca sheath reinforced polyvinyl alcohol composite prepared by injection moulding. The tensile, flexural and impact properties are studied by considering various weight percentages from 0 to 40 wt% of areca fiber. The optimum weight fraction for the mechanical property is determined by using regression analysis.

Some of the researchers also worked on dynamic mechanical properties and thermal properties of biodegradable composites. Amaresh *et al.* (2019) worked on alkali-treated plain-woven banana fabric reinforced biodegradable composites by varying concentrations of NaOH treatment from 2 to 10%. The mechanical and thermo-mechanical properties are found to be better for 6% NaOH treated composite. The storage and loss modulus enhanced with chemical treatment even at elevated temperatures.

Ione *et al.* (2001) analyzed dynamic mechanical properties of  $\text{CoFe}_2\text{O}_4$  particles filled PVA nanocomposite. The PVA-based composite films are obtained by mixing the appropriate amount of ferrofluid with an aqueous solution of PVA. When homogenization is achieved, polymer films are prepared by pouring the solution onto glass plates and allowing the water to evaporate at room temperature. The films are dried under vacuum at 50 °C for 10 days. The glass-transition temperature of PVA increases with filler content up to 10 wt %, probably as a result of polymer–filler interactions that reduce the polymer chain mobility.

Xiaohong *et al.* (2013) worked on PVA nanofiber mats formed using electrospinning process, which is chemically cross-linked with Glutaraldehyde. The PVA mat of 5 cm x 5 cm was immersed in GA and trace hydrochloric acid in acetone solution for 0.5 hr. They found that as the concentration of GA increases the weight loss percentage and swelling degree decreases. It is also observed by thermal analysis that cross-

linking with GA decreases chain mobility of PVA which causes a change in the stiffness of the chains.

Jibril *et al.* (2013) studied the effect of untreated and treated single-walled carbon nanotube reinforced PVA film nanocomposites. The dynamic mechanical property is measured under tensile mode with a preload force of 0.01 N at 5 Hz frequency. The storage modulus of pure PVA is 717.52 MPa and it is decreased drastically at around 80°C. By adding 1 wt% of untreated single-walled nanotube the storage modulus improved marginally 798.4 MPa and follows the same trend as pure PVA. But by adding 1 wt% of treated single-walled nanotube the storage modulus the storage modulus enhanced significantly to 1430.9 MPa. The enhancement of dynamic mechanical, electrical and thermal properties are due to incorporation of ozone treatment which improved the dispersion of nanoparticle and its interfacial adhesion.

Shadpour and Dinari (2013) observed that the reinforcement of the Al<sub>2</sub>O<sub>3</sub> nanoparticles with PVA resulted in an improvement of thermal properties. The thermal stability is improved by adding nanoparticle in the polymeric matrix. This can be attributed to homogeneous mixture and good dispersion of Al<sub>2</sub>O<sub>3</sub> and also strong hydrogen bonding between O-H groups of PVA and the O-H groups of the Al<sub>2</sub>O<sub>3</sub> nanoparticles.

Teresa *et al.* (2014) studied the effect of cloisite Na<sup>+</sup>, Nanofil (NF) and Cloisite (30B) montmorillonites as filler materials for PVA and found that composites with organically modified montmorillonites exhibited the lowest water absorption compared to the base materials. Composites with organically modified montmorillonites have a micro-morphology and the lowest water absorption. Young's modulus, tensile strength, and percentage of strain of sodium montmorillonites composite are 143.4 MPa, 41.2 MPa, and 2.30%, respectively, which is better as compared to other montmorillonites composites.

Parinaz *et al.* (2017) investigated Polyvinyl Alcohol (PVA) and polyvinyl alcohol/Polyvinyl Pyrrolidone (PVP) bio-medical foams prepared by high-speed mechanical stirrer and freeze-drying process. The gamma irradiation used for cross-

linking the foams structures without using any harmful chemicals. These biocompatible foams possessed interconnected open-cell structure, which helps to absorb and retain water. These foams are soft and flexible during wet conditions. By adding 20 wt% polyvinyl pyrrolidone increased the size and interconnectivity of the cell structure and rendered more flexible foams than the pure polyvinyl alcohol.

Jin and Seungsin (2018) demonstrated that PVA nanofibrous membranes containing *Coptidis Rhizoma* extracts have considerable potential to ensure the effective antimicrobial wound dressings. The nanofibrous membranes are fabricated via electrospinning process by varying the wt% of *Coptidis Rhizoma* extracts as 10, 20, and 30%. These nanocomposite fibers exhibited a high drug-loading efficiency ranging from 92% to 97%. The release profile from the nanofibrous membranes of *Coptidis Rhizoma* showed an initial fast release followed by a gradual release for 48 hr.

Eunsil *et al.* (2019) worked on an eco-friendly cross-linking method to improve stability of lignin/PVA nanocomposite fiber in aqueous media. The cross-linking and insolubilization is achieved by combining several cross-linking techniques: water vapour treatment at 80°C for 180 min, photo-irradiation for 30 min under visible light at a distance of 17 cm, and heat treatment at 200°C for 60 min. They concluded that the PVA nanocomposites have advanced functions and they are eco-friendly.

Jagadish *et al.* (2019) carried out experiments on proton-conducting solid polymer electrolyte films, which are composed of Diazanium Hydrogen Phosphate (DAHP) and PVA. The specimens are prepared by a solution casting method and it is observed that the addition of nanofillers enhanced the physicochemical properties of DAHP/PVA composites. With increase in DAHP content in PVA the optical activation energy and band gap also increases. The sample containing 15 wt% DAHP shows highest Alternating Current (AC) conductivity of the order of  $10^{-4} \text{ S cm}^{-1}$  and Direct Current (DC) conductivity about  $4.27 \times 10^{-7} \text{ S cm}^{-1}$  at ambient conditions. Crystallinity decreased and glass transition temperature ( $T_g$ ) increases with an increase in DAHP content.

Daehee *et al.* (2019) worked on mechanical and swelling behavior of PVA/alginate carriers by cross-linked GA. The chemical bonding between GA and hydroxyl/amino groups minimized their concentrations and the carriers became hydrophobic. The swelling ratio is decreased by the addition of catalyst and had a minor effect that generally increases with GA addition. This indicates that the swelling ratio opposed the cross-linking extent. The porosity showed minor variation with increasing GA cross-linking as the carrier physical structure was already developed during the boric acid cross-linking. During GA cross-linking, the acetal group replaced the borate group and is expected to retain the existing physical structure. As cross-linking increases, the porosity, and the swelling ratio of carriers decrease, which in turn decreased the average porosity of the carriers. The mechanical strength is improved with increasing cross-linking effect due to GA weight percentage.

Ravindra *et al.* (2019) studied the cross-linking effect of GA on thermal and mechanical properties of starch and PVA blended films. They observed that strong cross-linking is due to the reaction of hydroxyl group of PVA with GA through the formation of acetal bonds. Increases in storage modulus is observed for the starch cross-linked with 1.5 wt% of GA.

Renbo *et al.* (2019) studied the static and dynamic mechanical properties of PVA fiber reinforced ultra-high-strength concrete. They reported that PVA fiber reinforced concrete showed relatively good ductility, toughness, and deformability when compared to steel reinforced concrete under static loading conditions.

Shanshan *et al.* (2019) used PVA cross-linked GA nanosphere as a modifier to form polymer particles on the surface of Corn Straw Fiber (CSF). They observed that the flexural strength of 30 wt% modified corn straw fiber Wood Plastic Composite (WPC) is 62 MPa, which is 12.3% higher than that of WPC untreated CSF composite.

Ting *et al.* (2019) worked on self-standing and flexible regenerated cellulose membranes fabricated by using a facile  $ZnCl_2/CaCl_2$ /cellulose dissolution system. The tensile strength and strain to failure of PVA cross-linked GA membrane are found 66.3 MPa and 2.6%, respectively.

From the exhaustive literature review, it is found that biomaterials are the alternatives for environmental hazardous synthetic materials. Moreover, several researchers also focused on enhancing the behavior of PVA by cross-linking with glutaraldehyde and found that the cross-linking exhibited a promising enhancement in mechanical and other properties (Wang and Hsieh 2010, Rudra *et al.* 2015).

Thermoplastic biodegradable polymers are widely used in various applications today such as disposable food packaging products and biomedical materials. Polylactic Acid (PLA) is one of the most popular renewable resource-based biodegradable polymers, due to its excellent biodegradability and compostability, as well as attractive cost structure. However, the poor mechanical properties of the PLA polymer in bulk form restricts its use as high-performance material. The mechanical properties can be improved by introducing foreign fillers into the biodegradable polymer to produce a composite material.

In line with PLA, PVA is also one of the promising polymer as it has favorable biodegradable characteristics. However, the application of PVA materials is limited due to its high cost and slow degradation process especially under anaerobic conditions (Takasu *et al.* 2002). Considering these limitations, PVA is often blended with other low-cost biodegradable polymers and their properties like tensile strength, elongation, and toughness of PVA blends and its composites are enhanced as reported in literature (Guo *et al.* 2006; Ramesan *et al.* 2018).

Natural and synthetic fiber reinforced biodegradable composites reduce waste disposal challenges. Many of the researchers have motivated to do research on the development and characterization of biopolymer films and their composites (Abdul Khalil *et al.* 2018; Asem *et al.* 2018).

## **2.2 Short and Long Sisal Fiber Composites**

In order to find mechanical properties of natural fiber reinforced composites, most of the researchers reinforced natural fiber in short and random orientation form in the polymer.

Kuruvilla *et al.* (1993) analyzed short sisal fiber reinforced Low-Density Polyethylene (LDPE) composite. The impacts of the processing method, effect of fiber content, fiber length and orientation on the tensile properties of the composites are analyzed. The optimum tensile property is found for 6 mm fiber length and 30 wt%. They found that unidirectional alignment of the short fibers obtained through an extrusion method improved the tensile strength and modulus of the composites along the fiber orientation axis by more than double relative to randomly directed fiber composites.

Kalaprasad *et al.* (1997) analyzed the influence of fiber loading, fiber orientation and fiber length on mechanical properties of low-density polyethylene composite. They observed correlation between experimental data and multiple theoretical models. Theoretical models including parallel and sequence, Hirsch, Cox, Halpin – Tsai, modified Halpin – Tsai and modified Bowyer and Bader are analyzed and results are compared with experimental data.

Joseph *et al.* (2002) studied short sisal fiber reinforced polypropylene composite for various chemical treatments prepared by mixing in a Haake Rheocord mixer at a temperature of 170°C and with a rotor speed of 50 rpm for 10 min duration. This mix was rolled in two roll mill followed by compression moulding at a pressure of about 8 MPa at 170°C. The tensile strength, tensile modulus, elongation at break of 30 wt% fiber content 6mm length untreated sisal fiber composite is 44.35 MPa, 1194 MPa, and 7.4%, respectively. The urethane derivative of Polypropylene Glycol (PPG) treated NaOH washed fiber exhibit better mechanical properties as compared to other treatments. It is observed that surface fibrillation occurs during alkali treatment, which improves interfacial adhesion between the fiber and matrix materials.

Hari *et al.* (2015) worked on short sisal fiber reinforced epoxy composites prepared by hand lay-up method with various fiber lengths (5, 10, 15 and 20 mm) at 30 wt%. The tensile and flexural strength increases with fiber length up to 15 mm, whereas better impact strength is observed for 20mm fiber length.

Rajesh *et al.* (2015) worked on untreated and treated short sisal reinforced Polylactic Acid (PLA) biocomposite for various weight proportions up to 25%. The sisal fiber is



treated with 10% NaOH followed by H<sub>2</sub>O<sub>2</sub> treatment and found that 20% fiber loaded composite exhibits better tensile and flexural strength. The impact strength of the untreated composite is found to be better than the treated composite. The untreated composite observes more water than that of the treated composite, but the thermal degradation temperature is increased.

Maya *et al.* (2017) worked on sisal fiber reinforced phenol formaldehyde composite by varying fiber length as 10, 20, 30, 40 and 50 mm using hand layup process followed by compression moulding. The prepared samples dried at 30°C to 70°C to avoid residual stress development during the processing. The composites are prepared for different fiber loading 38, 46, 54 and 70 by weight fraction (wt%). Through the flexural and impact strength analysis it is found that the better fiber length and wt% are 40 mm and 54 wt%, respectively.

Naushad *et al.* (2017) studied the effect of sisal fiber reinforcement on recycled polypropylene composites prepared using melt blending technique. The marginal improvement in mechanical properties is observed for the 40 addition of weight percentage of untreated sisal fiber. Reinforcement of mercerized sisal fiber with compatibilizer (maleic anhydride grafted polypropylene) enhanced tensile, flexural and impact properties due to improvement in interfacial bonding.

Rajashekarani *et al.* (2017) studied on sisal fiber reinforced silicone matrix composite prepared by compression moulding process. They found that the incorporation of sisal fiber enhances the tensile strength, tear strength and hardness of the composite. The silane-treatment of fiber enhances the adhesion between fiber and matrix of composite and exhibit better mechanical properties.

Saurabh and Inderdeep (2017) investigated effect of processing of sisal fiber (3 and 8 mm) reinforced poly-lactic acid biocomposite using direct-injection molding and Extrusion-Injection Molding (E-IM). The mechanical properties like tensile, flexural and impact properties are compared with extracted fiber morphology and fiber orientation. The long fibers in D-IM is found to bind and entangle with each other forming fiber clusters, hindering uniform dispersion and orientation of fibers within

the biocomposite. However, in the case of E-IM biocomposite, an improvement in the fiber orientation and distribution is observed. In the case of short sisal fiber composite, the dispersion and orientation is enhanced significantly. In short fiber composite, more number of fiber are aligned in the direction of extraction as compared to long fiber reinforced biocomposites.

Bernardo and Giuseppe (2018) analyzed short and discontinuous sisal agave fibers reinforced green epoxy biocomposites. They found that the tensile property is found to be better at 35 volume fraction with 3 to 4 mm short sisal fiber reinforcement. They also reported that incorporation of sisal mat fabric the tensile properties enhanced drastically as compared to discontinuous sisal fiber composite.

Jiratti *et al.* (2018) analyzed surface modifications effect on PLA and its composites with silver nanoparticles (AgNPs, size range between 120 and 150 nm) with and without additional melamine–formaldehyde-coated short sisal fibers. The composites are prepared by varying AgNP content as 100, 300 and 500 ppm (parts per million) in a constant mass percentage of constant sisal fiber. The PLA-based systems with a fully amorphous matrix are irradiated with 1–256 laser pulses at a constant fluence of  $0.32 \mu\text{J} \mu\text{m}^{-2}$ . Changes in the irradiated surfaces are assessed and quantified by light and scanning electron microscopic pictures. Protrusion with bubbling, bubbled protrusion with cratering and crater formation with more or less bubbled ridges are found as characteristic ablation features.

Qi *et al.* (2018) studied effect of fiber content and alkaline treatment on sisal starch fully biodegradable composite cushioning products through energy absorption performance, cellular microstructure and fiber-starch compatibility. The composite with a fiber and Thermoplastic Starch (TPS) mass ratio of 4:13 shows the optimum cushioning property. Alkaline treatment improves contact between sisal fiber and TPS, and thus strengthens composite cushioning properties. After biodegradability tests for 28 days, the weight loss of the composites is 62.36%. Composites have been found to be a promising replacement for Expandable Polystyrene (EPS) as packaging material, particularly under high compression load (0.7–6 MPa).

Adewale *et al.* (2019) studied the elastic properties of sisal fiber reinforced polystyrene composite analytically and numerically using numerical homogenization approach. The experimental result of longitudinal modulus ( $E_1$ ) shows a good agreement with the phenomenological model predictions at lower fiber loading. However, the Finite Element Model (FEM) gives higher longitudinal modulus results compared to both experimental and phenomenological model results. The experimental result of transverse modulus ( $E_2$ ) agrees favorably with both FEM and phenomenological model results for higher fiber loading cases. However, for lower fiber loading cases, a contrasting behaviour is observed. The experimental result of in-plane Poisson ratio ( $\mu_{12}$ ) favorably agrees with the phenomenological model and FEA circular–square Representative Volume Element (RVE) predictions but does not agree with FEA circular–hexagonal RVE prediction. The study indicates that the effective elastic properties of sisal fiber-reinforced polystyrene composites are affected by parameters such as fiber loading, cross-sectional area, and RVE.

Aiju *et al.* (2019) studied on L-lactide (LA) grafted sisal fiber (SF-g-LA) and untreated sisal fiber (USF) in a poly (lactic acid) (PLA) matrix are prepared with SF-g-LA/USF fibers ratios of 0, 1:9, 3:7, 5:5, 7:3, 9:1, and 1. The tensile and flexural properties of treated sisal fiber show better properties as compared to untreated fiber composite. The tensile strength and modulus, flexural strength and modulus found to be better for the fiber to matrix ratio of 7:3.

Bing *et al.* (2019) investigated sisal fiber reinforced polylactic acid biocomposites prepared using melt mixing and subsequent compression molding. The effect of fiber content and sodium hydroxide (NaOH) concentration on mechanical properties is analyzed. The tensile strength and impact strength are improved for the addition of sisal fiber up to 20 wt% and then decreases. 6% NaOH treated fiber reinforced composite exhibits better mechanical properties.

Florencia *et al.* (2019) analyzed short sisal fiber pectin matrix composites by varying fiber content from 1 to 30 weight percentages. Theoretical models are used to obtain the maximum packing or volume fraction of randomly oriented short fibers and its relationship with the mechanical parameters. A higher elastic modulus and tensile

strength are observed when the fiber content is increased in the composite at a fixed aspect ratio (length/diameter = 2.8).

Juliana *et al.* (2019) studied the influence of hydrothermal carbonization treated sisal fibers reinforced recycled polypropylene prepared using extrusion and injection processes. They found that hydrothermal carbonized sisal fiber raises the crystallinity of fibers, resulting in greater conformity to the interface fiber/polymer matrix as per the scanning electron microscope images.

Mengyuan *et al.* (2019) studied discontinuous sisal fiber reinforced high density polyethylene composite using continuous pre-pregs via hot-pressing. The interfacial bonding is found to be improved by treating fiber in 2% of sodium hydroxide solution at 60 °C. Another three types of coupling agents ( $\text{NH}_2\text{C}_3\text{H}_6\text{Si}(\text{OC}_2\text{H}_5)_3$ ,  $\text{C}_2\text{H}_3\text{Si}(\text{OC}_2\text{H}_5)_3$  and  $\text{C}_{51}\text{H}_{112}\text{O}_{22}\text{P}_6\text{Ti}$ ) are used to prepare the composite. These coupling agents react with hydroxyl groups on sisal fibers, resulting in polymerization or physical entanglement with the matrix via  $\text{CH}_2=\text{CH}-$ ,  $\text{NH}-\text{CH}-\text{CH}-\text{CH}-$ , and  $-\text{OR}$ , respectively.

Namrata *et al.* (2019) carried out studies on modified sisal fiber reinforced agro-waste derived resins from nonedible protein and starch composites. The composites are prepared using hand-lay-up process, followed by drying process for 18 hr in an air-circulating oven maintained at 40°C, then placed in hot press at 130°C for 20 min under a pressure of 6 MPa. The sisal fiber is modified using a novel combination of mercerization followed by heat treatment under a pre-determined tension which enhanced Young's modulus and tensile strength of the composites. The non-edible protein and starch were extracted from defatted karanja (*Pongamia pinnata*) and mango (*Mangifera indica*) seed cake wastes, respectively, to prepare the green resins. It is found that tensile strength of modified sisal fiber composite was better as compared to raw sisal fiber composite.

Saurabh *et al.* (2019) analyzed recyclability of PLA/Sisal biocomposites comprising sodium bicarbonate treated sisal fibers (30 wt%). The composite is recycled eight times using the extrusion process and found that the tensile strength of three times

recycled samples is decreased by 20.9%. It is also found that beyond third recycle, storage and loss modulus found to decrease drastically and it is not recommended for structural applications. However, the biocomposites recycled up to third recycle can be used for making products for low to medium strength non-structural applications.

Yashwant *et al.* (2019) carried out studies on short sisal fiber reinforced polypropylene polymer-based composites. Short sisal fibers of 3 mm length are incorporated into Polypropylene (PP) in three different fiber loading conditions (10, 20 and 30). Composites are fabricated through extrusion, followed by injection moulding process. The tensile strength, tensile modulus and percentage of elongation at break are found to be better at 30 wt%.

### **2.3 Mechanical and Dynamic Mechanical Properties**

Many researches also investigated on dynamic mechanical properties of short and long sisal fiber reinforced polymer composites and are presented below.

Kuruvilla *et al.* (1993) studied dynamic mechanical properties of short sisal fiber reinforced low-density polyethylene composite. The storage modulus and loss modulus increase, whereas the  $\tan \delta$  decreases with increase in fiber content. The effect of fiber-matrix adhesion on the viscoelastic properties of the composites is studied and found that the increase in adhesion increases the storage modulus. The effects of fiber length, fiber orientation, and fiber loading on the dynamic mechanical properties also investigated. In all cases, storage modulus ( $E'$ ) and loss modulus ( $E''$ ) decrease with temperature and increase with fiber loading.

Manikandan *et al.* (2001) investigated the effect of fiber loading, fiber orientation and fiber modification of short sisal fiber reinforced with Polystyrene (PS) composites reinforced on thermogravimetric and dynamic mechanical characteristics. The storage modulus decreases with increasing temperature due to increased segmental mobility. The glass transition temperature of the composite is shifted to lower temperature compared to pure PS and can be attributed to the presence of residual solvent in composites. The storage modulus increases with an increase in fiber loading and

chemical treatment. It is also found that storage and loss moduli are greatly influenced by fiber orientation.

Ghamsari *et al.* (2015) studied sisal fiber reinforced syntactic foam composites for the mechanical and dynamic mechanical properties by varying the volume fraction of short sisal fiber. The thermo-mechanical property of composite is measured under tension-compression mode. They found that storage and loss modulus are enhanced drastically in the glassy region due to the addition of sisal fiber as compared to the rubbery region. The storage modulus of pure epoxy is 2.20 GPa, which is enhanced to 2.47 GPa by adding 3.5% sisal fiber. The  $\tan \delta$  peak decreases by adding sisal fiber which indicates that enhancement in interfacial bonding between fiber and matrix material. The decrease in the magnitude of  $T_g$  is observed for the addition of sisal fiber due to plasticizing effect of epoxy matrix.

Sushanta *et al.* (2017) worked on short sisal fiber reinforced with soybean oil-modified toughened epoxy blends. The tensile modulus and tensile strength enhanced by reinforcing 15 wt% of sisal fiber as compared to bio-based epoxy blend. The Derivative Thermogravimetry (DTG) analysis clears that the rate of degradation peak is shifting to a higher temperature, which indicates that enhancing thermal stability as compared to base epoxy. The dynamic mechanical analysis reveals that improvement in the storage and loss modulus by adding sisal fiber.

Jiratti *et al.* (2018) analyzed the effect of Melamine-Formaldehyde (MF) coating of sisal fiber on PLA composite prepared using compression moulding technique. The MF coating is confirmed using FTIR and SEM images. It is observed that 1:1 combination exhibits better tensile strength and tensile modulus. The thermal stability is also enhanced by the coating, due to the strong interfacial bonding. In addition, the water absorption of MF coated sisal fiber PLA composite reduces the hydrophilic properties.

Gupta and Singh (2019) studied water absorption, static, and dynamic mechanical properties of alkali-treated and polylactic acid-coated sisal fiber reinforced polyester composite. Sisal fiber is processed by two methods; one is treating with 5% NaOH

solution at 30°C for 30 min, and another method is immersing sisal fiber in 60°C PLA chloroform solution for 5 min. The treated sisal fibers are chopped into 10 mm length and the composite is prepared by keeping 20 weight fraction of fiber using hand-lay-up process. They reported that PLA coated sisal fiber composite shows enhanced the resistance to water absorption. They also observed that mechanical and dynamic mechanical properties of the composite are enhanced by PLA coated sisal fiber.

Sahoo *et al.* (2019) studied unidirectional sisal fiber reinforced bio-epoxy composites for shock-absorbing applications. Cardanol based phenalkamine, a bio-renewable crosslinker, is used to develop well toughened sustainable composite materials. The dynamic mechanical properties are enhanced by cross-linking co-polymers and mobility of polymer chains is restricted enough to behave as rigid/stiff materials. These bio-composites are suggested for many engineering applications like automotive, structural, construction, and building sectors.

#### **2.4 Natural Fiber Fabric Reinforced Bio-Degradable Composites**

Some researchers demonstrated that mechanical properties of natural fiber composite can be improved by reinforcing the natural fiber in woven fabric form instead of the typical short and random orientation form.

Garkhail *et al.* (2000) analyzed the influence of composite fabrication method on mechanical properties of flax-polypropylene composite. They compared the mechanical properties of the composites prepared using film-stacking method based on random fiber mats with a papermaking process based on chopped fibers. It is observed that random fiber mat composite enhances the properties of composite material.

Processing of plant-based natural fiber composites have issues like fiber alignment, resin-rich area due to the short and random fiber reinforcement. In case of short natural fiber composites, fibers are cut into small lengths to get uniform mixing and distribution during its preparation. However, this reduces the strength of the composites; this can be overcome by using woven fabric reinforcement. However, in woven fabric composites, fabric properties play a major role in deciding the

composites mechanical properties. Most of the reinforcements in composite material have a close relation with textile materials and textile forms especially when the fibrous reinforcement is concerned. However, it also depends on the type of fiber, woven structures, yarn direction, and its strength, the weight of the fabric, and its volume fractions (Ping *et al.* 2000, Cevallos and Olivito 2015, Rajesh and Jeyaraj 2017).

In the mid-twentieth century onwards, fabric composites and modern polymers enabled the fabrication of performance geotextiles and specialized textile products for the civil, automobile, aeronautical and marine engineering industries (Khan *et al.* 2018, Krivoshapko 2018).

However, many researchers demonstrated that woven composites show promising mechanical properties and dynamic mechanical properties, and these composites are easy to process also (Rajesh and Jeyaraj 2016).

Pothan *et al.* (2008) investigated the effect of weave architecture on the ultimate mechanical properties of plain, twill and matt woven sisal fiber reinforced polyester composites prepared by the resin transfer molding technique. They observed that fabric weave architecture enhances tensile properties compared to other patterns.

The literature survey encourages moving towards the sisal fiber as it possesses excellent mechanical properties. It is also an alternative for jute, wood, hemp, and banana fibers.

It is difficult to evaluate the quality of natural fibers, which generally extracted from nature, and thus it is challenging to develop a generic formula to predict the structural and mechanical properties of Natural Fiber Reinforced Polymer (NFRP) composites. Hydrophilic and hydrophobic properties of natural fibers and polymers respectively cause poor bonding interaction at the fiber-matrix interface. Traditional shear-lag model was popularly used to study the stress transfer mechanism between fiber and matrix of advanced composites. However, such model is not applicable to NFRP composites due to the imperfect shape of natural fibers along their longitudinal direction and irregular shape of fibers cross-section.



The strength of composite materials mainly depends on properties of reinforcement material and current work focuses on to study the influence of woven fabric reinforcement in a polymer composite. In case of woven fabric, the major influencing fabric properties are woven structure and gram per unit area (GSM) in addition to cover factor, crimp, number of warp, and weft yarns and mechanical properties of the fabrics. However, many researchers have worked on the effect of a gram per unit area of woven materials (Rajesh and Jeyaraj 2017, Icten and Karkuzu 2008) and weight fraction (Naik *et al.* 2002, Senthilkumar *et al.* 2018) of woven fabric in composites. But limited literature is available on the studies related to influence of cover factor, crimp, yarn linear density, number of warp and weft yarns and mechanical properties of fabric on composites. Further, it is evident that fabric reinforced composites exhibit better properties in all directions because of their enhanced structural integrity.

Tan *et al.* (2000) studied the effect of stuffer (x direction) and filler yarn (y direction) and found that Young's modulus in filler yarn direction is higher than in the stuffer yarns direction, with lower strain rate in filler yarn direction. Mouritz (2008) studied the effect of z-reinforcement type woven z-binder, stitch or pin on composite materials and observed that in-plane Young's modulus of the composites are not affected by the type or volume fraction of the z-reinforcement. Cevallos and Olivito (2015) observed that fiber content, fiber type, fabric geometry mainly affect the behaviour of the composites. However, by considering environmental considerations and accessibility, availability of comprehensive data, and sustainability render these composites eminently suitable for various applications (Huang and Netravali, 2007). Superficially, many industries like automobile, marine, and aerospace, are moving towards the replacement by natural fiber composite components as an alternative to the traditionally used synthetic and man-made fibers. The major limitation is to control the orientation or alignment during processing and ensure that the mechanical properties of the fibers are utilized with optimum efficiency and that the fiber content is maximum. These limitations/drawbacks can be overcome using textile techniques, where the natural fibers are converted into yarn (Yang *et al.* 2007). Very few researchers have reported on the effects of processing on mechanical properties of natural fiber textile fabrics materials. Processing the natural fibers to form textile

fabrics is very difficult, because of many limitations in producing fine and clean fibers, fibers remain short, some fibers become hard, and the process is time-consuming during spinning and weaving. In the second type of non-woven fabric, fabric fibers become scattered, sheets are bulky and less flexible, and possess lower mechanical properties compared to woven fabric (Mishra *et al.* 2002, Rajesh and Jeyaraj 2016). These textile fabrics, because of their non-uniform properties, can result in variation in the composite properties, as in fabric warp and weft direction of fabrics. Therefore, a study needed to comprehend the mechanical properties of textile fabrics before processing the composite.

Literature survey reveals that reinforcement of natural fibers in short and random orientation in most of the polymer composites investigated. Discontinuity in the fiber creates amorphous nature in the composite which creates a non-uniform stress distribution in the matrix during loading. Due to this non-uniform stress distribution, composite fails early with lower strain rate. This short fiber reinforcement reduces the performance of composite material. In order to improve the performance of natural fiber composite, researchers suggested to use natural fiber in woven fabric form in the polymer matrix which carries more load than composite with short natural fiber reinforcement. Some researchers demonstrated that when these natural fibers are reinforced in woven fabric form, it carries more load and experience uniform stress distribution during loading. However, detailed investigation of textile properties of woven fabric and its influence on biodegradable natural fiber composite is yet to be carried out.

Literature survey also reveals that natural fiber reinforced with non-biodegradable matrix materials are investigated by many of the researchers. These types of materials are partially biodegradable: reinforcement fiber material is fully eco-friendly and matrix materials are non-biodegradable. Due to global warming issues, drastic development needs to be carried out to develop eco-friendly materials. In view of this, a fully biodegradable composite is yet to be carried out. However, only limited research work is available on dynamic mechanical properties characterizations of synthetic biodegradable materials. From the literature, Polyvinyl Alcohol (PVA) is found to be the most common bio-material used in many applications. Hence, in this

work, PVA thermoplastic polymer used as matrix material and cross-linked the same with Glutarahydrate (GA) for better mechanical and thermal properties.

As per previous discussion, it concluded the woven fiber reinforced composite carries more load with uniform stress distribution during loading. Hence, natural fiber reinforced in woven form, using fully biodegradable matrix material need to be investigated.

## **2.5 Applications**

James and Houston (2006) surveyed the natural-fiber composites with thermoplastic and thermoset matrices that have been embraced by European car manufacturers and suppliers for door panels, seat backs, headliners, package trays, dashboards, and interior parts. Natural fibers such as kenaf, hemp, flax, jute, and sisal offer such benefits as reductions in weight, cost, and CO<sub>2</sub>, less reliance on foreign oil sources, and recyclability. They also reported many challenges like homogenization of the fiber's properties and a full understanding of the degree of polymerization and crystallization, adhesion between the fiber and matrix, moisture repellence, and flame-retardant properties, to name but a few.

Dweib *et al.* (2004) studied development an all natural composite roof for housing application, structural panels and unit beams using soybean oil-based resin and natural fibers (flax, cellulose, pulp, recycled paper, chicken feathers) using Vacuum-Assisted Resin Transfer Molding (VARTM) technology. Physical and chemical investigations and mechanical testing of the beams yielded good results in line with the desired structural performance.

Mohini *et al.* (2011) reported that natural fiber reinforced composite depleting at a faster rate due to an increase in global warming and pollution hazards. In recent years, there has been increasing interest in the substitution of synthetic fibers in reinforced plastic composites by natural plant fibers such as jute, coir, flax, hemp, and sisal. Sisal is one of the natural fibers widely available in most parts of the world; it requires minimum financial input and maintenance for cultivation and is often grown in wastelands, which helps in soil conservation. The advantages of sisal fiber are low

density and high specific strength, biodegradable and renewable resource, and it provides thermal and acoustic insulation. Sisal fiber is better than other natural fibers such as jute in many ways, including its higher strength, bright shiny color, large staple length, poor crimp property, variation in properties and quality due to the growing conditions, limited maximum processing temperatures. In recent years, there has been an increasing interest in finding innovative applications for sisal fiber-reinforced composites other than their traditional use in making ropes, mats, carpets, handicrafts, and other fancy articles. Composites made of sisal fibers are green materials and do not consume much energy for their production. Sisal fiber is a potential resource material for various engineering applications in the electrical industry, automobiles, railways, building materials, geotextiles, defense and in the packaging industry.

Plastic/wood fiber composites are being used in a large number of applications in decks, docks, window frames and molded panel components (John *et al.* 2008). Satyanarayana *et al.* (2009) reported that natural fiber composites having many application like automobiles include parcel shelves, door panels, instrument panels, armrests, headrests and seat shells. Recently, banana fiber reinforced composites are coming into in interest due to the innovative application of banana fiber in under-floor protection for passenger cars (Samal *et al.* 2009). The passenger car bumper beam is manufactured by kenaf/glass epoxy composite material (Davoodi *et al.* 2010). Jitendra *et al.* (2010) studied the recent applications of natural fiber reinforced polymer composites and suggested making them a conceivable alternative to traditional fillers like mica, calcium carbonate and glass. By modifying either the resin system or the natural fiber, biocomposites can be designed for different applications ranging from products of commodity to aerospace, examples including electroactive papers, fuel cell membranes, controlled drug release mechanisms, and biosensors. This review aims to analyze the advancement in the application of cellulose based materials in different sectors with a discussion of fundamental research in these areas.

Nadir *et al.* (2011) studied the physical, mechanical, and flammability properties of coconut fiber reinforced Polypropylene (PP) composites. The flexural and tensile strength and hardness of the composites improved with increase in the coir fiber

content up to 60 wt %. The flame retardancy of the composites also improved with increase in coir fiber content.

Phillips *et al.* (2012) studied on flax-reinforced sandwich structure suitable for replacing wood in the top plates of string musical instruments. The mechanical properties of Sitka spruce, the most widely used wood species for this application, were taken as a benchmark when the new materials were developed. The materials enhanced using dynamic methods to determine the dynamic Young's modulus, shear modulus, internal friction, and static mechanical properties. The results show that the flax-reinforced sandwich structure can successfully act as a top plate and that an efficient manufacturing process can be developed to produce monocoque string musical instruments out of composite materials.

Automobile parts such as rearview mirror, visor in two-wheeler, pillion seat cover, indicator cover, cover L-side, nameplate are fabricated using sisal and roselle fibers hybrid composites (Chandramohan *et al.* 2013).

Faris *et al.* (2014) worked on date palm fibers reinforced polymer composites and suggested for automobile applications. This gap leads to disregard of potential natural fiber types in industrial applications and keep it no more than an environmental waste problem.

Furqan *et al.* (2015) reviewed the applications of natural fibers that have been used for making baskets, clothing, and ropes. Comparisons of material indices for beam and panel structures were made to investigate the possibility of using natural fiber composites instead of conventional and non-conventional

Kin *et al.* (2018) reviewed the use of natural fibers as reinforcement in cementitious and polymer based structural applications. They concluded that Natural Fiber Reinforced Polymer (NFRP) composites have been widely used in automotive and building industries, it is still possible to promote them to high-level structural applications like primary structural components of aerospace and maritime structures.

## **2.6 Motivation**

Natural fibers have several advantages such as low density, inexpensive and eco-friendly compared to synthetic fibers like glass, kevlar and carbon fiber. These natural fiber reinforced polymer composites can be used as an alternative material to conventional metals and non-biodegradable composites in structural applications where the load carrying capacity of a structure is not vital. However, the fulfillment of literature gap is essential to analyze the structural behaviour of both reinforcing and matrix materials subjected to several loading conditions. It is important to understand the influence of reinforcement and matrix material properties upon properties of the composite. The present work is focused on the investigation of the characterization of both reinforcing and matrix materials on mechanical and thermo-mechanical loading conditions.

## **2.7 Objectives**

From the foregoing literature survey, it is clear that there is needs for developing natural fiber woven fabrics reinforced completely bio-degradable composites and characterize its mechanical and thermo-mechanical behavior. It is also important to investigate the effect of different physical properties of yarn and fabric on textile and mechanical properties of the natural fiber fabric bio-degradable composites. Sisal fiber is considered as the reinforcement and PVA is considered as the matrix material to perform various studies in the present work.

Main objectives of the proposed work are:

- To determine different textile properties of sisal fabrics.
- To investigate the mechanical and thermo-mechanical properties of Polyvinyl Alcohol - Glutaraldehyde (PVA-GA) cross-linked polymer.
- To analyze the influence of sisal fabric reinforcement on the mechanical and thermo-mechanical properties of PVA-GA cross-linked polymer composites.

## CHAPTER 3

### MATERIALS AND METHODS

Natural fibers such as jute, sisal, silk, and coir are inexpensive, abundantly available, lightweight with low density, high toughness, and are biodegradable. Some natural fibers have the potential to be used as a replacement for traditional reinforcement materials in composites for applications which require a high strength-to-weight ratio and further weight reduction. Among other natural fibers, the sisal fiber is abundantly available in south India. Literature survey revealed that limited work has been carried out on woven sisal fabric reinforced with a biodegradable matrix material. Polyvinyl Alcohol (PVA) is a hydrophilic synthetic polymer generated by the hydrolysis of poly(vinyl acetate), which is formed by the polymerization of vinyl acetate. PVA is selected as the matrix and it is biodegradable. This chapter focuses on materials selection and its processing, experimentation and different testing-standards. Initially, the matrix material is prepared by mixing Polyvinyl Alcohol (PVA) with Glutaraldehyde (GA) for various volume fractions (Ravindra *et al.* 2019). Followed by this, the processed polymers are immersed in 2 mole of Sulphuric acid ( $H_2SO_4$ ) for 24 hours for complete cross-linking (Kumbar *et al.* 2019). The chemical structural characterization of PVA and GA is analyzed using Fourier Transform Infrared spectroscopy (FTIR). Sisal fiber extracted from leaves of sisal plant and processed into yarn, then into three types of fabrics such as Plain 1 (P1), Plain 2 (P2) and Weft Rib (WR) fabrics. The two plain fabrics are prepared to analyse the effect of gram per unit area (GSM): plain 1 and plain 2 have GSM of  $161.02 \pm 0.17$  and  $296.60 \pm 1.75$  respectively. The one weft rib fabric with GSM  $300.45 \pm 1.67$  is prepared to analyse the effect of woven pattern by comparing with plain 2. The basic physical and mechanical properties of these fabrics are analysed using various textile testing standards. These fabrics are further used to prepare the biodegradable composites with different weight fractions using conventional compression moulding technique.

The materials selection, processing, testing and characterization details are discussed in the following sections.

### **3.1 Materials Selection**

#### **3.1.1 Matrix material**

PVA and GA are procured from M/s. Leo Chem India, Bengaluru, India. PVA ( $\text{CH}_2\text{CH}(\text{OH})_n$ ) used as biodegradable matrix material and has a molecular weight of 85000 to 124000 g/mol with a degree of hydroxylation varying from 87 to 89. The viscosity of 4% aqueous solution at 20 °C is varies from 23 to 38 Cps (Centipoise), pH varies from 4.5 to 6.5 and has an ash content maximum of 0.75%. The melting point and boiling points are 200 °C and 228 °C respectively. The density of PVA is 1.19 g/cm<sup>3</sup>. Glutaraldehyde ( $\text{OHC}(\text{CH}_2)_3\text{CHO}$ ) is a 25% aqueous solution with a density of 1.06 g/cm<sup>3</sup>. Glutaraldehyde is a colourless liquid with a pungent odour and readily changes to a glossy polymer. The Odor threshold is 0.04 ppm (parts per million) as per Society of the Plastics Industry Inc., New York, USA. Molecular weight is 100.13, specific gravity ( $\text{H}_2\text{O}:1$ ) is 1.10, boiling point is 100 °C, freezing/melting point is -13.8°C, vapor pressure is 17 mmHg. Hazard identification (based on NFPA-704 M Rating System): Health 3, Flammability 0, Reactivity 0 and soluble in water.

#### **3.1.2 Sisal fiber and its processing**

Sisal fibers extracted from plants in southern part of Karnataka state, India. These sisal fibers are used to prepare three types of plain woven fabrics (two plain and one weft rib) in M/s. OM Textile Industries, Bengaluru, India. The sisal fibers are extracted from the leaves in the same plantation to get similar properties of all fibers. These fibers are sun-dried for seven days and washed several times using fresh water and again sun-dried for four days under normal climatic conditions. The extracted fibers are converted into yarn, and these yarns are then converted into fabric by hand weaving process. The schematic diagrams of plain woven and weft rib fabric structures as shown in Figure 3.1. As referred to plain woven, the vertical yarn is known as warp while the other direction is weft. The plain weave structure can be



categorized by observing the warp yarn (lengthwise or longitudinal or end yarns) which alternately and repeatedly goes over and under the weft yarn (woof or filling or pick or horizontal yarns). Similarly, weft rib structures can be categorized by observing the warp yarn which alternately and repeatedly goes over and under the two weft yarn. However, weft rib also comes under the category of plain woven, but two weft yarns are crossed with one warp yarns.

It is necessary to investigate the textile properties of three woven fabrics. For comparing purposes, the three sisal woven fabrics will be denoted as Plain 1 (P1), Plain 2 (P2) and Weft Rib (WR). The basic properties of various sisal woven fabrics given by manufacturer which are listed in Table 3.1. Figure 3.1 shows the schematic picture of plain and weft rib weave fabric structure, whereas Figure 3.2 shows the photographic view of P1, P2 and WR woven sisal fabrics used in this work.

Woven sisal fabrics are characterized through physical properties like mass per unit area, thickness, fabric density or fabric count. The sisal yarns are characterized for its yarn size (linear density) and crimp (for warp and weft). These fabrics are characterized by employing many textile standard methods which are generally used in textile industry. Table 3.2 shows the list of standards used to characterize all the three woven sisal fabrics, at Department of Fashion and Apparel Design, Acharya Institute, Bengaluru and Central Silk Technological Research Institute, Bengaluru, India. The details of experimental setup and its testing procedure for fabrics are explained in Section 3.4.

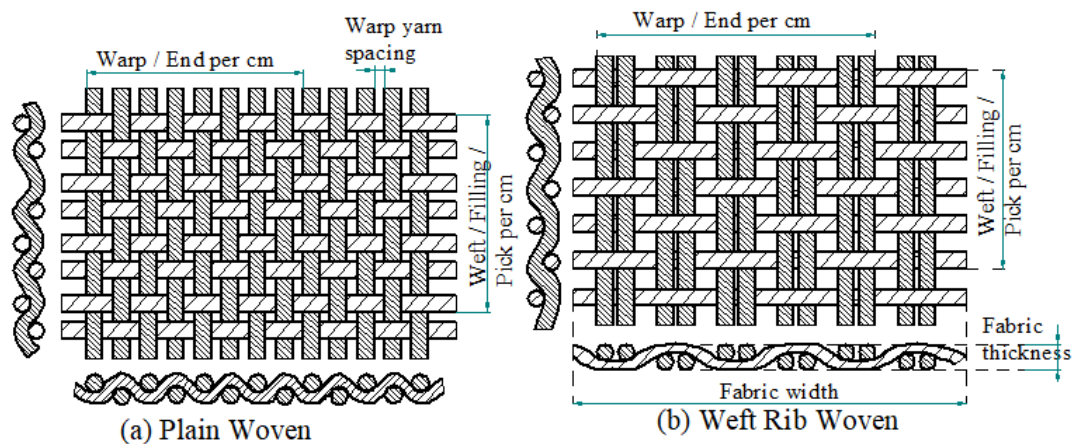


Figure 3.1: Schematic diagram of (a) Plain and (b) Weft rib woven fabrics and cross-section

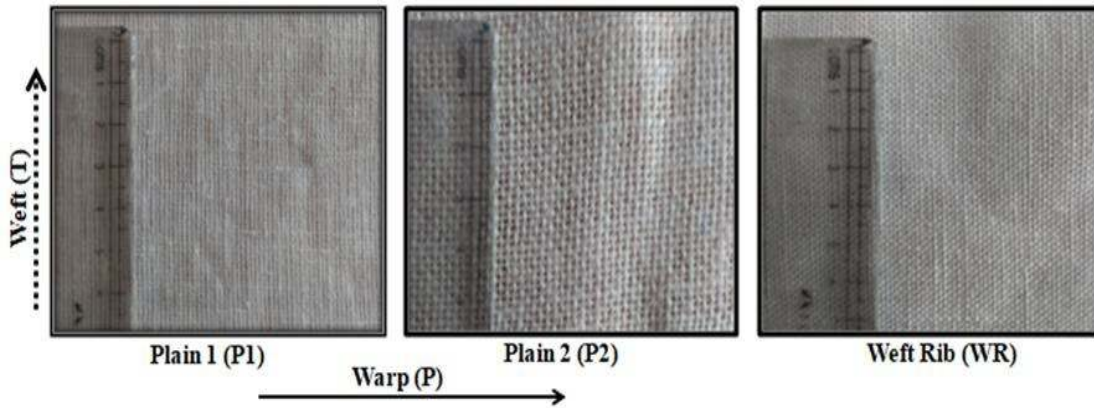


Figure 3.2: The photographic view of plain and weft rib woven sisal fabrics used

Table 3.1: Representation of different woven fabric of sisal textile fabric analyzed and their basic properties given by manufacturer

Sl. No	Woven type	Code	Fabric Thickness in mm	Mass per unit area	No of yarns per cm	
					Warp(P)	Weft(T)
1	Plain-1	P 1	0.42	160	18	20
2	Plain-2	P 2	0.73	300	12	12
3	Weft Rib	WR	0.72	300	22	11

### 3.2 Processing of Matrix and Composite

Sisal fabric reinforced composites are prepared using conventional vacuum-assisted pressure compression method. Figure 3.3 shows the schematic diagram of different steps involved in the present work from extraction of sisal fiber to testing of composites. Figure 3.3(a) shows extracted sisal fiber and then converted into woven sisal fabrics. The resin and fabric materials are loaded into mild steel mould having dimensions of 250mm x 200 mm x 4 mm and kept in the vacuum-assisted pressure compression moulding machine as shown in Figure 3.3(b). The prepared laminated composites are post-cured for 24 hours at 60 °C using conventional air oven, and then immersed in 2 mole of Sulfuric acid (H<sub>2</sub>SO<sub>4</sub>) for 24 hours to attain complete cross-linking. Further these samples are cut in to required dimensions for different mechanical and thermo-dynamic properties characterization. Figure 3.3(c) represents Universal Testing Machine (UTM) and Dynamic Mechanical Analyzer which are used to characterize the mechanical and thermo-mechanical properties of the composites respectively.

Table 3.2: Different standards used for characterization of textile properties of fabrics

Methods	Properties	Testing	Standard method
Yarn testing methods	Twisting strength of yarn	Untwist-retwist method	IS: 832-1985
	Yarn crimp	Yarn crimp and yarn take-up in woven fabrics	ASTM: D3883
	Yarn size	Yarn number (linear density)	ASTM: D1907
Fabric basic properties testing methods	Fabric density	Warp (end) and filling (pick) count of woven fabrics	ASTM: D3775
	Fabric weight	Mass per unit area of fabric	ASTM: D3776
	Fabric thickness	Thickness of textile materials	ASTM: D1777
Fabric mechanical properties testing methods	Tensile Strength	Fixing fabric two ends	IS: 1969-1985
	Stiffness Strength	Bending through the angle of 41.5°	ASTM D 1388-96
	Bursting Strength	79.8mm diameter of subjected to bursting	IS: 1966-1976
	Fabric Stretch and recovery test	Applying and removing the load	ASTM D 1388-96
	Elmendorf Tearing Test Method	Impact testing method	ASTM D1424
	Single Rip Tear Test Method	Tongue tear	ASTM D 2261

### 3.3 Fourier Transform Infrared Spectroscopy

The chemical compounds of PVA and sisal fiber are examined to understand the effect of chemical compounds upon mechanical behaviour of the composites. In order to identify the organic and polymeric compounds, the Perkin Elmer Fourier Transform Infrared Spectroscopy [FTIR] is used to study compounds of PVA, sisal fiber and its composites with high accuracy (Banafsheh *et al.* 2019, Muhammad *et al.* 2019). All samples are completely dried to avoid unwanted peaks (Madhuri and Rukmani 2019). Then, the FTIR spectroscopy is recorded by accumulating 16 scans at 4 cm<sup>-1</sup> resolution between 500 cm<sup>-1</sup> to 4000 cm<sup>-1</sup> range. Further, the sisal fiber chemical compositions are analyzed at M/s. Intertek Testing Services India Pvt Ltd, Bengaluru, India.

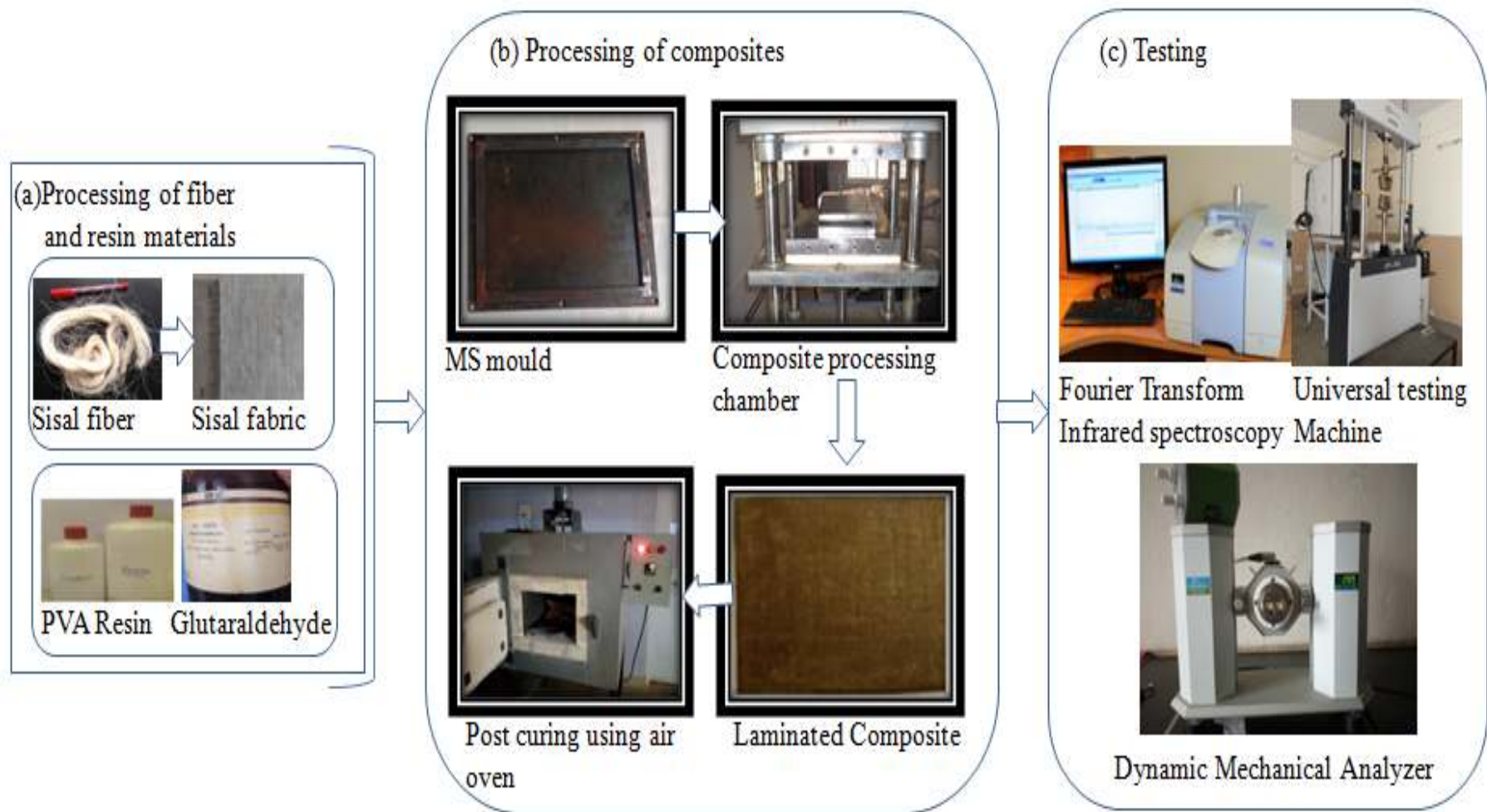


Figure 3.3: Schematic representation preparation steps of woven sisal fabric composite

### 3.4 Methods Used for Fabric Physical Properties

#### Yarn twisting

The spiral disposition of the woven fabric of yarn, which is generally expressed as the number of turns per unit length of yarn (turns per meter). The twist of the yarns measured using direct counting method, which is also called untwist-retwist method. From each woven sample, five specimens of 500 mm length are selected from different parts of the woven fabric. The twist test is conducted in accordance with IS: 832-1985 method having gauge length of 250mm. A dead weight of 0.5g/tex is applied to the specimen and the tension is maintained till permitted elongation is obtained with an accuracy of  $\pm 0.5$ mm.

#### Yarn crimp

The physical property of yarn crimp is evaluated as per ASTM D3883 standards. The fabric is cut in weft direction for length 300 mm and warp direction for length 200 mm. Two parallel lines are marked on the fabric which are parallel to the yarns and are 200mm apart (width of fabric  $-Y_1$ ). Minimum of ten yarns are unravelled from the cut fabric to determine the yarn crimp percentage (Equation 3.1) (Misonon *et al* 2015).

$$\text{Yarn Crimp (\%), } C = \frac{Y_2 - Y_1}{Y_1} \times 100 \dots\dots\dots (\text{Eqn. 3.1})$$

where  $Y_1$  = Length of yarn in fabric,  $Y_2$  = Measured length of yarn after unravelling without external force and  $c$  = yarn crimp in percentage.

#### Yarn linear density

The ASTM D1907 standard is used to determine the linear density of the prepared yarn. Minimum of ten unravelled yarns of 1 meter length are considered to determine the linear density of the yarn (Equation 3.2) (Misonon *et al* 2015).

$$\text{Yarn size (tex), } N = \frac{w \times k}{l} \dots\dots\dots (\text{Eqn. 3.2})$$

Where,  $l$  = length of yarn in meter,  $w$  = yarn weight in grams and  $k$  is the constant ( $k = 1000$  m/g) in tex.

### **Yarn density / Fabric density**

The fabric properties could be significantly affected by the compactness of the fabric related yarn spacing. “Yarn density” or ‘fabric density’ is the number of yarns in fabric, it is generally known as ‘fabric count’. Number of yarns in both warp and weft direction are measured according to ASTM: D3775 standard by placing fabric on the glass surface using a pick counter in a 20 mm length.

### **Weight and thickness of fabric**

The fabric weight is calculated as per ASTM: D3776, five specimens are used to measure in gram per square meter (GSM). Fabric thickness is measured as per ASTM: D1777 at thirty locations. Thickness of the fabric is measured using Askhi fabric thickness indicator which is having least count of 0.01 mm.

## **3.5 Fabric Mechanical Properties**

### **Tensile strength**

Tensile properties of sisal fabrics are measured using Instron make Universal Testing Machine (UTM). The test specimens are cut by maintaining equal number of yarn in both the directions. The width and thickness are considered to evaluate the cross-sectional area of the specimen (Huang and Netravali 2007, Yahya *et al.* 2011). Tensile test is conducted according to IS: 1969-1985 to find the influence of mass per unit area and woven structure with a gauge length of 200mm, width of 50mm, and speed of 3 mm/min. Specimen is gripped between two clamps of the tensile testing machine in such a manner that the same set of yarns are gripped by both the clamps, and load is equally distributed on each yarn. Further increasing in load longitudinally to the specimen by moving one of the clamps until the specimen fails. The maximum load and corresponding deformation are noted during experimentation.

### **Flexural rigidity**

Flexural rigidity is a bending moment which is required to produce a given curvature in mg-cm. Fabrics are cut according to ASTM D 1388-96 having dimension of 152.4

mm x 25.4 mm. This is mounted on the horizontal platform with an overhang like a cantilever. It will bend downwards along the length, due to its own weight. This cantilever principle testing method is also known as Shirley stiffness testing method and shown in Figure 3.4. The fiber is allowed to bend through the angle of  $41.50^\circ$  under its own weight, then flexural rigidity of the fabric is calculated.

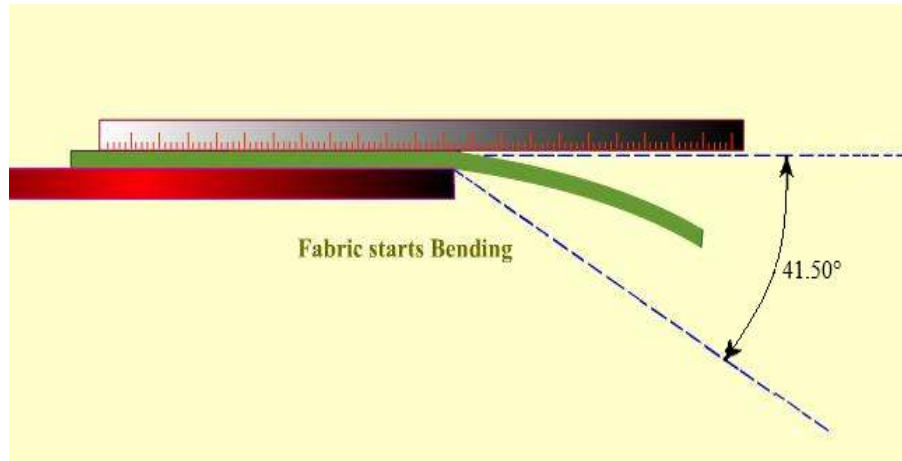


Figure 3.4: Schematic to determine flexural rigidity of fabric

### **Bursting strength**

Bursting strength of all the three fabrics were determined according to IS: 1966-1976 standards. Test specimens are cut in to a circle of 79.8mm diameter and area is free from folds or crease and selvage of the fabric. Test specimen is kept over the diaphragm so that it lies in a flat tensionless condition, and is clamped securely with a holder. The pressure is applied to test specimen until the fabric bursts. Bursting strength is calculated by subtracting the initial diaphragm pressure from the mean busting pressure.

### **Fabric stretch and recovery**

Fabric stretch and growth test are conducted according to ASTM D 1388-96. A fabric is stretched from its original length ( $L_1$ ) to a specified extension length ( $L_2$ ) for the prescribed period of time. The fabric doesnot reach original length after release of load. However, length of the fabric is extended after release ( $L_3$ ). The fabric growth at time interval is calculated from the distance between the bench marks of the specimen

prior to stretching and the length after relaxation period. The percentages of fabric stretch and fabric growth are calculated using below equations.

$$\text{Fabric stretch} = \frac{(L_2 - L_1)}{L_1} \times 100 \quad \dots\dots \text{(Eqn. 3.3)}$$

$$\text{Fabric growth} = \frac{(L_3 - L_1)}{L_1} \times 100 \quad \dots\dots \text{(Eqn. 3.4)}$$

### **Elmendorf tearing test method**

The force in grams required to propagate tearing across the fabric specimen is measured according to ASTM D1424 both along warp and weft directions. Elmendorf Method is also known as impact testing method which is shown in Figure 3.5 (a). The sample is cut randomly from a 3 meter length of fabric and 0.2 meter away from the selvage edges. Two sets of sample are obtained, one is warp sample and the other is weft sample. The specimen is held by two clamps as shown in Figure 3.5 (b). The pendulum swings through an arc, tearing the specimen from a pre-cut slit. The loss in energy by the pendulum is indicated by a pointer. The scale indication is a function of the force required to tear the specimen. When the specimen is cut out, a slit of 20 mm deep has been made at the centre of the edge perpendicular to the direction to be tested. Four adjustable weights are used to determine tearing strength of fabric based on fabric strength. The average value of five trials of tear strength in warp and weft direction respectively is calculated using Equation 3.5. Figure 3.5 (c) shows the template used to mark the sample size.

$$\text{Tearing strength of fabric} = K \times \text{average pointer reading in gram force} \dots \text{(Eqn. 3.5)}$$

where, K is four weight constants i.e., A=16, B=32, C=64, D=128

### **Single rip tear method**

The tearing strength of the fabrics are determined using single rip static tear method also called as Tongue tear. This test carried out using Universal Testing Machine at National Institute of Technology Karnataka, Surathkal, India. The samples are cut according to ASTM D 2261 as shown in Figure 3.6. One end of the sample is clamped to lower jaw (fixed jaw) another end of tear sample connected to upper jaw



(moveable jaw). The crosshead speed varied from 50mm/min to 200mm/min at an interval of 50 mm/min in both warp and weft directions.



Figure 3.5: Impact tearing tester (a) Elmendorf tear tester (b) Fabric mounted by fixing both the ends of fabric (c) Tearing testing template which is placed on P1 types of sisal fabric

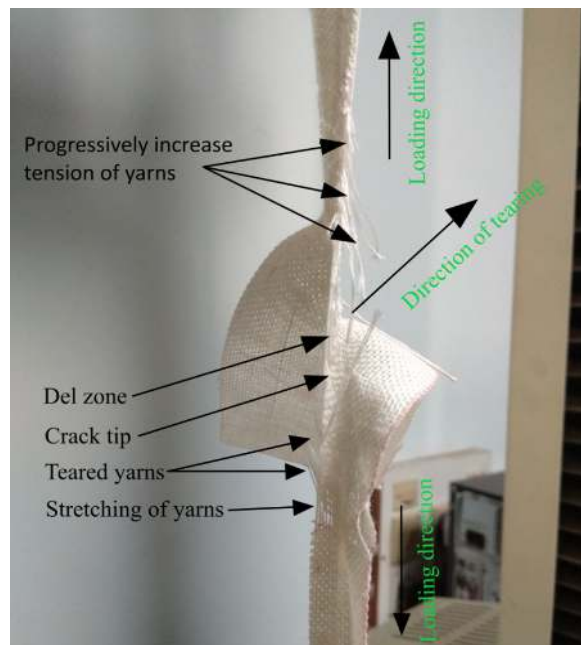


Figure 3.6: Single rip tear method and its details

### 3.6 Mechanical Properties of Matrix and Composites

All structural parts are subjected to static loading, so it is necessary to determine the mechanical properties of fabric reinforced composite. It is a basic fundamental testing

which helps to understand the influence of cross-linking and reinforcement both in warp and weft directions. The computerized Universal Testing Machine (UTM) used to evaluate mechanical properties of the composites under tensile and flexural loadings. Similarly, impact strength is analyzed through the impact test conducted using Izod Impact tester. The mechanical properties of both resin and composites are evaluated based on the average value of tests conducted on five identical samples.

### **Tensile properties**

Tensile properties of the composite samples are determined according to ASTM D638-03 with samples of size dimensions of 160 mm length, 12.5 mm width and 4 mm thickness. The tensile test is conducted at a rate of 10 mm/min with a gauge length of 100 mm using the Universal Testing Machine available at National Institute of Technology Karnataka, Surathkal, India.

### **Flexural properties**

Flexural tests are conducted according to ASTM D790 standard using samples with size 127 mm length, 12.7 mm width, and 4 mm thickness. The point load is applied with a crosshead speed of 2 mm/min at middle of the span length of 90 mm. which is carried out using the Universal Testing Machine available at National Institute of Technology Karnataka, Surathkal, India.

### **Impact strength**

The impact properties of composite are evaluated at M/s. GLS Polymers Pvt Ltd, Peenya Industrial Area, Bengaluru, Karnataka. The impact test is conducted using Izod Impact Tester according to ASTM D 256 standard and a sample with dimensions of 64 mm length, 12.7 mm width, and 4 mm thickness.

### **3.7 Dynamic Mechanical Analyzer**

The Perkin Elmer Dynamic Mechanical Analyser (DMA) 8000 Model is used to study the thermo-mechanical behaviour of both matrix and composite materials over a range of temperature.

Initially, matrix material is analyzed using DMA under 3 point bending mode. The storage modulus, loss modulus, and tan delta values are directly recorded from DMA. Several tests are carried out to evaluate adhesion factor, activation energy, and estimation of the operating life, cross-linking density, effectiveness, and displacement. Further matrix material's storage modulus, loss modulus and tan delta are evaluated using various modes, like dual cantilever, single cantilever and tensile modes.

### 3.7.1. Temperature sweep

#### Three point bending

Thermo-mechanical properties of both polymer and composite are measured using DMA 8000. The instrument used in a three point bending mode with a nitrogen flow rate of 20 mL/min. Two ends of the sample are simply supported and sinusoidal frequency is applied at the middle of the span length. Initially, the sample is maintained at the isothermal condition for 5 minutes in order to obtain thermal stabilization of sample at 2 Hz. The test is conducted at temperature sweep mode at 2 Hz with temperature scan from 25-160°C at the heating rate of 2°C/min, and strain of 0.050 mm. The rectangular samples of dimensions 50 mm mm xx 6 mm mm xx 4 mm is used with a span length of 45 mm is shown in Figure 3.7.

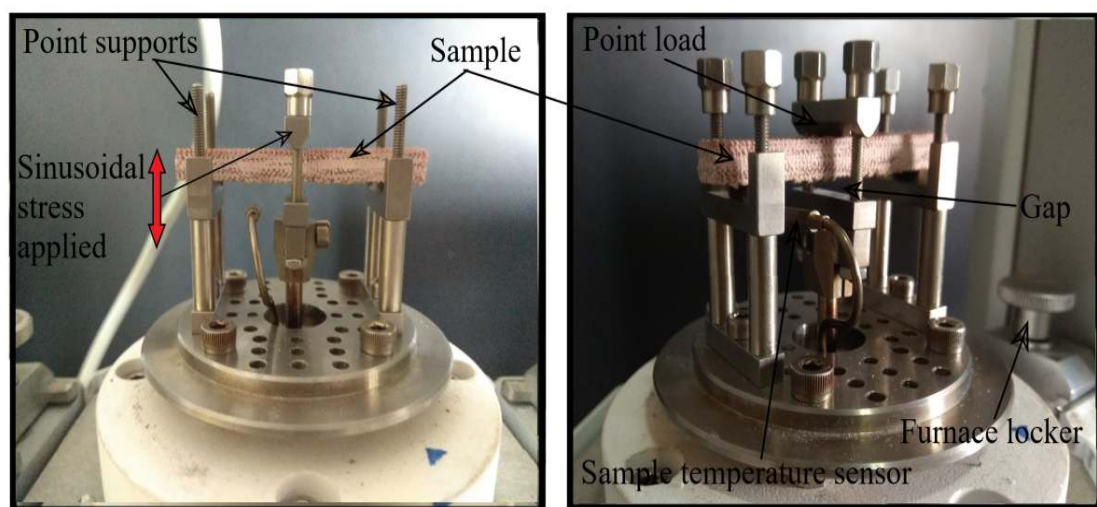


Figure 3.7: Dynamic mechanical analyzer under three point bending mode

## Tensile mode

DMA 8000 instrument is used under tensile mode with a nitrogen flow rate of 20 mL/min. Initially, the sample is maintained at the isothermal condition for 5 minutes in order to obtain thermal stabilization of sample at 2 Hz. The test is conducted at temperature sweep mode at 2 Hz with temperature scan from 25-160°C at the heating rate of 2°C/min, and strain of 0.050 mm. The samples of dimensions 20 x 8 x 2 mm with a gauge length of 10 mm shown in Figure 3.8.

### 3.7.2 Multi frequency sweep

#### Three point bending mode

The thermo-mechanical responses of the both matrix and composites are measured using Dynamic Mechanical Analyzer Perkin Elmer model 8000 instrument in three-point bending mode in a nitrogen environment with a flow rate of 20.0 ml/min. The test is conducted at multi-frequency from 2 Hz to 20 Hz at intervals of 2 Hz linearly with temperature scan from 20-160°C with heating rate of 2°C/min, and strain of 0.050 mm on rectangular samples with an approximate dimension of 50 mm x 6 mm x 4 mm. The sample maintained isothermally for 5 minutes under 3-point bending mode before the starting of multi-frequency mode for better stabilization.

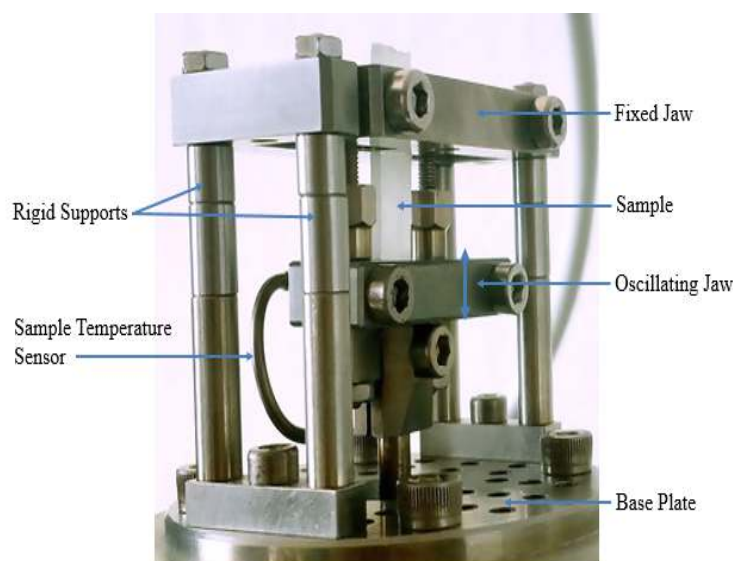


Figure 3.8: Dynamic mechanical analyzer tensile mode setup

### **3.8. Hardness and Microstructure Studies**

#### **Hardness**

Shore D hardness is used to measure PVA and PVA-GA samples according to ASTM D-2240 standard. Shore D hardness testing is the preferred method for rubbers/elastomers and is also commonly used for 'softer' plastics. Shore D hardness is measured using Excel make tester at room temperature ( $28^{\circ}\text{C}\pm 1$ ).

#### **Microstructure of fractured surface**

The microstructures of sisal fabric reinforced composite are analyzed to understand the influence of textile microstructure on mechanical properties. Also, the interfacial bondings between the matrix and fabric material are studied using Scanning Electron Microscopy (SEM) images. The fractured specimens of tensile, flexural and impact sample are analyzed using SEM to understand the fractured mechanism.



## CHAPTER-4

### CHARACTERIZATION OF PVA WITH GA

This chapter analyses the influence of various volume fraction of Glutaraldehyde (GA) cross-linking in Polyvinyl Alcohol (PVA) on mechanical properties (tensile and flexural), and dynamic mechanical characteristics (storage and loss modulus, material loss factor, and deflection). Along with the adhesion factor, activation energy, estimation of the operating life, cross-linking density, and effectiveness are determined by further processing of DMA data. The optimum volume fraction of GA cross-linker in PVA is determined based on mechanical and thermo-mechanical properties and same is used as a matrix material to prepare the composite.

#### 4.1 Cross-linking of PVA with GA

PVA is cross-linked with GA for different volume fractions using conventional vacuum-assisted pressure compression methods as discussed in Section 3.2. After processing of polymers, the mechanical properties like tensile and flexural properties are analyzed as per ASTM standards as described in Section 3.6. Similarly, dynamic mechanical properties of PVA cross-linked GA are investigated under tensile mode using temperature scan method as represented in Section 3.7.1. Further, these polymers are tested under three-point bending mode under the multi-frequency temperature scan method as reported in Section 3.7.2. This DMA data is also used to analyze the activation energy, adhesion factor and shift factor. Further, some additional studies are carried out to study GA cross-linking effect on cross-linking density and cross-linking effectiveness.

#### 4.2 Mechanical Properties

##### Tensile strength

The tensile property of matrix is characterized as per ASTM D638-08 standard to study the effect of cross-linking GA with PVA. Figure 4.1 shows that ultimate stress increases by adding GA up to 20% and beyond that the tensile strength tends to

decrease. In case of pure PVA the necking takes place at very less magnitude of load and the fracture is observed with lower toughness. For the GA loading up to 20% load carrying capacity and strain shows improvement. It is also evident from the relatively high toughness and mechanical properties exhibited compared to pure PVA. The better combination of PVA-GA is found at 20% of GA with maximum tensile strength 14.96 MPa. The area under the curve represents the strain energy absorption of matrix material which is found to be highest at 20% GA due to the establishment of effective cross-linking.

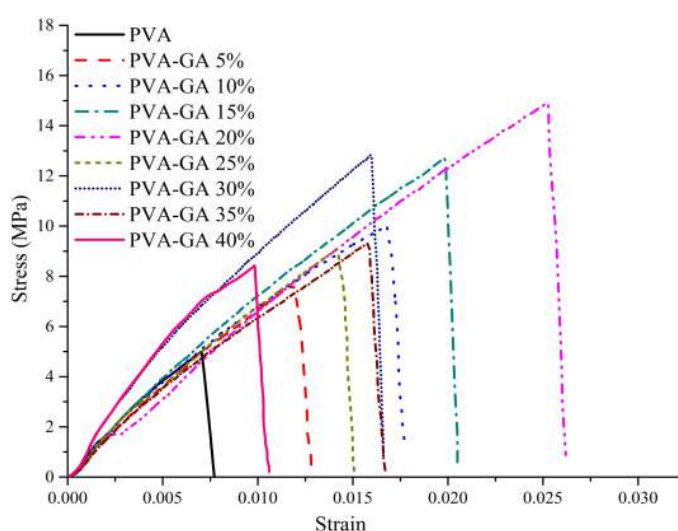


Figure 4.1: Tensile stress-strain plot for various percentage of GA in PVA

### Flexural strength

The flexural property of matrix is characterized as per ASTM D790 standard to study the cross-linking effect of GA with PVA, and results are shown in Figure 4.2. Figure 4.2 shows that load carrying capacity under flexural load increases with the addition of GA. However, the same composition 20% GA cross-linked PVA exhibiting favourable bending properties and allows better deformation compared to other cases. As the percentage of GA increases the flexural resistance increases drastically from 10 MPa (neat PVA) to 26 MPa 20% GA, which also indicates relative inflexibility. There is an improvement of 2.6 times in flexural strength, for 20% of GA in PVA. This may be due to cross-linking the polymer network, which promotes the breaking and re-forming of bonds can make the polymer stiffer. The flexural strain increases for the addition of GA up to 15% drastically, further it decreases. Comparing to tensile mode, in flexural mode cross-linked polymer is exhibiting good ductility and



energy absorption capability. The optimum combinations of GA in PVA are found to be at 25% by considering flexural stress.

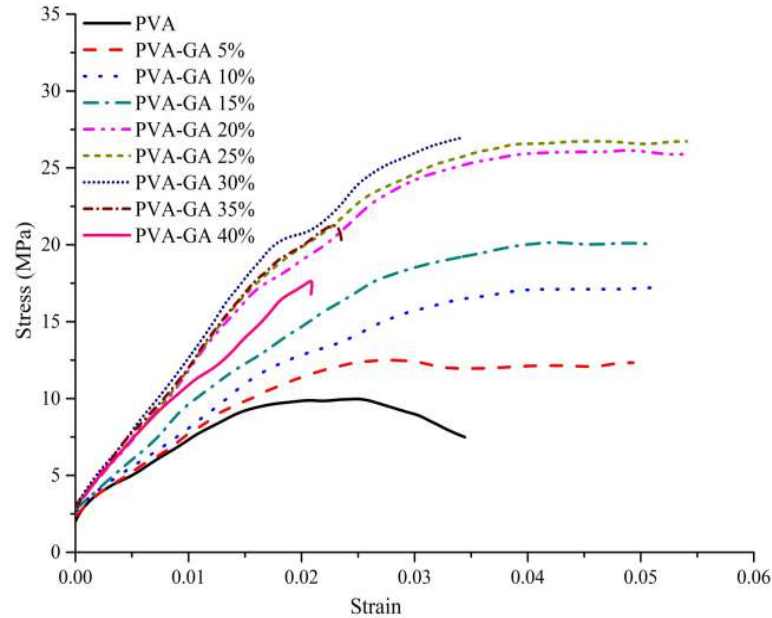


Figure 4.2: Flexural stress-strain plot for a various percentage of GA in PVA

### Surface morphology study

Fractured samples of PVA and PVA-GA tensile and flexural test are considered for the surface morphology study.

### Microstructure of tensile fracture surfaces

Figure 4.3 shows the SEM images associated with fractured surfaces of PVA-GA polymers under tensile loading. Tensile loading of PVA-15%GA generates dendritic structure due to material drawing/stretching and microscale cavitations near the origin of fracture, indicative of craze formation and rupture. SEM images shows in Figure 4.3 (c) also reveals evidence of macro- or micro-ductility. Instead, microscale ridges and plateaus can be seen, likely due to small crack deflections under fast fracture propagation for PVA-30GA. This is followed by fast, multi-planar fracture that resulted in fragmentation PVA-40GA under tensile loading. This indicates PVA-40GA having relatively low ductility compared to PVA-20GA. The concentric rib markings seen on fractured surface of tensile samples are also seen on the representative fracture surfaces for each material and loading mode.

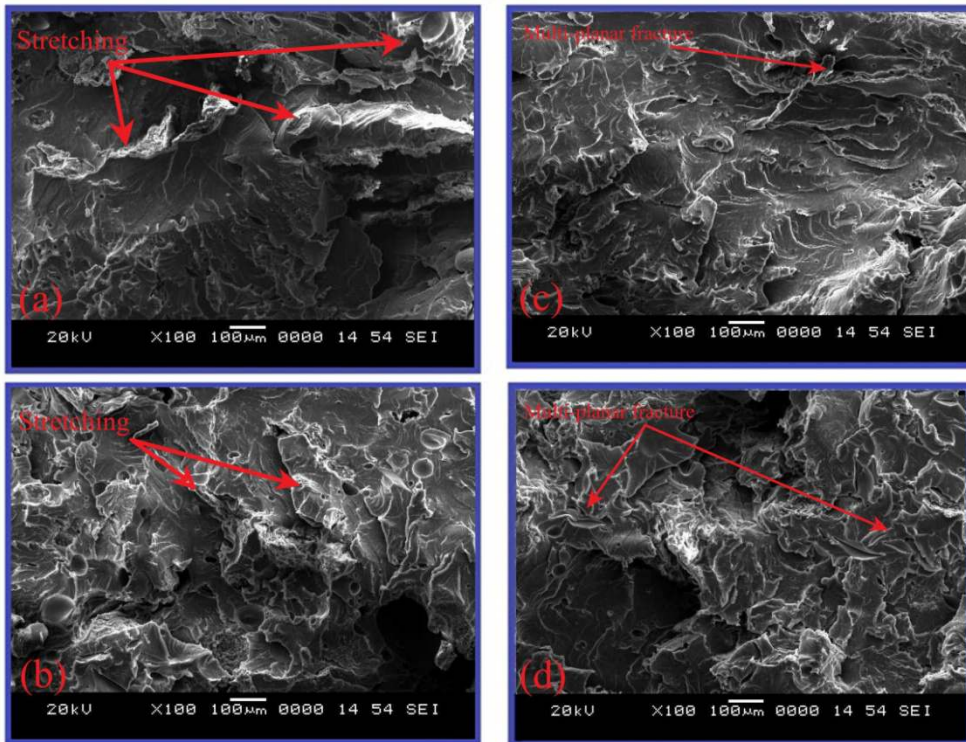


Figure 4.3: Tensile fractured images (a) 15% GA in PVA, (b) 20% GA in PVA (c) 30% GA in PVA and (d) 40% GA in PVA

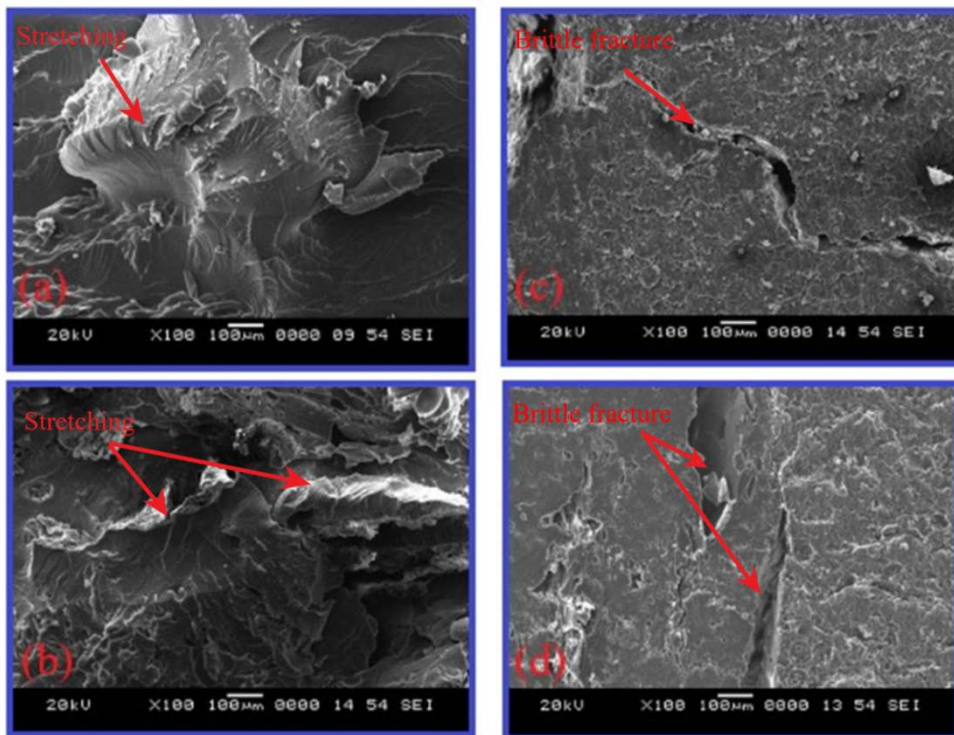


Figure 4.4: Flexural fractured images (a) 15% GA in PVA, (b) 20% GA in PVA (c) 30% GA in PVA and (d) 40% GA in PVA

### **Microstructure of flexural fracture surfaces**

In flexural mode, the point load is applied at the mid of the sample with a span of 90 mm. Due to this the top surface is subjected to compression, and bottom surface is subjected to tension. So fractured images associated with the bottom surface are analyzed the ductile behaviour. Figure 4.4 shows the fractured images of different PVA-GA samples under flexural loading. Ductile failure is observed in both PVA-15GA and PVA-20GA polymers, as seen in SEM images in Figure 4.4 (a) and (b) respectively. This is also evident in flexural stress-strain graph discussed in Section 4.1. As the percentage of GA increases more than 20%, the ductile fracture is converted to brittle fracture as shown in Figure 4.4 (c) and (d) for PVA-30GA and PVA-40GA polymers respectively.

### **4.3 Dynamic Mechanical Properties Under Tensile Mode**

The temperature scan method is used to analyze the cross-linking effect of GA with PVA for various volume fractions on dynamic mechanical behaviour. The thermo-mechanical properties of PVA cross-linked with the extent of GA from 0 to 40 volume fractions are analyzed via Dynamic Mechanical Analyzer (DMA) under tensile mode. The storage modulus, loss modulus, and  $\tan \delta$  are used to analyze the thermo-mechanical tensile behaviour of GA cross-linked PVA.

#### **Storage modulus**

The softening behaviour, heat resistance, glass transition temperature ( $T_g$ ), the phase characteristics effect are analyzed using storage modulus, loss modulus,  $\tan \delta$ , and elongation plots. The polymers exhibit different properties depending on the cross-linking densities. Figure 4.5 clearly shows the effects of GA cross-linking on various regions of storage modulus under tensile mode. The storage modulus is used to measure the elastic response of materials. The storage dynamic module as a function temperature is divided into four regions, I. hard plastic region, II. leathery region, III. rubber region, and IV. liquid region (soft rubber).

In region I (hard plastic region), it is observed that the storage modulus is depends on the degree of cross-linking. In region II, storage modulus decreases drastically with

increase in temperature but increases with GA cross-linking. This enhancement of storage modulus in this region is due to the decrease in chain mobility. This increase in storage modulus is because of high physical interactions between the polymer chains due to the existence of hydrogen bonding between the hydroxyl groups (Krumova *et al.* 2000). In region II, magnitude of storage modulus is improved due to cross-linking effect. At the end of this region, storage modulus values reach the lowest value. In region III, storage modulus is stable and improved with GA cross-linking. This is due to the interconnection between different long backbone chains increase the elastic energy of the polymer even at a higher temperature. In other words, cross-linking increases the rigidity of the polymer. For PVA, the hydroxyl group contributes via hydrogen bonding to the stiffness of the polymer (Jun *et al.* 2001). This clearly shows both physical and chemical cross-linking. In physical cross-linking due to increased entropy, modulus increases, while chemical cross-linking because of formation of a network and due to no slippage of chains, the physical properties are improved. This can also refer to some physical forces of attraction like hydrogen bonding or charge transfer complexes etc. The effect of cross-linking is clearly observed in the regions II & III (glass transition region 1 and 2) as well as the rubbery plateau region (IV). This indicates that PVA-GA can resist the load at higher temperature.

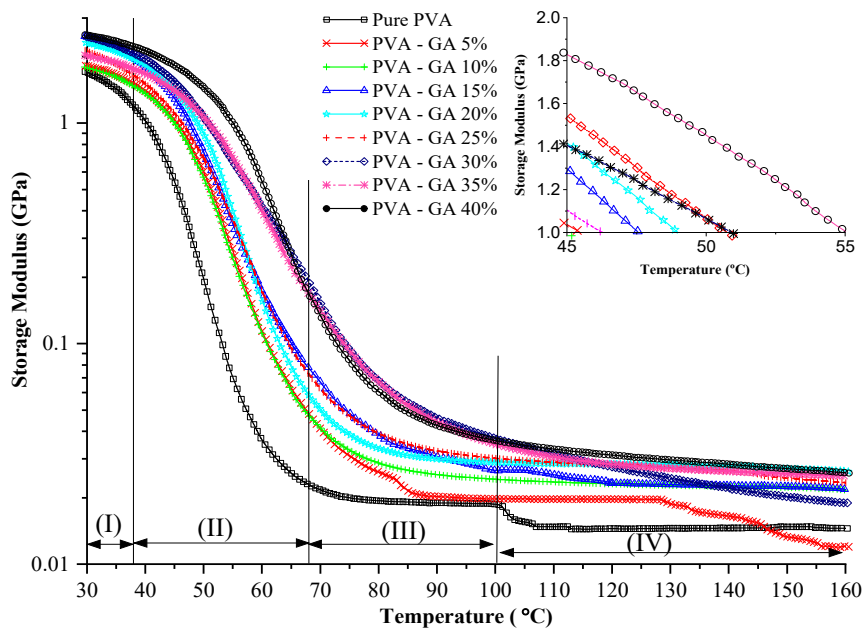


Figure 4.5: Tensile storage modulus for GA cross linked PVA

## Loss modulus

Similar to storage modulus, the loss modulus under tensile loading is also divided into four different regions, as shown in Figure 4.6. It is observed that in transition region I, with increase in GA loading peak of the loss modulus curve is shifting towards higher temperature and the decreasing rate of loss modulus also reduced. This is due to the existence of hydrogen bonding between the hydroxyl groups leads to reduce mobility even at higher temperature. However, it is observed that pure PVA is very soft and flexible at higher temperature. Due to the bonding between PVA and GA the loss modulus of PVA-GA polymer is reduced and makes PVA-GA stiffer. This shows that shifting for softening, glass transition temperature, and phase change region of PVA materials to a higher temperature by GA cross-linking. In region II, the loss modulus decreases further. However, the magnitude of loss modulus gets improved due to the cross-linking effect. Significant improvement in the dynamic modulus in the rubbery plateau region (IV) is observed which indicates higher visco-elastic nature. The highly cross-linked polymer has a much larger loss modulus indicating the tighter network structure and higher stiffness (Richeton *et al.* 2005).

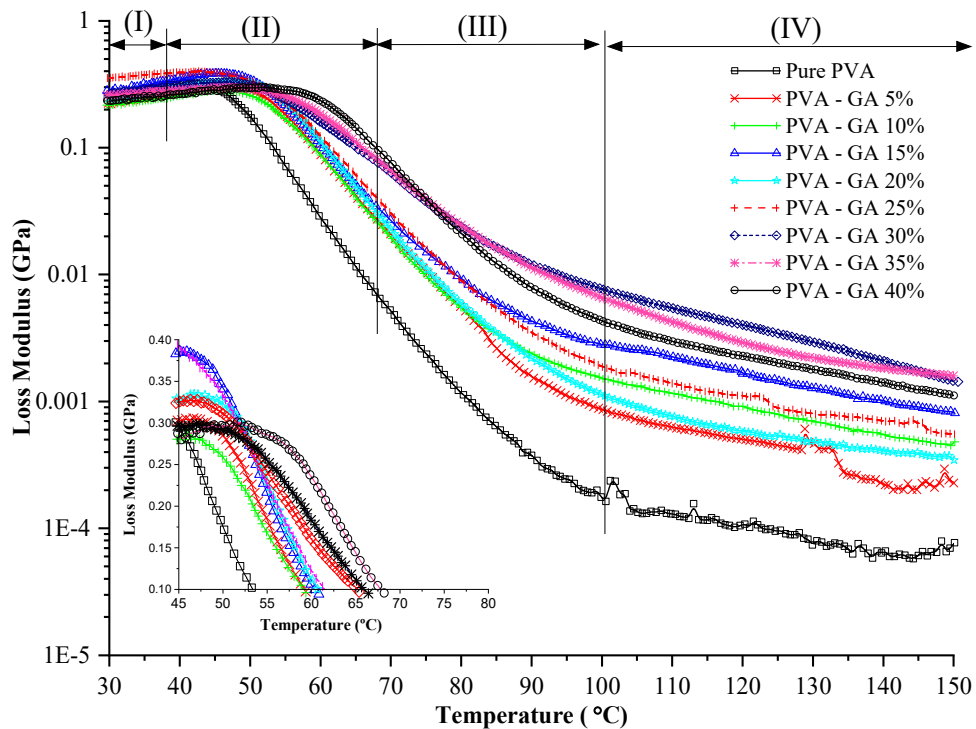


Figure 4.6: Tensile loss modulus for GA cross-linked PVA

## Tan $\delta$

Tan  $\delta$  is the ratio of loss to the storage modulus and is called damping factor or loss factor of polymer. It is a measure of energy dissipation of materials and expresses how good materials will be at absorbing the energy. As  $\delta$  approaches 0, it shows purely elastic behaviour, and as  $\delta$  approaches 1 or more, the material shows a purely viscous behaviour. The tan  $\delta$  of the different PVA-GA are shown in Figure 4.7. Similar to the earlier cases tan  $\delta$  curve also divided into four regions.

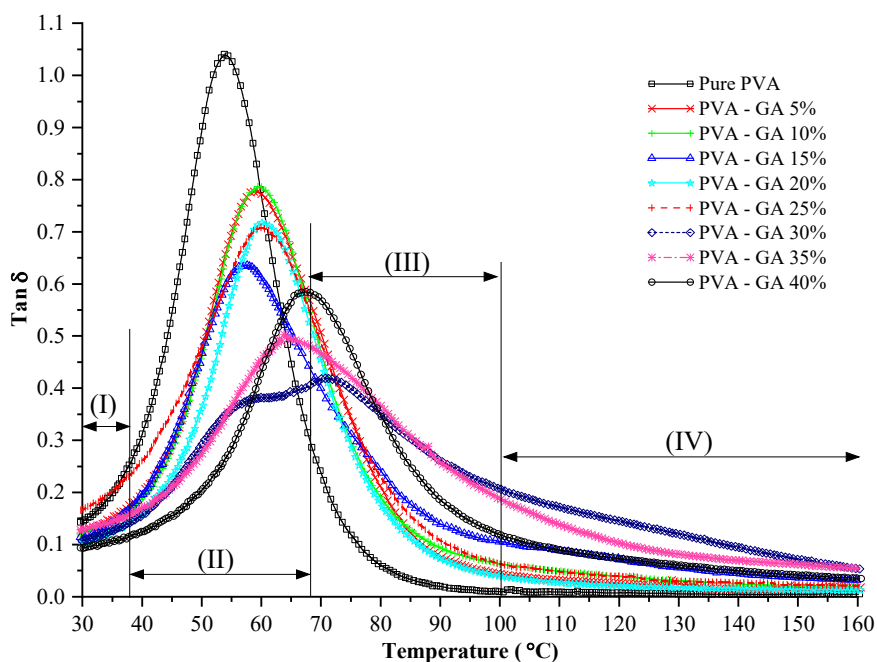


Figure 4.7: Tensile tan  $\delta$  for GA cross-linked PVA

In the region I, negligible change in the loss factor is observed due to the cross-linking effect. The region II, (the transition region) indicates that pure PVA has lower  $T_g$  and the curve reaches peak value at a faster rate. Due to the cross-linking effect, the tan  $\delta$  peak decreases and shifts towards higher temperature. For pure PVA the tan  $\delta$  peak is higher and narrow which indicates higher energy dissipation. By cross-linking, peak value is reduced and wider the tan  $\delta$  curve is observed which indicates lower energy dissipation of material. It acts as being elastic to store the load rather than dissipating it. This relaxation represents the glass transition temperature of the PVA at which the Micro-Brownian motions of the molecular chains become appreciable, and the elastic modulus ( $G'$ ) also decreases drastically (Akio *et al.* 2003). However, by adding GA,

the  $\tan \delta$  peak decreases and also the slope is improved. The presence and good diffusion of GA retard the segmental motions (restrictions against molecule motion of polymer chain) of the polymer during the transition. Table 4.1 shows the peak values of  $\tan \delta$  and shifting of the  $\tan \delta$  peak to higher temperature with cross-linking effect. The  $\tan \delta$  peak value is at around 53.8 °C for pure PVA material by adding GA, the shifting of peak up to 70.7 °C.

Table 4.1: Dynamic mechanical properties of PVA cross-linked with GA

% GA	Loss Modulus (GPa)		Tan $\delta$	
	Temperature at peak	Magnitude at peak	Temperature at peak	Tan $\delta$ at peak
Pure PVA	41.36	0.323	53.8	1.040
5	45.82	0.305	59.3	0.776
10	46.01	0.291	59.3	0.787
15	46.67	0.381	57.6	0.635
20	46.74	0.334	61.1	0.717
25	42.67	0.401	59.9	0.708
<b>30</b>	45.50	0.326	70.7	0.418
35	46.15	0.296	62.9	0.494
40	51.63	0.301	67.5	0.584

#### 4.4 Dynamic Mechanical Properties Under Three Point Bending Mode

Studies carried out to analyse the cross-linking effect of GA with PVA on dynamic mechanical properties under three point bending mode is presented in this section. Influence of GA cross-linking with increase in its volume fraction on dynamic mechanical properties such as storage modulus, loss modulus, and  $\tan \delta$  is studied. Further, the DMA results are used to investigate the cross-linking effect of GA on activation energy, adhesion factor and shift factor.

##### Storage modulus

Influence of GA cross-linking on storage modulus of PVA under three point bending mode is shown in Figure 4.8. From Figure 4.8, it is clear that the cross-linking enhances storage modulus of PVA significantly with increase in volume fraction of GA. It is evident that the enhancement of storage modulus is significant until 20 % GA and further increase with GA shows a marginal improvement in storage modulus. The variation of storage modulus with respect to temperature can be divided into four

different segments for better understanding. The four regions are (I) hard plastic region, (II) leathery region, (III) rubber region, and (IV) liquid region.

In region I, storage modulus decreases with increase in temperature but the rate of change is marginal compared to other regions. The storage modulus of this region shows similar behaviour to conventional mechanical properties (Section 4.2.1). This is due to the effect of decrease in molecular mobility and increases degree of cross-linking in hard plastic region. This may also be due to interlinking by any means (atoms, electrons or ions) between different long backbone chain in a polymer and it is called cross linking. This enhances the binding chain in three dimensional way such that, the mobility or movement, sliding, breaking of long chain by external condition is prevented even at higher temperature. Cross-linking always enhances the storage modulus by decreasing chain mobility (Cauich *et al.* 1996, Sonker *et al.* 2016). Three point bending is the right technique to identify changes in storage modulus due to changes in cross-linking.

The variations of storage modulus with respect to temperature in region II is similar to the region I. However, the rate at which the storage modulus decreases is significant at higher temperature as compared to the region I in general, for all cases. In region II, it is also observed that the decrease in loss modulus associated with pure PVA is much higher than other GA cross-linked polymer. In region II, it is also observed that the gap between storage modulus curve of pure PVA and 5% GA widens with increases in temperature. This clearly indicates that, storage modulus increases considerably with increase in GA in leathery region.

The variation of storage modulus in region III is similar to the variation in the region I and II. But, the rate at which the storage modulus decreases with respect to increase in temperature is less compared to region I. This is due to the mobility of the molecules in polymer which creates strain hardening effect with the improvement in the storage modulus (Richeton *et al.* 2005). This shows that cross-linking enhances stiffness (storage modulus) of PVA by cross-linking even at higher temperature. PVA contains hydroxyl groups (OH), which have the potential to form hydrogen bonds between



molecules, resulting in a significant change in surface bond strength between PVA and GA matrix.

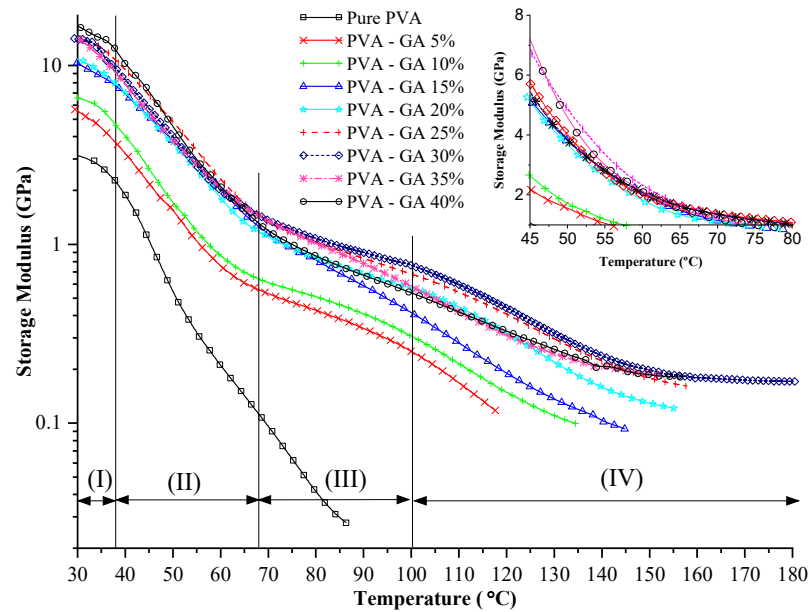


Figure 4.8: Influence of GA volume fraction on storage modulus

From region IV, it is observed that increase in volume fraction of GA increases storage modulus even at the higher temperature and this may be due to the reason that, PVA is self-cross-linking due to the high density of hydroxyl groups located on its side chains. It also clears that cross-linking results bond formation between chains, which decreases chain mobility. The decrease in chain mobility means that chains can't flow past one another upon deformation of the bulk. The chain reaches its mobility limit in smaller deformations, causing the external load to strain the chemical bonds (trying to "bend" them). In case of pure PVA material, the modulus is driven by the difficulty of chains to flow past one another due to entanglements. Cross-links form a more rigid, non-flowing bulk compared to entanglements. This storage modulus can be correlated with flexural strength as discussed in Section 4.2.1. The flexural modulus increases up to 30% GA even at room temperature testing and beyond that volume percentage it decreases significantly.

For the 5% addition of GA the storage modulus increases by 1.6 and 12.33 times at 30°C, and 86 °C respectively compared to pure PVA. There is a considerable amount

of increase in storage modulus at higher temperature. The same trend of improvement is observed for the addition of GA in PVA as shown in Figure 4.2.1 under flexural mode. However, 20% GA addition shows improvement in storage modulus, which increases by 3.29 and 26.17 times at 30°C and 86 °C respectively compared to pure PVA. Further addition of GA above 20% doesn't show much significant improvements in storage modulus at higher temperatures. The results clearly indicates that there is an increase in storage modulus and working temperature due to the cross-linking of GA. Pure PVA fails at less than 90°C, however cross-linking with GA increases the operating temperature of PVA by up to 140°C.

### **Loss modulus**

Similar to the storage modulus curve, loss modulus curves also grouped into four different regions. Figure 4.9 shows that the cross-linking of PVA with GA significantly increases the loss modulus, and the variation with increase in temperature is similar to storage modulus with temperature. Variations in loss modulus with respect to increase in temperature at different regions are observed as follows: region I – no significant variation, region II- significant reduction, region III – reduction is not so significant, and region IV -reduction is significant. This clearly shows that due to the GA cross-linking, energy loss decreases and improves the thermal stability even at higher temperatures. This is due to the presence of glutaraldehyde as a bifunctional molecule and can react either with other PVA chain yielding a polymer network or with available NH<sub>2</sub> group from proteins. This GA reaction most probably involves due to the conjugated addition of protein aminogroups to ethylene double bonds of  $\alpha$ ,  $\beta$ -unsaturated glutaraldehyde oligomers, since the linkages formed between the protein and glutaraldehyde are irreversible and survive extremes of pH and temperature (Araujo *et al.* 1997, Katia *et al.* 2009, Uma *et al.* 2014).

Figure 4.9 shows that the addition of 5 % GA improves loss modulus ( $G''$ ) by 2.83 times and 11.28 times at 30 °C and 86 °C respectively compared to pure PVA. Similarly for the addition of 20% of GA, loss modulus increases by 4.84 times and 24.22 times at 30 °C and 86 °C respectively. This shows that there is an improvement

in modulus by adding GA up to 20% at higher temperature compared to pure PVA. Further variation of  $G''$  value is not so significant with further increase in GA percentage. This improvement in loss modulus may be due to the higher crystallinity content. When PVA is exposed to heat, the supplied energy is used to modify the spatial organization of the chains and to establish stronger hydrogen bonding among hydroxyl groups, which leads to a higher crystallinity content. The physical aging of PVA aqueous solutions may cause network formation because of chain entanglements, especially when the system undergoes heating and post curing consecutively. On the other hand, chemically cross-linked polymer is based on the reaction between the cross-linker and the high amount of hydroxyl groups of PVA (Shadpour and Dinari 2013). Due to this cross-linked polymer exhibits better loss modulus, as energy dissipation or loss is very less.

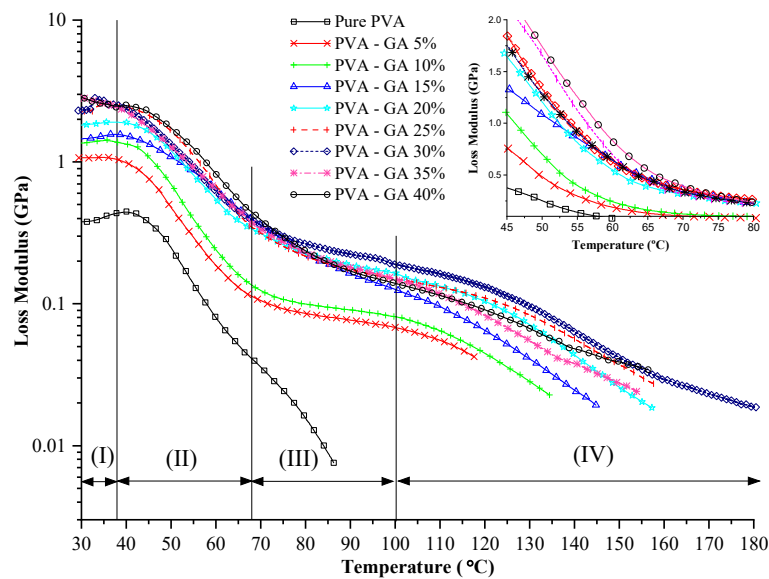


Figure 4.9: Influence of GA volume fraction on loss modulus

### Tan $\delta$

Influence of GA cross-linking on Tan  $\delta$  of PVA is shown in Figure 4.10. From Figure 4.10, it is clear that prediction of  $T_g$  is very difficult as DMA is a sensitive method to determine the  $T_g$ . Incorporation of GA in PVA did not show any distinct effect on  $T_g$ , although the cross-linking of the polymer is effective. The reason is GA effect, which shifts the  $T_g$  to lower temperature and acts in opposite direction to the cross-linking

effect. Increase of the GA up to 15% or more resulted in a more distinct increase in  $T_g$ . A higher GA loading results in an increase of the cross-linking density of the polymer and to higher  $T_g$  due to decreased chain mobility. The ability of the polymer to dissipate energy decreases as a result of the decreased chain mobility. This is reflected in decrease in magnitude of  $\tan \delta$  which is clearly seen in results. Increasing the cross-linking density of the polymer by increasing the GA loading enhances the storage modulus in the rubbery region as observed in Figure 4.5 and Figure 4.8. The variation of  $\tan \delta$  with temperature is shown in Figure 4.10 for various GA-PVA cases.  $\tan \delta$  curves are also divided into four regions as discussed in earlier sections. The peaks of  $\tan \delta$  are observed in the regions II and III for pure PVA and II, III and IV for cross-linked GA material. These regions quantify the way in which a material absorbs and disperses energy. It is also observed that in the region I  $\tan \delta$  increases at a faster rate and reaches a peak at the end the region I. However, pure PVA shows peak with higher value and it clearly shows higher material loss factor of pure PVA. By cross-linking with GA peaks of  $\tan \delta$  shifting to higher temperature. This is due to the movements of the PVA chain segments thus became restrained by these cross-linking points of GA, driving the  $T_g$  to higher values (Uma *et al.* 2014). For example, the sample with the highest content of PVA showed the lowest  $T_g$  and is the most flexible. The magnitude of  $\tan \delta$  peak decrease with increase in GA volume due to the better cross-linking.

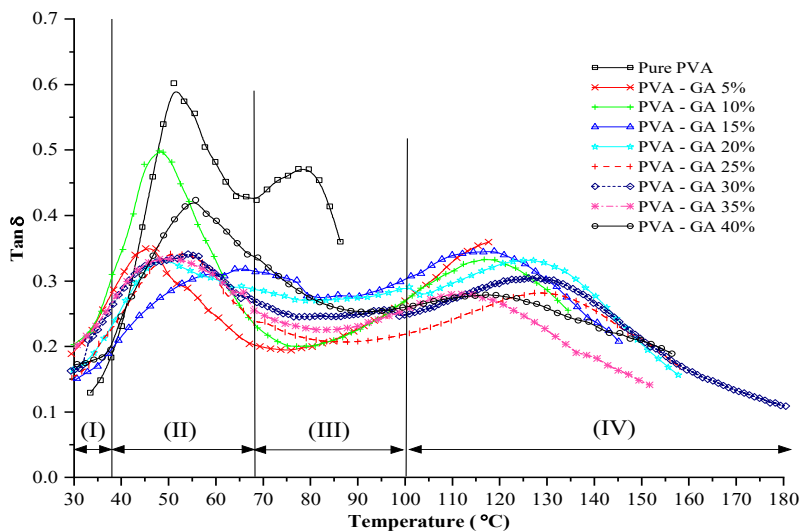


Figure 4.10: Influence of GA cross-linking on  $\tan \delta$

In the region II, significant variation in  $\tan \delta$  is observed in terms of first peak of the curve.  $\tan \delta$  curve is having narrow peak for up to 10% of GA and the curve is having wider peak for the higher values of GA volume fraction. This means that, addition of GA in PVA the area under the curve increases, which indicates the material loss factor decreases as reported in literature (Amaresh *et al.* 2019, Uma *et al.* 2014). The area under the curve represents energy required or stored in the material before its failure; this energy is called modulus of toughness. The second peak of  $\tan \delta$  curve occurs between 120 to 140 °C except for pure PVA case and shows an intimate mix (solubility) between the GA and PVA. From this, it is evident that by adding GA in PVA the stability can be improved even at a higher temperature. In region IV, the material loss factor once again decreases with increase in temperature. The  $\tan \delta$  curve indicates that damping factor can be retained even at higher temperatures. From the  $\tan \delta$  results, it is evident that two peaks corresponding to two glass transition temperature are observed due to the presence of GA in PVA, as reported by Romo *et al.* (2017).

### **Deflection**

The bending strain is applied at the middle of the test sample and the deflection over a range of temperature is studied to analyze the cross-linking effect on bending response. Similar to the earlier cases the deflection - temperature response curve also divided into four regions for the analysis of the mechanical response of the cross-linked polymer. Cross-linking effect on bending with temperature is shown in Figure 4.11. Region I: negligible change in deflection, this is due to hard plastic state at lower temperature. So, very difficult identify the influence of GA in PVA in this region. In region II, as temperature increases the energy is lost from the sample, and leads to its stiffness loss. This behaviour also clearly observed in storage and loss modulus plots refers. Whereas in pure PVA, material becomes soft at higher temperature and further material does not sustain any load. The softening is also observed in storage and loss modulus curves as seen in earlier sections. It is also observed that the increase in deflection associated with pure PVA is much higher than other GA cross-linked polymer. By adding 5% of GA the value of deflection decreases drastically and reaches stagnant level at the end of this region. In region III,

no significant variation in deflection with increase in temperature is observed. However, the deflection reduces significantly with increases in GA volume %. In region IV, the pure PVA does not withstand any further stain and fails to work under dynamic conditions. By adding GA the thermal stability of PVA improved to a greater extent and dynamic operating temperature is also enhanced. It is also observed that there is no much variation in the deflection curve at higher temperature with increases in GA%. This clearly indicates that cross-linking enhances stiffness of PVA even at higher temperature (Richeton *et al.* 2005).

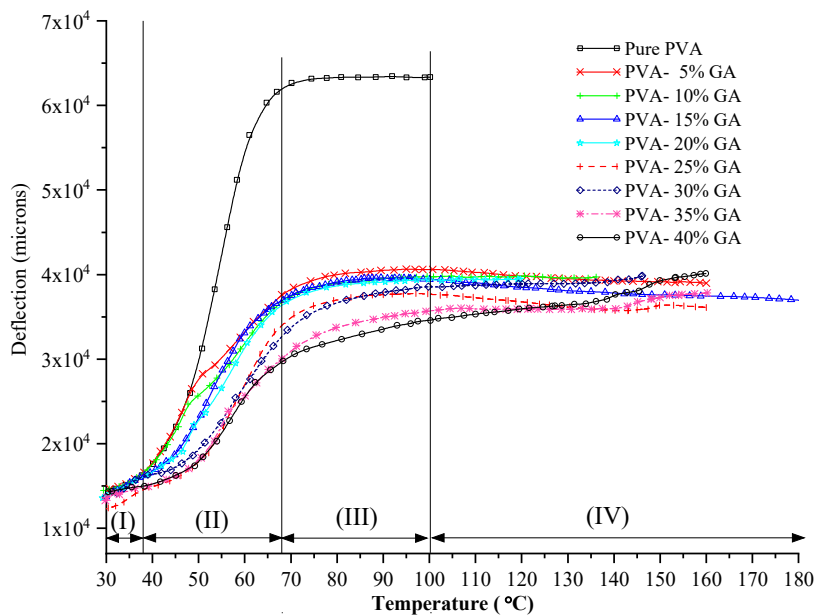


Figure 4.11: Effect of deflection with temperature of extent GA cross-linking

### Cole-Cole plot

Cole-Cole plot is used for analysis of the cross-linking effect on structural behaviour of the matrix material, homogeneity of PVA. Figure 4.12 shows the Cole-Cole plot of different cases of PVA-GA cross-linked polymer. From the results, it can be observed that pure semi-circle in the Cole-Cole plot indicates the homogeneity of the material. But by cross-linking GA in PVA changes the semi-circle into imperfect semi-circular shape which indicates change of material from homogeneity to heterogeneity.

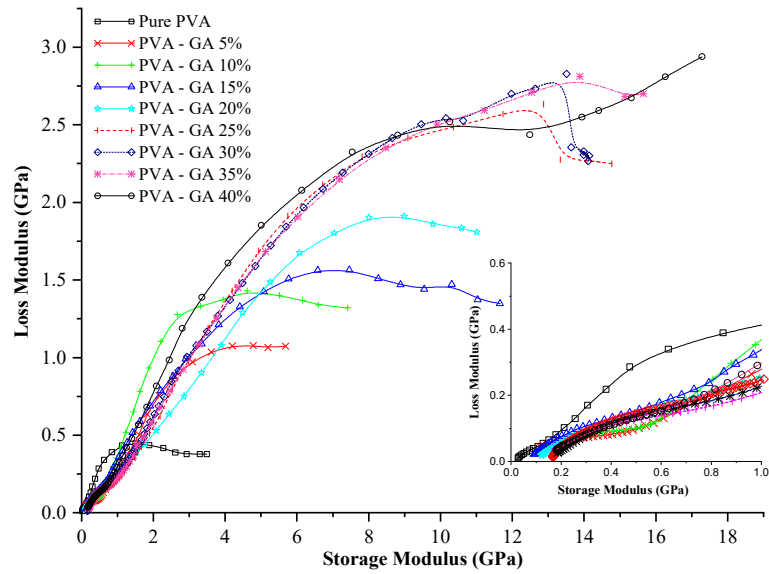


Figure 4.12: Cole-cole plot used to understand the effect of cross-linking of GA in PVA

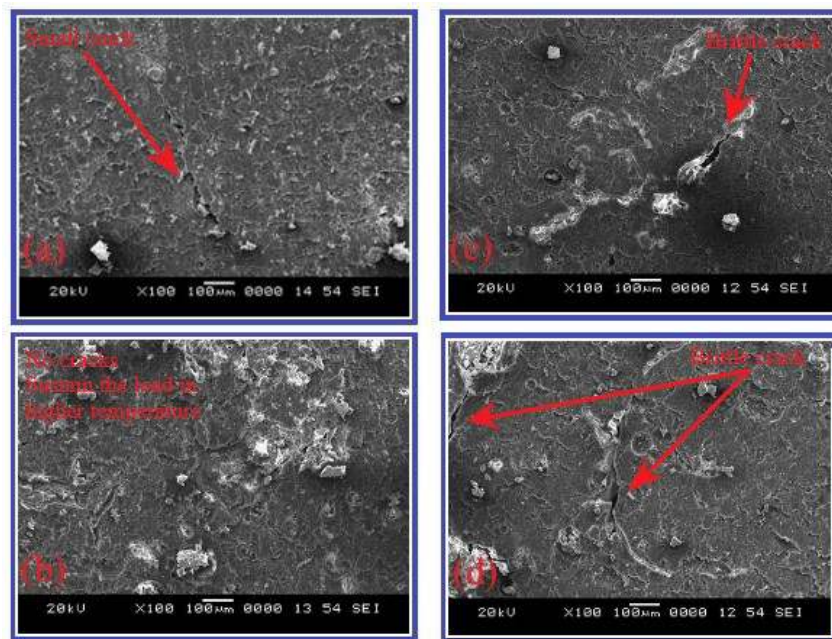


Figure 4.13: SEM image after DMA analysis (a) Pure PVA, (b) 20% GA in PVA (c) 30% GA in PVA and (d) 40% GA in PVA

### Microstructure of dynamic mechanical analyzed samples

Figure 4.13 shows the SEM images of dynamic mechanical analyzed samples. Samples are exposed to dynamic working condition at frequency (1 to 20 Hz) and

temperature (30-180°C). So, it is necessary to understand the morphology after the test. Figure 4.13 a) shows the morphology of PVA samples, small crack is observed and failure occurs within 90°C. Figure 4.13 b) shows morphology of 20% GA in PVA sample and it is observed that samples sustain the load in higher temperature. Figure 4.13 c) shows SEM images of 30% GA in PVA samples and a brittle crack is found after exposed to 180°C. Figure 4.13 d) shows SEM image of 40% GA in PVA sample and brittle nature of failure is seen. From these morphology studies, it is concluded that between 15 to 25% GA in PVA exhibit ductile fracture. If GA increases to more than 25%, the ductile fracture is converted into a brittle fracture.

### Adhesion factor

Adhesion factor ( $A_f$ ) of a cross-linked polymer refers to the molecular mobility of the polymer matrix. Improved adhesion between constituents of polymer reduces the molecular mobility of polymer chain. Adhesion factor also used to study the molecular coupling which can occur at the interface. This also helps to analyze the coupling mechanism which initiates deflection and energy dissipation in the polymer. Adhesion factor can be calculated with the help of DMA results of PVA-GA polymer in comparison with pure PVA. The expression given by Kubat *et al.* (1990) to calculate adhesion factor is as follows.

$$\text{Adhesion factor } (A_f) = \left( \frac{1}{1-V_f} \left( \frac{\tan\delta_c}{\tan\delta_p} \right) \right) - 1 \quad \dots\dots\dots (4.1)$$

where,

$V_f$  is volume fraction of GA in PVA,  $\tan \delta_c$  is  $\tan \delta$  value of cross-linking polymer (GA),  $\tan \delta_p$  is  $\tan \delta$  value of polymer (PVA)

The variation of adhesion factor for various temperatures in shown in Figure 4.14. From Figure 4.14, it is clear that initially the adhesion factor is high and there is a significant variation in adhesion factor up to 35 °C. This can be attributed to the hard-plastic region and absence of molecular mobility and hence adhesion factor is high. But the magnitude of adhesion factor increases with respect to cross-linking percentage for GA more than 25%. As the temperature increases, the adhesion factor



decreases drastically at around 40 °C and reaches a negative value at around 45°C. This is due to temperature and frequency increase continuously upto certain point say 40°C and the bonding between the PVA and GA are weaker due to the viscoelastic behaviour (Xiaohui *et al.* 2017). This is because of the molecular stick-slip phenomena between PVA and GA. Around 50°C the adhesion factor reaches the lowest value, which shows weaker adhesion between GA to PVA. However, the variation of adhesion factor is marginal from 50°C to 80°C and magnitude of adhesion factor increases with an increase in GA cross-linking percentage. The variation of adhesion factor of 40% GA in PVA polymer is much significant and it shows only positive value.

This indicates by adding GA, stiffness of the polymer increases and adhesion between two polymers is also improves (Richeton *et al.* 2005). This in turn, maintains constant bonding factor which can also be seen in Figure 4.8 and Figure 4.9 in region - I. Hence, there is a strong adhesion between GA and PVA polymers at ambient temperature.

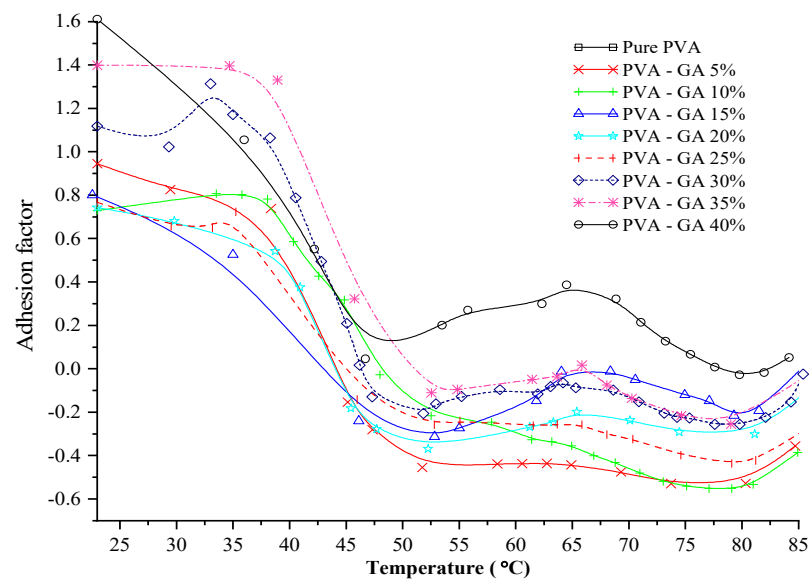


Figure 4.14: Influence of cross-linking percentage of GA on adhesion factor

#### 4.5 Activation Energy

Activation energy is the minimum energy that is required to initiate a chemical reaction. Activation energy analysis is carried out to further understand the thermo-

mechanical response of pure PVA and PVA-GA composites (Fauziyah *et al.* 2017, Rudin and Choi 2013).

$$\text{Activation Energy} = \Delta E = 2.305 \times R \times \frac{d(\log f)}{d\left(\frac{1}{T}\right)} \dots\dots\dots (4.2)$$

where,

R is Universal gas constant 8.134 J/mol-K.,  $d(\log f)$  and  $d\left(\frac{1}{T}\right)$  are the slope from activation energy plot.

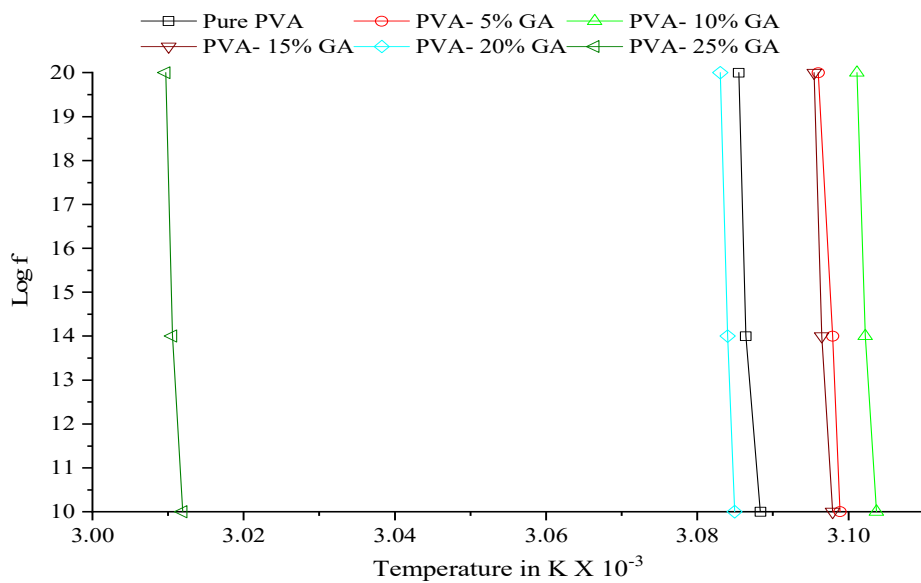


Figure 4.15: Log frequency plot for pure PVA and various percentage of GA

Table 4.2: Slope data from Figure 4.8

% GA	Slope	R <sup>2</sup>	ΔE in KJ/mol
Pure PVA	3297.8	0.9096	63.143
5	3425.0	0.9944	65.579
10	3827.6	0.9666	73.288
15	4002.0	0.9535	76.626
20	5262.3	0.9891	100.76
25	4359.5	0.9875	83.472

By substituting slope data from Table 4.2 (from Figure 4.15) in Equation 4.2, the activation energy is computed and noted in Table 4.2. The pure PVA shows 63.14 kJ/mol (Khalifa *et al.* 2015, Zhan *et al.* 2017) by cross-linking the significant

improvement due to the addition of GA in PVA and maximum activation energy is observed for 20% GA.

#### 4.6 Estimation of the Operating Life of PVA-GA Polymer

The linear relation between  $\log f$  versus  $1/T$ , observed during the activation energy analysis for pure PVA and PVA-GA polymer suggested that these materials exhibit Arrhenius relationship and that the Williams-Landel-Ferry model (Liu *et al.* 2019, Williams *et al.* 1955) given below can be applied to determine the shift factor.

$$\text{Shift factor for temperature } < T_g = aT = \exp \frac{\Delta E}{R} \left[ \frac{1}{T} - \frac{1}{T_r} \right] \dots\dots\dots(4.3)$$

where,

$T$  = Test Temperature in K,  $R$  = Universal Gas Constant in KJ/mol K,  $T_r$  = Room Temperature in K,  $\Delta E$  = Activation energy in kJ/mol

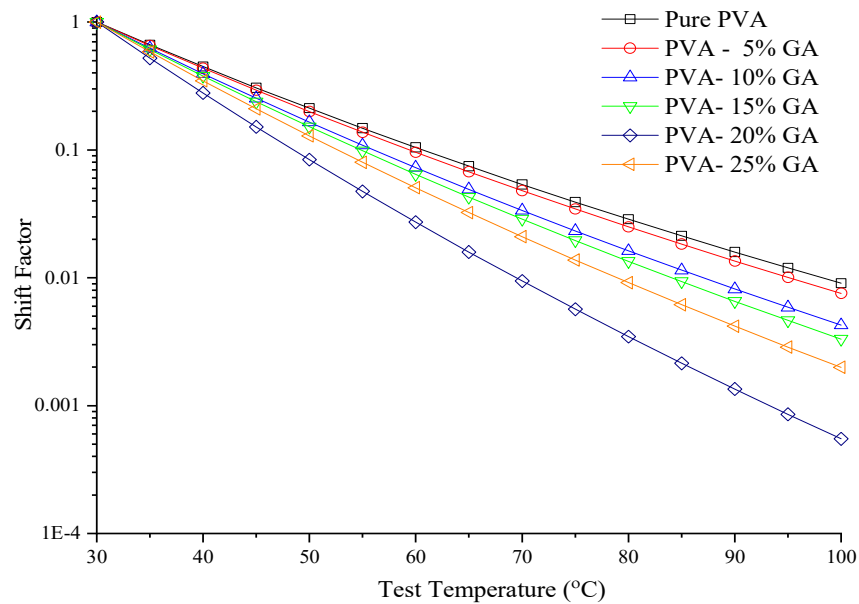


Figure 4.16: Shift factor for time-temperature superposition analysis

Time Temperature Superposition (TTS) is used to determine the accelerated test conditions to estimate the operational life of polymer and its composites since these materials undergo time-dependent decay in properties. For example, if the properties of 20% PVA-GA part after 10 years of operation under ambient condition are required, then accelerated tests can be conducted at 70 °C and 100 °C. The test duration can be computed using Equation 4.3 and the shift factor is taken from Figure

4.16 corresponding to pure PVA and PVA-GA polymer. The computed estimated test duration is 35 days at 70 °C and 2 days at 100 °C respectively. Similarly, the calculation is performed for different GA percentages and results are shown in Figure 4.17. From Figure 4.17, it is evident that cross linked PVA with GA has higher operational life than pure PVA. As the operating temperature is higher the test duration decreases to predict the life of the material. Figure 4.17 shows testing duration with respect to temperature and GA cross-linking.

$$\text{Test Duration} = 365 \alpha T Y \quad \dots\dots\dots(4.4)$$

where,

Test duration in days,  $\alpha T$  is shift factor, Y is required years of operation of the polymer at ambient temperature.

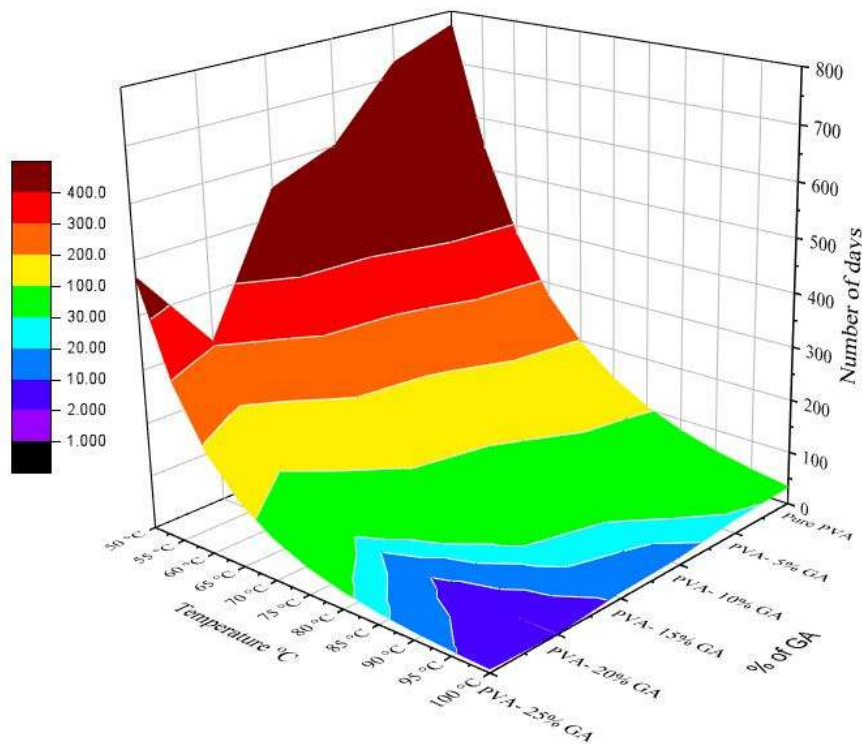


Figure 4.17: Test duration in days for Pure PVA and PVA-GA at different temperatures

#### 4.7 Cross-linking Density ( $M_c$ )

The cross-linking density is determined using dynamic mechanical analysis results (Xia *et al.* 2013, Berean *et al.* 2014). In this case, evaluations are performed under

low deformations (<100 %) and  $M_c$  is calculated from experimental results. The  $M_c$  is cross-link density as the inverse of the molecular volume between cross-links for chemically cross-linked polymers, is given by

$$\frac{M_c}{\rho} = \frac{3RT}{E'} \quad \dots\dots\dots (4.5)$$

where,

$E'$  is the storage modulus in GPa.,  $R$  is universal gas constant.,  $T$  is the temperature in K near to  $T_g$ .

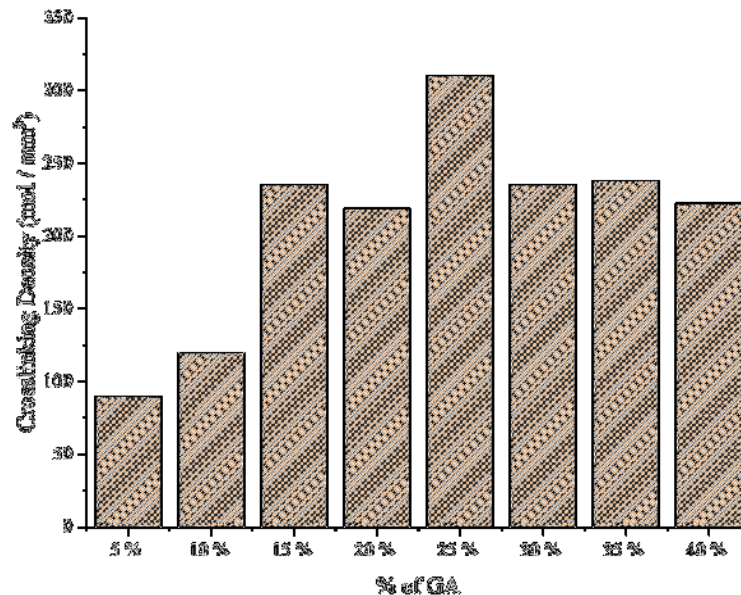


Figure 4.18: Cross-linking density of PVA-GA.

Figure 4.18 shows the cross-linking density of PVA-GA polymer, by adding Glutaraldehyde the cross-linking density increases up to 25% GA beyond that it decreases and maintains stagnant behavior up to 40%. This is also evident from storage modulus, loss modulus, adhesion factor and shift factor results. It is clear that 20 to 25% GA cross-linked polymer is stiffer than other compositions even at higher temperature (Richeton *et al.* 2005). This is directly related to the extent of cross-linking, the higher the degree of cross-linking the greater the storage modulus.

#### 4.8 Effectiveness

The effectiveness of cross-linking on the modulus of the polymer can be represented by a coefficient  $C$  defined as follows (Poathan and Thomas 2003, Poathan *et al.* 2003).

$$C = \frac{\left[ \frac{E'_g}{E'_r} \right]_{PVA \text{ cross-linked GA}}}{\left[ \frac{E'_g}{E'_r} \right]_{PVA}} \dots\dots\dots (4.6)$$

where,

$E'_g$  and  $E'_r$  are the storage modulus values in the glassy and rubbery region respectively.

Higher the value of constant C, lower the effectiveness of the glutaraldehyde cross-linking. The value of  $E'_g$  and  $E'_r$  is used at 30°C and 80°C in case of pure PVA, similarly the value  $E'_g$  is used at 30 °C and  $E'_r$  is used at 70, 80 and 90°C of PVA-GA for better understanding of effectiveness. The values obtained for the different cases at frequency 10 Hz are given in Table 4.3. In this case, the lowest value is obtained at 15% of GA at 70°C, less than 20% GA at 80 °C. It is important to note that the modulus in the glassy state is determined primarily by the strength of the intermolecular forces and the way the polymer chain is packed.

Table 4.3: Effectiveness of cross-linking agent

% GA	C at 70 °C	C at 80 °C	C at 90 °C
5	0.332	0.176	0.081
10	0.339	0.177	0.079
15	0.296	0.178	0.089
20	0.316	0.178	0.081
25	0.346	0.200	0.086
30	0.331	0.183	0.077
35	0.326	0.192	0.088
40	0.428	0.256	0.121

#### 4.9 Hardness

For hardness test, the shore D tester is used and measurements are taken on flat surface of specimen placed over a rigid, flat surface. Five points are marked with a 6 mm distance apart between each other and from lateral margins of the test specimen. Average of these 5 readings is reported as the hardness value. Readings are taken after stable contact over the specimen. Shore D hardness of PVA and GA cross-linked

PVA are shown in Table 4.4. It is found that the hardness increase with the GA cross-linking content in the PVA polymer. Up to 10% GA increase the hardness from 59.8 to 69.6 drastically and further increase in GA it has raised to up to 75.2. Further, the hardness values varied marginally with GA cross-linking.

Table 4.4: Shore D hardness for a various percentage of GA

% GA	Trial 1	Trial 2	Trial 3	Trial 4	Trial 5	Average
Pure PVA	60	59	61	59	60	59.8
5	69	68	70	71	69	69.4
10	71	70	69	70	68	69.6
15	74	72	75	74	75	74.0
20	73	76	76	75	74	74.8
25	75	74	75	76	74	74.8
30	76	75	76	75	74	75.2
35	75	76	75	74	75	75.0
40	74	75	76	74	75	74.8

#### 4.10 Summary and Conclusion

The mechanical and dynamic mechanical properties of PVA cross-linking with GA are studied and concluded that thermal and mechanical stability of the PVA improved drastically.

- The tensile strength of pure PVA is 4.98 MPa by cross-linking with GA the tensile strength enhanced and found to be highest at 20% GA, which is 14.96 MPa. Similarly, the tensile strain of pure PVA is 0.0071 by adding GA the tensile strain enhanced and 20% cross-linking exhibits higher strain of 0.0253 shown in Table 4.5.
- The flexural strength of pure PVA is 10 MPa by adding GA the strength increases significantly and found to be highest at 20% of GA. Further adding GA marginal variations are observed up to 25%.
- The storage and loss modulus of PVA enhanced with GA cross-linking under tensile mode. But a marginal improvement in dynamic properties at a higher temperature.
- Storage modulus increases marginally with the addition of GA up to 20% at room temperature and also higher temperature. But the influence of cross-

linking is observed significantly at the higher temperature. The pure PVA fails at 85°C with the addition GA the thermal stability improved drastically and operating temperature enhanced up to 150°C.

- The Loss modulus also improved by adding GA even at a higher temperature.
- Shift factor and Activation Energy are determined to estimate the life cycle of PVA. The cross-linked polymer of all the GA cases shows enhanced behaviour and hence the strength is found to be dependent on the percentage of the cross-linking. Equations are proposed on the Williams-Landel-ferry model, is used to predict the testing duration for different cross-linked polymers at different working temperature.
- Adhesion factor, effectiveness index and cross-linking density are improved favourably by GA addition.
- The influence of cross-linking is found to be significant in three-point bending mode as compared tensile mode under dynamic mechanical properties.

Table 4.5 Summary of mechanical property of PVA for various percentage of GA

% of GA	Tensile		Flexural	
	Strain	Stress MPa	Strain	Stress MPa
PVA	0.0071	4.98	0.0252	10.012
PVA-GA 5%	0.0119	7.70	0.0276	12.516
PVA-GA 10%	0.0168	10.04	0.0519	17.233
PVA-GA 15%	0.0198	12.72	0.0424	20.189
PVA-GA 20%	<b>0.0253</b>	<b>14.96</b>	0.0485	26.164
PVA-GA 25%	0.0142	9.08	<b>0.0526</b>	<b>26.730</b>
PVA-GA 30%	0.0161	12.86	0.0340	26.918
PVA-GA 35%	0.0158	9.34	0.0229	21.447
PVA-GA 40%	0.0098	8.44	0.0210	17.799

On the whole, it observed that PVA cross-linked with 20% GA as shown improvement in tensile and flexural properties. But thermo-mechanical properties like storage modulus, loss modulus and  $\tan \delta$  improved significantly up to 20% GA cross-linking. Further, additions of GA in PVA marginal variations in thermo-mechanical properties are observed. Adhesion factor, cross-linking density, activation energy and



effectiveness are also improved with GA cross-linking. Therefore, PVA cross-linked with 20% GA optimized and carried to prepare the composite material.

## CHAPTER-5

### CHARACTERIZATION OF SISAL FABRICS

The exhaustive literature survey clearly describes the need of using advances in textile fabric engineering in composite preparation. Physical properties of the fabric influences mechanical behavior of the fabric and in turn mechanical properties of fabric reinforced composites. So, it is necessary to study the important textile physical properties such as gram per unit area and woven pattern.

This chapter analyses the influence of various physical properties of a fabric on mechanical properties of a textile fabric. Three types of woven fabrics are prepared using hand-weaving process and considered as the reinforcement. Two plain woven (Plain 1 and Plain 2) are prepared with different grams per unit area to analyze the effect of GSM on mechanical properties of the fabric. One WR woven pattern is also prepared by keeping the same GSM and compared with P 2 woven pattern fabric to analyze the effect of nature of woven pattern on mechanical properties of the fabric.. Initially, different physical properties of the fabrics are analyzed. Then the different types of the fabrics are investigated for their tensile, flexural, bursting, stretch and recovery, and tearing characteristics. For comparing purposes, the three sisal woven fabrics will be denoted as Plain 1 (**P1**), Plain 2 (**P2**), and Weft Rib (**WR**).

#### 5.1 Sisal Yarn Characterization

##### Sisal fiber

The cross sections of single sisal fiber are analyzed using SEM analyzed and shown in Figure 5.1 (a). The chemical composition of extracted sisal fiber which is available in Karnataka, India has 62-76% cellulose, 23-36% hemicellulose, 6-9% lignin, 0.8-1.3% wax and 5-10% moisture. The average diameters of the sisal fiber were found to be

varying from 100 to 350 micrometers shows in Figure 5.1 (a). The sisal fiber available in various parts of India is compared from the literatures. *Khan et al.* (2012) reported that sisal fiber which is available in Bhopal has 65-73% cellulose, 9-11% hemicelluloses, 5-6% lignin, 0.9-1.2% wax and 9-11% moisture. Sreekumar *et al.* (2009) studied the southern part of Indian sisal fiber which is available in Kerala region and found that 100-300 $\mu$ m diameter 65-78% cellulose, 10-14% hemicellulose, 9.9% Lignin, 2% Waxes. Figure 5.1 (b) shows the structure of sisal fiber and its details.

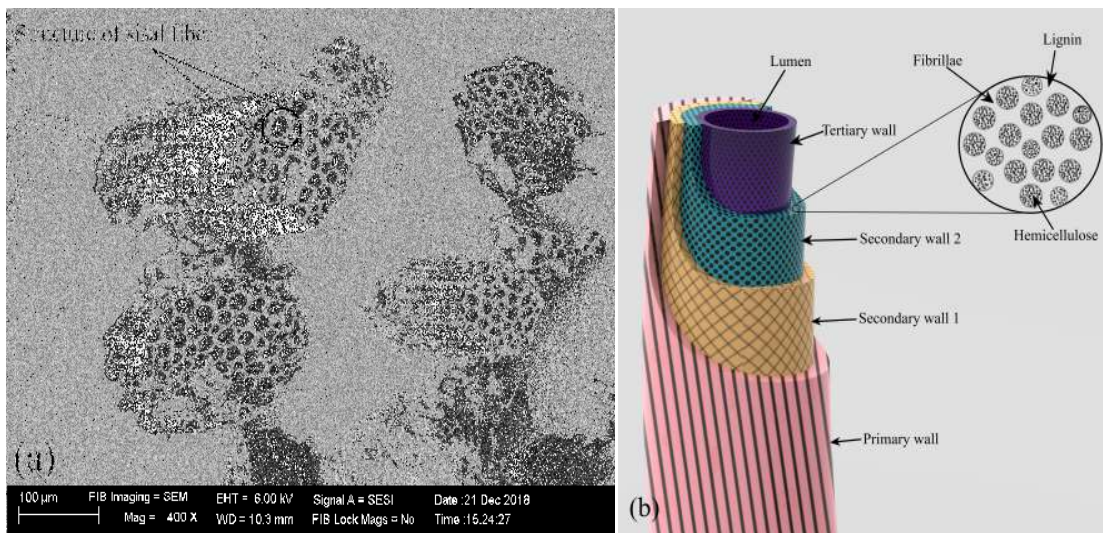


Figure 5.1: (a) Cross section of sisal fibers (b) Structure of sisal fiber

### Twist of yarn

Twist of yarn affects many factors such as water absorption, abrasion resistance, pilling resistance, feeling effect (hard or soft) and fabric strength. However, the prepared sisal fabrics are studied to find the effect of nature of reinforcement in composites. Right-handed angle twists are observed in the prepared fabrics. It is necessary to identify the type of twist of the yarn as it influences fabrics properties as well as composite properties and S type twist is found in all three sisal fabrics. The average twists (one full spiral threads) per meter length of yarns vary from 425 to 645.

### **Yarn crimp**

Yarn crimp is the waviness of the yarn in the fabric due to the interlacing of warp and weft yarns. It is also known that yarn crimp in a woven fabric is an important parameter that affects most of its physical properties, which include the thickness and the weight of fabric (Sule 2012).

### **Yarn count**

Yarn size or yarn linear density or yarn count has a close relation with the fabric weight. For this reason, warp and weft yarn linear density of all three fabrics are determined and shown in Table 5.1. P1 is having fabric yarn linear density of 80.1 tex in warp and 85.1 tex in weft direction and P2 is having 182.3 tex in warp and 166.8 tex in weft direction. Similarly, WR fabric is having 65.3 tex in warp direction and 182.9 tex in weft direction.

## **5.2 Basic Physical Properties of Sisal Fabric**

### **Fabric density**

Fabric density is the number of yarns along warp and weft directions of the fabric. The yarn spacing is indicated by fabric density which also relates to fabric compactness. The typical properties between two plain fabrics are related to their fiber density in fabric and weight. The metric system is used to measure the number of yarns that are in centimeter (mm). Table 5.1 shows the different densities for both plain fabrics. i.e., P1 having 18 warps/1 cm and 20 wefts/1 cm and P2 having 12 warps/1 cm and 12 wefts/1 cm. Similarly, the WR is having 22 warps/1 cm and 11 wefts/1 cm.

### **Weight and thickness of fabric**

Because of some limitations in the weaving technique, it is difficult to process the natural sisal fiber. It is also quite challenging to maintain the same grams per area. But the weight of the fabric influences many of the physical and mechanical properties of the fabric and its composites. So it is very important to measure the weight of the fabrics. The supplier specifications for the selected fabrics are P1 fabric should have 160 g/m<sup>2</sup>

(GSM) and P2 and WR fabric have similar aerial density or fabric weight of 300 g/m<sup>2</sup>. The experimental measurement of fabric density shows that P1 fabric had a lighter weight (161.02 g/m<sup>2</sup>) than P2 (296.6 g/m<sup>2</sup>) and WR fabric (300.45 g/m<sup>2</sup>) noted in Table 5.1.

The results from fabric measurement give an idea about how P1 and P2 fabrics are designed to get the same woven structure with different GSM. Also, P2 and WR fabrics gives an idea how mechanical properties vary with woven structure. The properties are also influenced by number of warp and weft yarns when it is designed mechanically with equal number of yarns in warp and weft direction. The total weight of warp and weft yarn are given in Table 5.2 for the three different fabrics considered. Influence of number of yarns, crimp, and yarn linear density on mechanical properties are discussed in Section 5.3.

Table 5.1: Physical properties of three fabrics

Sl. No	Woven type	Fabric thickness in mm	GSM	Cover factor (%)		Yarn count in Tex		Yarn crimp (%)		Number of yarns per cm	
				Warp (P)	Weft (T)	Warp (P)	Weft (T)	Warp (P)	Weft (T)	Warp (P)	Weft (T)
1	<b>Plain-1</b>	0.42	161.02 ±0.17	79.18 ±0.46	91.78 ±0.69	80.1 ±0.56	85.1 ±1.67	7.23 ±0.26	9.54 ±1.12	18 ±0.95	20 ±1.06
2	<b>Plain-2</b>	0.73	296.60 ±1.75	74.28 ±2.80	80.24 ±3.75	182.3 ±4.43	166.8 ±8.41	6.53 ±0.97	11.06 ±1.09	12 ±0.74	12 ±0.67
3	<b>Weft rib</b>	0.72	300.45 ±1.67	82.12 ±3.09	53.01 ±3.06	65.3 ±2.51	182.9 ±4.04	10.05 ±0.94	5.96 ±1.22	22 ±1.03	11 ±1.05

Note: Standard deviations are in (±) for 10 trials.

Table 5.2: Fabrics weight in warp and weft directions

Fabric types	Direction of yarn	Plain 1	Plain 2	Weft Rib
Weight (g/m <sup>2</sup> )	Warp	70.57	142.88	61.6
	Weft	90.45	153.72	238.85
Fabric weight (g/m <sup>2</sup> )		161.02	296.6	300.45

The fault/defect observation in the fabric has revealed that there is no missing pick found along the fabric length for at least 5 m in all the three fabrics. Missing or out-of-sequence yarn in the woven fabric refers to the disappeared pick. In the current study, three fabrics are tested and observed that they are free from loom's fault (Misnon *et al.* 2015). Hence, the prepared fabrics are suitable in loom and exhibited better-quality. Because of

variations in cross-sectional dimensions of prepared fabrics, the yarns are not homogenous (having a lot of thick and thin yarns) in the fabrics.

To analyze the effect of woven structure WR and P2 fabrics are considered. The yarn size is determined for all three fabrics and the average of the trials is considered. Irregularities and inconsistencies with the yarn are expected in the fabric as the fabrics have been derived from the natural fibers. The yarns are produced in the large production line known as 'spin'. It is known that there are lots of drawing steps involved while measuring the yarn size. Because of irregularities of natural fibers, it is challenging to get the desired size of the yarn even if perfect drawing is done (Mishra *et al.* 2003).

The thickness of the fabrics is measured and tabulated in Table 5.1 The average fabric thickness for P1, P2, and WR fabrics are 0.42 mm, 0.73 mm, and 0.72 mm, respectively.

### **5.3 Mechanical Characterization of Fabrics**

#### **Tensile strength**

The load-elongation curve for the different woven sisal fabrics under tensile loading are depicted in Figure 5.2 (a). The curve is divided into three phases for the better study of test results. Initial stage of the curve represents the gradual slope and at the end of this stage fabric reaches settlement with linear increase until it reaches the third stage. During the first stage of the curve, elongation increases drastically with a moderate load. This could be attributed to decrimping and crimping interchange and internal crossover between warp and weft yarns of the fabric. The sisal fabric is extended in principal direction and the straightening of crimped yarns is observed in the direction of the applied force. The yarns become less flattened and appear like a compacted into more circular cross-section. The pressure in the yarns along the direction of force is continuously interchanging between two yarns. Consequently this results in the increase in crimp of the yarn along the normal to the direction of force. Further, yarns in the fabric continuously become round and less flattened. Fibre and yarn elongation is occurred at this stage. However, elongation is minimal as compared to the first stage. This little elongation of the yarn is due to the twist, the fiber in tighter and stronger yarn build up

pressure and resist tensile force. At this stage, load carrying capacity is found to be maximum and break down of yarn takes place.

From Figure 5.2 (b) it is noticed that initial portion of curves are raised due to the decrimping and crimping interchange along warp and weft direction. However, this initial slope in the load- extension diagram is due to higher crimp percentage in weft direction (9.54) and lower crimp percentage in warp direction (7.23). This also may be due to the manufacturing effect, as always weft properties are better than warp directions propertiese (Mishra *et al.* 2003). After the decrimping and crimping state at initial stage, the curve rose steeply until the peak (ultimate point) is reached.

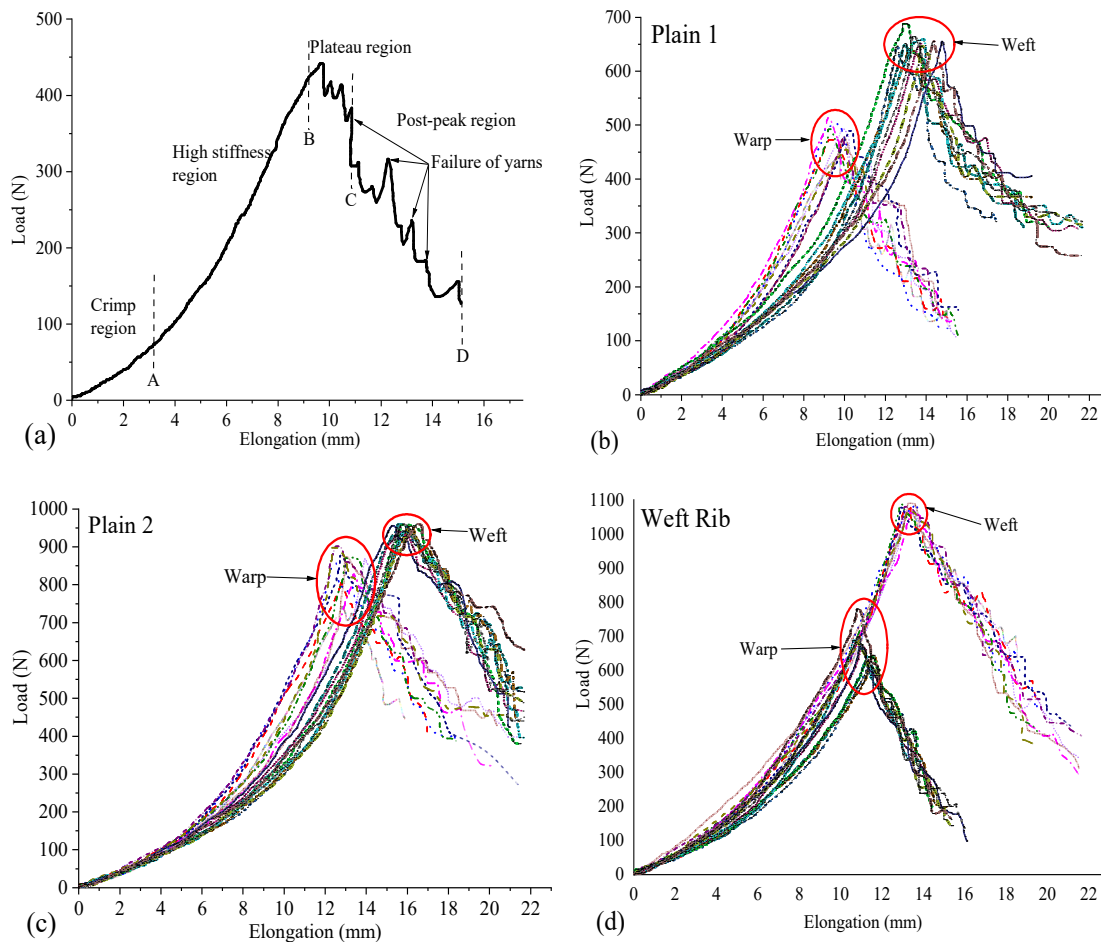


Figure 5.2: (a) Schematic load- elongation plot for fabric and its phases, (b) P 1, (c) P 2 and (d) WR fabrics load- elongation plot for in weft and warp directions

P1 type of fabric fails at 481.2 N for warp loading and 655.9 N for weft loading as seen in Figure 5.1 (b). This indicates that even though same numbers of yarns are present in warp and weft, the weft exhibited better properties (1.3 times) than warp directions. This increase in the ultimate tensile strength depends on yarns linear density which is more in weft (85.1) as compared to warp (80.1). Therefore, most of the weft specimens had stretched to their settlement state at approximately 12 to 14 mm elongation while for warp side of the fabric are decreased to about 9 to 10 mm.



Figure 5.3: The fractured fabrics after tensile test, (a) P1, (b) Magnified fracture area of P2, (c) Magnified fracture area of P2, and (d) Magnified fracture area of WR.

Table 5.3: Tensile properties of fabrics

Type of fabric	Directions	Ultimate Point		Breaking Point		Ultimate Point		Tensile Modulus (N/mm <sup>2</sup> )
		Load (N)	Elongation (mm)	Load (N)	Elongation (mm)	Stress (N/mm <sup>2</sup> )	Strain	
Plain 1	Warp	481.2 ±21.5	9.67±0.39	159.72±83.5	14.74±1.28	22.91±1.02	0.048±0.0019	474.743
	Weft	655.9 ±13.1	13.51±0.69	322.53±39.0	20.24±1.55	31.23±0.62	0.068±0.0034	463.237
Plain 2	Warp	869.2 ±31.0	12.88±0.50	405.80±79.3	19.14±2.02	23.81±0.85	0.064±0.0025	370.233
	Weft	952.8 ±8.0	15.85±0.35	471.60±72.8	21.55±0.21	26.10±0.21	0.079±0.0018	329.419
Weft Rib	Warp	672.0±48.2	11.02±0.30	223.40±98.4	14.77±0.96	18.66±1.34	0.055±0.0015	339.405
	Weft	1074.5±10.0	13.21±0.18	421.81±103.3	20.40±1.21	29.84±0.28	0.066±0.0009	451.716

\*Note: (±) standard deviation for ten tensile samples



Both P2 and WR are having almost same GSM, but ultimate tensile load found to be highest in WR weft direction which is 1.6 times to that of warp direction. This is due the two weft yarns are interlocked over warp yarns (yarn density) in WR fabric which enhances the tensile strength. This demonstrates that woven physical properties having significant impact on tensile properties (Maria *et al.* 2013). Figure 5.3 shows direction of propagation of yarns fracture in P1, P2 and WR fabrics under tensile loading.

The ultimate load for P2 type woven fabric is 869.2 N and 952.8 N in warp and weft directions respectively. This also indicates that marginal variation in the maximum (ultimate) tensile load for P2 fabric in warp and weft as compared to P1 fabric. The yarn linear density is 166.8 in weft which is lesser than warp. However, the ultimate tensile load is high in weft direction as compared to warp due to the textile fabrication. Both P1 and P2 type fabrics are of same weaving structure, but their gram per square meter are 161.02 and 296.6 respectively. From the tensile results, it is clear that the load withstanding capacity of the fabric increases proportionally with weight of the fabric. However, the tensile modulus at ultimate point is decreased. The elongation/strain along warp is very less as compared to both the plain woven due to the effect of twist of yarns per meter length.

Table 5.4: ANOVA results for sisal fabrics for ultimate point elongation

Fabric		df	SS	MS	F	Sig.	Remarks
P1	Regression	5	75.12	15.02			
	Residual	14	4.45	0.32	47.22	0.00	Significant
	Total	19	79.57				
P2	Regression	5	43.74	8.75			
	Residual	14	3.71	0.26	33.04	0.00	Significant
	Total	19	47.45				
Weft rib	Regression	5	24.29	4.86			
	Residual	14	0.97	0.07	70.17	0.00	Significant
	Total	19	25.26				

\* df – Degrees of freedom, SS – Sum of squares, MS – Mean square, and Sig. – Significant level.

The experimental results (Table 5.3) obtained are not sufficient to determine the significance of output results like tensile ultimate load and elongation in both warp and

weft directions with the input variable (Table 5.1) of the fabric cannot be controlled accurately. The inferential statistical analysis is required to making decisions concerning a Summary only on sample data to test considerable variations among the mean values. Microsoft Excel is used to determine the analysis of variance (ANOVA) to study the significance variations between warp and weft directions for all types of fabrics. The confidence levels for each fabric are assumed as 95% and hypothesis are assumed based on P-value. The warp and weft direction have exhibited significant difference because the P-value is equal to 0.000 in all types of fabrics. If P-value is more than 0.05, results are insignificant, which means the difference is ‘insignificant’ or ‘not significant’. From Table 5.4, it clearly is seen that elongation of all three fabrics has a significant effect in both warp and weft directions. Similarly, Table 5.5 shows that ultimate point load having significant effect in both warp and weft directions.

Table 5.5: ANOVA results for sisal fabrics for ultimate point load

Fabric		df	SS	MS	F	Sig.	Remarks
P1	Regression	5	152311.51	30462.30			
	Residual	14	6110.51	436.46	69.79	0.00	Significant
	Total	19	158422.01				
P2	Regression	5	36930.76	7386.15			
	Residual	14	7147.68	510.55	14.47	0.00	Significant
	Total	19	44078.44				
Weft rib	Regression	5	812338.49	162467.70			
	Residual	14	19457.74	1389.84	116.90	0.00	Significant
	Total	19	831796.23				

### Stiffness strength

Stiffness or bending strength of the fabrics are measured according to ASTM D 1388-96. The flexural rigidity of sisal woven fabric is measured to analyze the effect of self-weight upon overhanging. P1 type of fabric exhibited a flexural rigidity of 2105.1 mg-cm along warp and 545.3 mg-cm along weft direction. It is due to the effect of greater yarn linear density (yarn strength) in weft direction (85.1) compared to warp direction. Higher cover factor along weft direction compared to warp direction which leads to increase in weight of the fabric in weft direction (Table 5.2) and resulted in less flexural strength due

to overhanging (self-weight) as seen in Table 5.6. P2 type of plain woven fabric also exhibited flexural behavior similar to P1 type of plain woven fabric. However, flexural strength of WR fabric is less due to less yarn count in warp direction (65.3).

### **Bursting strength**

Bursting strength is the amount of pressure required to rupture a fabric and bursting strength of different fabrics analyzed are given in Table 5.6. As the bursting strength depends on the cover factor of the fabrics, it is in turn linked to yarn count and yarn density of the fabric. The reinforcement fabrics materials should have good cover factor which permits resin to penetrate into it. However, these bursting properties are linked to tensile and flexural strength, high and low-velocity impacts strengths. So, it is necessary to characterize the fabric materials using bursting tester. Both P1 and P2 fabrics are of plain woven structure but differ by GSM. However, the bursting strength of P1 and P2 are 1.36 MPa and 2.47 MPa respectively. This variation in bursting strength might be due to the fabric weight (P1-161.02 g/m<sup>2</sup> and P2-300.45 g/m<sup>2</sup>), yarn count (P1-80.1 tex and P2-182.3 tex ) and cover factor (P1-79.18% and P2-74.28%). P1 type of fabric is thin (yarn count) as compared to P2 fabric and most likely to break at thin places as the fabric possess both thin and thick portions across it. It is noticed that fracture has happened at thin yarn area which is having less yarn coverage area in the fabrics. However, it can be concluded that bursting strength mainly depends on the strength of the yarn and the cover factor.

Table 5.6: Flexural strength, stretch and growth of fabrics

Properties	Directions	Plain 1	Plain 2	Weft Rib
Stiffness strength (mg-cm)	Warp	2105.1	2307	1146.7
	Weft	545.3	771	456.5
Turns per meter	Warp	584	433	436
	Weft	645	425	528
Bursting strength (MPa)	--	1.36	2.47	2.43
Fabric stretch (%)	Warp	0.40	0.8	0.27
	Weft	3.5	1.9	2.6
Fabric growth (%)	Warp	0.17	0.21	0.09
	Weft	1.4	0.9	0.55

Similarly, P2 and WR types of woven fabrics have almost same GSM and cover factor with variation in number of yarn in warp and weft directions (woven structure). The bursting strength of P2 and WR are 2.47 MPa and 2.43 MPa respectively. The variations in bursting strength of P2 and WR fabrics are found to be marginal. However, in case of WR fabric as the number of yarns is less in warp compared to weft, the failure is initiated by warp yarns and resulted in fibre pull-out from the fabrics. However, a pair of yarn interlaced in WR withstands better when the force is applied vertically during bursting strength tests (Hakan *et al.* 2013). P2 and WR fabrics have higher bursting strengths than P1. This is because of the fact that the average float length, fabric weight and cover factor of these weaves are higher than those of P1 and also count of yarns are higher in P2 and WR woven structures.

#### **Fabric stretch and recovery**

Composite structures may be subjected to constant load for a long period during their service. As the sisal fabrics are used as a reinforcement to prepare composites it is necessary to analyze the fabric stretch and recovery (growth) behavior. Results shown in Table 5.6 clearly indicate that fabric stretch percentage is more along the weft direction compared to the warp direction for all the three different types of fabric analyzed. This might be due to the higher crimp percentage associated with weft direction compared to warp direction in plain woven. In case of P1 type fabric 40% fabric growth is observed in weft direction and 42% in warp direction. For P2 fabric, growths along weft and warp direction are 47% and 26% respectively. Due to the higher crimp associated with P2 fabric the growth is more for P2 fabric in weft direction. P2 and WR fabrics are having same GSM, but WR weft direction showed lowest fabric growth due to woven structure. Therefore, even though crimp percentage plays a major role in fabric stretch and growth, it varies according to GSM and woven structure of a fabric.

## Tearing characterization

### Elmendorf tearing properties

Table 5.7 shows the impact tearing strength of all three fabrics in warp and weft directions. The average impact tearing value of P1 fabric indicates that warp direction exhibit 1.18 times higher resistance than the weft direction. This is due to the higher yarn count of weft yarn along with the higher cover factor. In case of P2 fabric tearing impact strength along warp direction is 1.13 times higher than that of the weft direction. P2 fabric exhibit better tearing strength than P1 fabric, this could be due to the influence of yarn count. The number of yarns is less in P2 (12) as compared to P1 (18). However, the yarn count is higher (182.3 tex) for P2 fabric compared to P1 fabric (85.1 tex). In case of WR fabric, tearing impact strength along warp direction is 1.93 times higher than that of the weft direction. This can be attributed to higher yarn count and cover factor associated with warp direction.

### Analysis of variance (ANOVA)

It is very difficult to control the input variable and its effect on the fabric properties due to many limitations. ANOVA analysis is preformed to study the statistically significant parameters that influence Elmendorf tearing properties.

Table 5.7: Impact tearing strength (gram force) of three fabrics

Woven type	Plain 1		Plain 2		Weft rib	
Direction	Warp (P)	Weft (T)	Warp (P)	Weft (T)	Warp (P)	Weft (T)
Trial 1	6656	7168	9728	8704	11392	5888
Trial 2	7552	5376	9600	7936	12032	6144
Trial 3	7296	6272	10112	8320	10368	4992
Trial 4	7424	6528	8704	7808	12288	5760
Trial 5	7936	5888	9472	9216	11008	6784
Average	7372.8	6246.4	9523.2	8396.8	11417.6	5913.6
Standard deviation	466.81	673.67	516.78	576.71	775.43	648.90

The P-value (probability of significance) is then determined from the F-value. The hypothesis assumed as follows: if P-value is equal to or smaller than 0.05 (confidence level 95%) then it suggests that the contribution of the factor is significant. Table 5.8

shows the variance of impact tearing testing between each group of fabric and Table 5.9 shows the significance test of fabric between the groups. The P-value of the present analysis is less than 0.05 which indicates that the data is significant. This also indicates that nature of fabric (P1, P2 and WR) and loading direction (warp and weft) influences impact tearing strength significantly.

Table 5.8: Variance for impact testing of fabric

<i>Groups</i>	<i>Count</i>	<i>Sum</i>	<i>Average</i>	<i>Variance</i>
Warp (P1)	5	36864	7372.8	217907.2
Weft (P1)	5	31232	6246.4	453836.8
Warp (P2)	5	47616	9523.2	267059.2
Weft (P2)	5	41984	8396.8	332595.2
Warp (WR)	5	57088	11417.6	601292.8
Weft (WR)	5	29568	5913.6	421068.8

Table 5.9: ANOVA for impact testing of fabric

Source of Variation	SS	df	MS	F	P-value	F crit
Between Groups	1.09E+08	5	21852870	57.16257	1.52E-12	3.89507
Within Groups	9175040	24	38229s3.3			
Total	1.18E+08	29				

### Single rip tear properties

The single rip tearing results of the three different woven fabrics in warp and weft directions are shown from Figure 5.5 to Figure 5.10. Figure 5.5 shows the tearing load carrying capacity of P1 fabric in weft direction at various crosshead speeds of 50, 100, 150 and 200 mm/min. The single tear test described in Figure 5.4 shows each cross-section of yarn is subjected to progressively increasing tension. The yarn fails individually in tension and for this reason, the fabric tear strength is much lower than its breaking strength where all the yarns fail at the same time. The mechanism of tearing in woven structures generally includes four main stages: in first stage the stretching and slippage of yarns occurs closest to the tip of the crack; In second stage, the crowding of these yarns on the edges of a Del Zone occurs. In third stage, the stretching and

alignment/jamming of these yarns occurs, and in last stage, final rupture of the outer transverse yarn takes place as shown in Figure 5.5. These stages occur cyclically until the tearing direction reaches the endpoint of loading. A typical tear test load- displacement plot has a saw-tooth shape as shown in Figures 5.5. The peaks in the load-displacement curve correspond to failure of each successive transverse yarn as the tearing progresses, and the same trend continued till the endpoint of loading i.e., 180 mm. The cross-yarn fails one by one, twice or even in a group of multiple yarns depending on the woven physical properties of the fabric such as yarn strength, elongation of yarn, cover factor, crimp, and woven pattern.

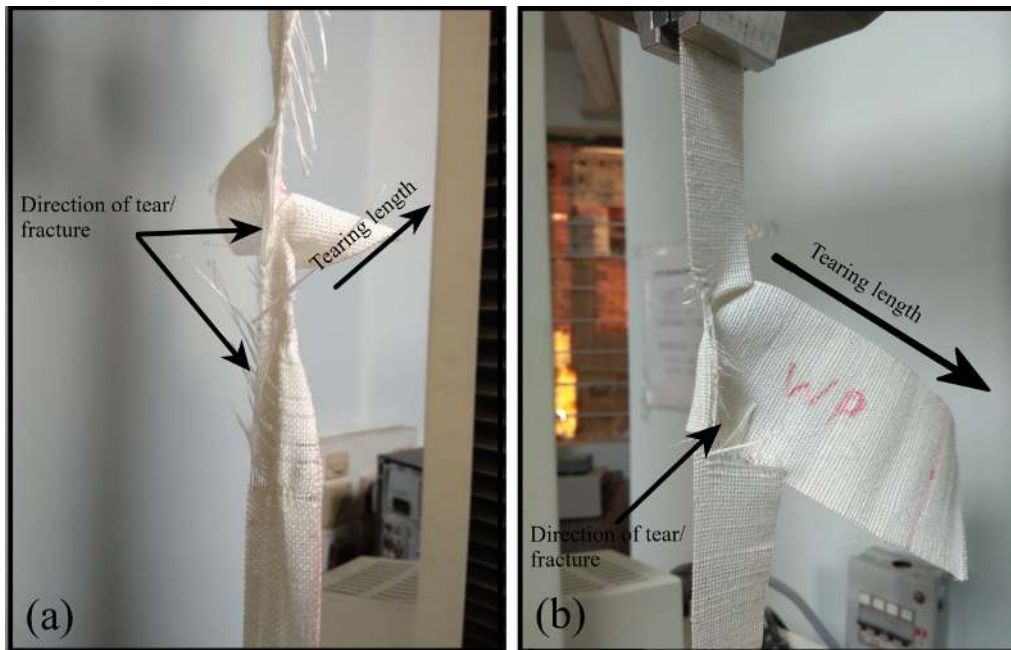


Figure 5.4: Tearing failure of fabric under single rip tear

Figure 5.5 and Figure 5.6 shows the tearing load-displacement curves of P1 fabric in both weft and warp direction respectively. It shows that up to the occurrence of the initial peak resistance against load increases as compared to the remaining tearing length. The increase in resistance against load will occur till the failure of first yarn. This results in stretching of the crack tip which further slip closely to the neighboring yarn and forms Del zone. After this, the crack corresponds to the initial peak propagates and continues along the direction of tearing. The crosshead speed is varied from 50 to 200 mm/min.

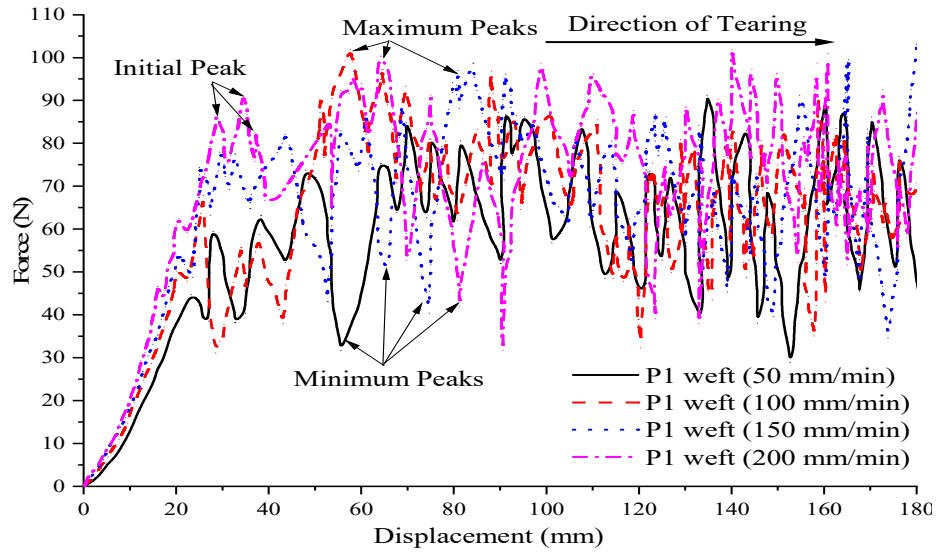


Figure 5.5: Tearing of P1 fabric in weft direction

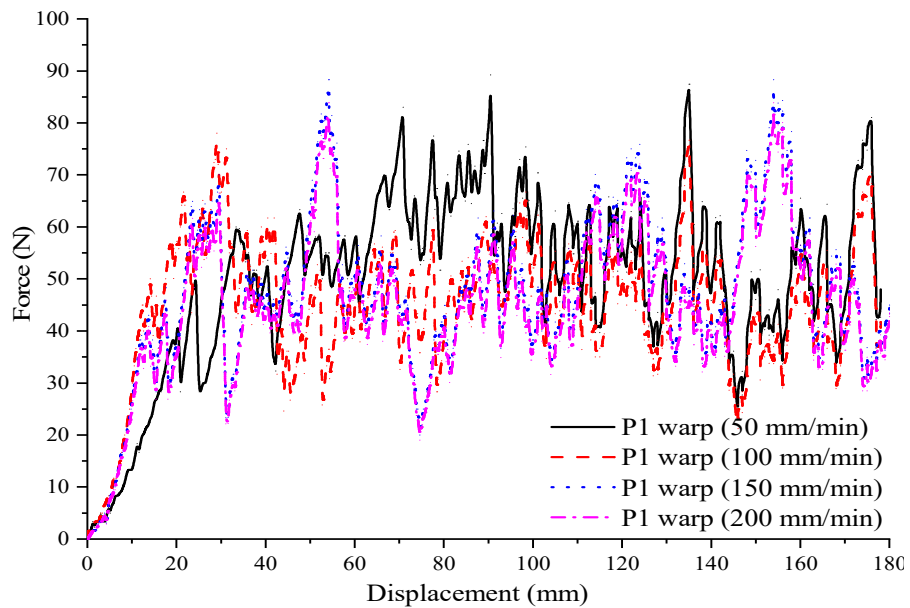


Figure 5.6: Tearing of P1 fabric in warp direction

Figure 5.6 clearly shows that at higher the crosshead speeds, initial peaks occurs at lower tearing length with a higher magnitude of tearing strength (force). The same nature of variation is observed in both warp and weft directions. However, occurrence of initial peaks is found to be at lower tearing length for warp compared to weft direction. This may be due to the higher yarn crimp in weft direction compared to the warp direction.



The displacement of the curve beyond the initial region clearly shows the progressive failure of single and multiple yarns along the tearing direction. The tearing force varies cyclically until the tearing direction reaches the endpoint of tear. However, the gap between two cyclic peaks is found to be higher and many small peaks are found throughout the tearing length. This gap between peaks of cyclic curves is due to the effect of fabric cover factor and the yarn count. The small peaks represent the failure of one or two yarns as there is more resistance for the mobility of yarn under the action of tearing load. However, the tearing strength of woven fabric by a single rip tear test method is very low as compared to Elmendorf tearing test method. This might be due to the effect of nature of clamping during the testing. In Elmendorf tearing test method both the sides of the fabric are held rigidly and impact load is applied. However, in case of single rip tear test, two ends are connected by two jaws and weft yarns are exerting tearing force on warp yarns. The yarn slips each other and forms the saw-teeth profile curve throughout the tearing length.

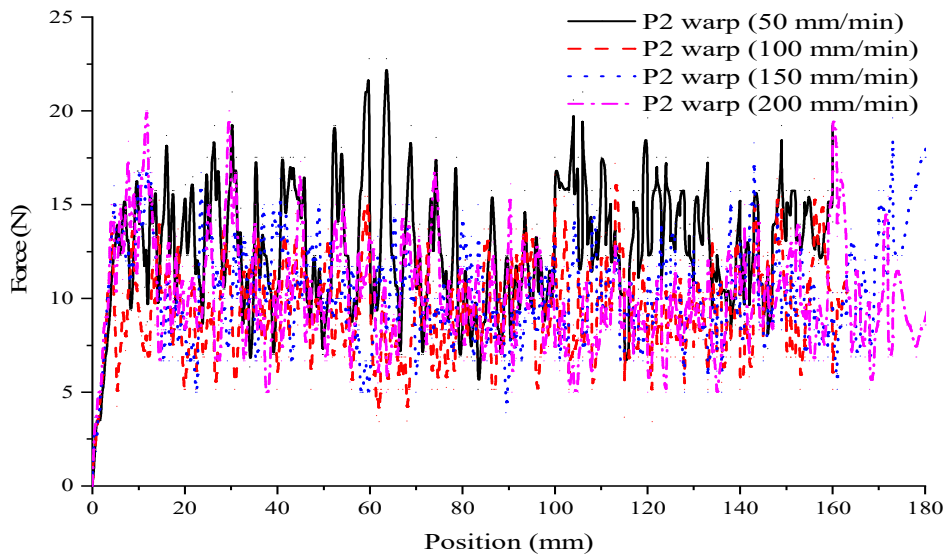


Figure 5.7: Tearing of P2 fabric in warp direction

Figure 5.7 and Figure 5.8 shows the tearing load-displacement curves of P2 fabric in both warp and weft direction respectively. The nature of tearing curve of P2 is similar to P1. As the crosshead speed increases, the tearing force value also increases. However, the

gaps between the peaks of force-tearing length curves are closer and variations of force value throughout the tearing length are found to be cyclic with a narrower bandwidth. This clearly shows slipping of yarns and formation of a Del zone. In case of P2, the initial peaks are found to occur at lower tearing length as compared to P1. This may be due to the influence of the cover factor. The number of yarns in both warp and weft directions of P1 fabric are higher than that of P2 fabric. As cover factor is less in P2 fabric, many of the loose yarns in both warp and weft directions lead to the slipping of yarns from the fabric. The mobility of these yarns led to lower tearing resistance and observed like a zigzag pattern of failure of P2 fabric as compared to P1 fabric. In other words, the number of cyclic curves is higher in P2 as compared to P1. Similar to P1, weft direction of fabric exhibited excellent tearing strength than the warp direction for the P2 fabric also. However, the tear strength values of P1 fabric are better than P2 fabric. Since P2 has a loose fabric structure as compared to P1, it allows greater yarn mobility as compared to P1. The decrease in yarn mobility leads to a more rapid crowding of the yarns in the Del zone shown in Figure 5.4 (a).

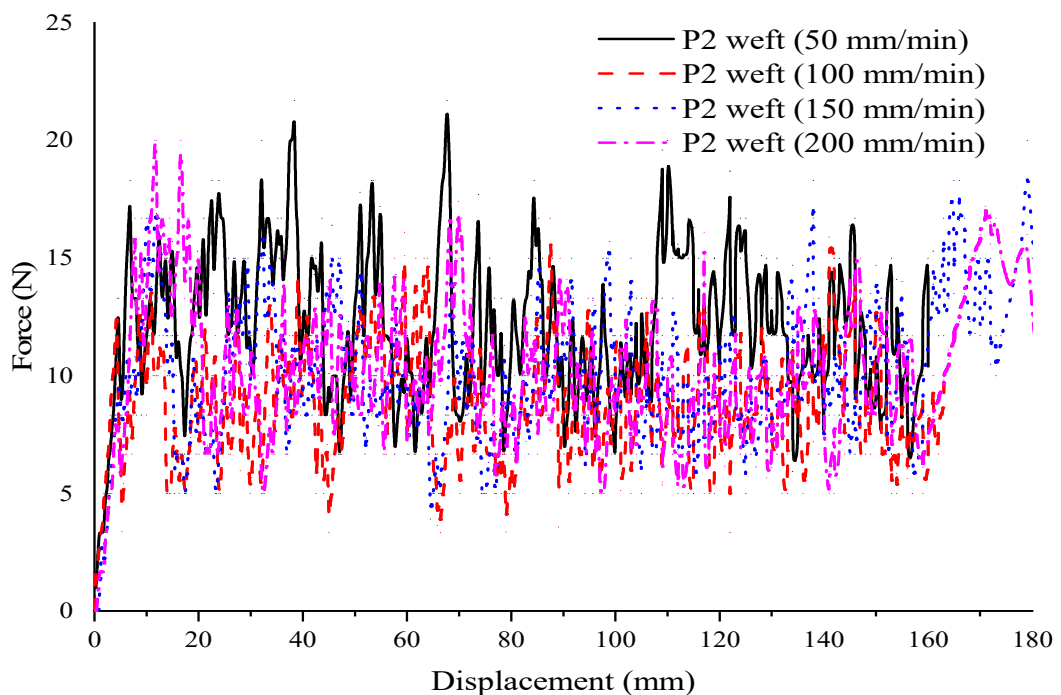


Figure 5.8: Tearing of P2 fabric in weft direction

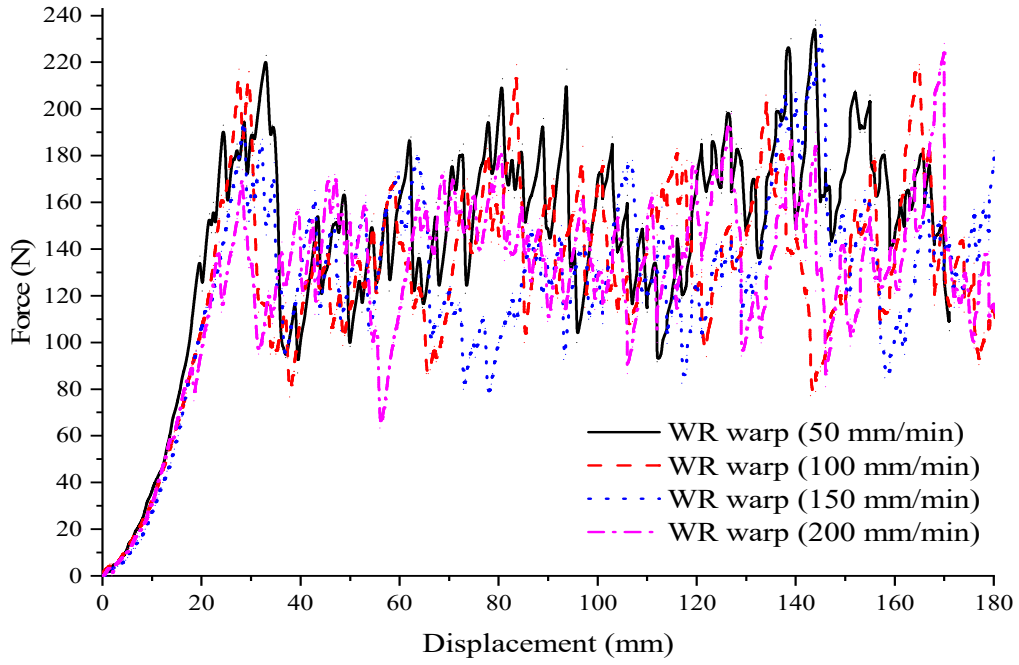


Figure 5.9: Tearing of WR fabric in warp direction

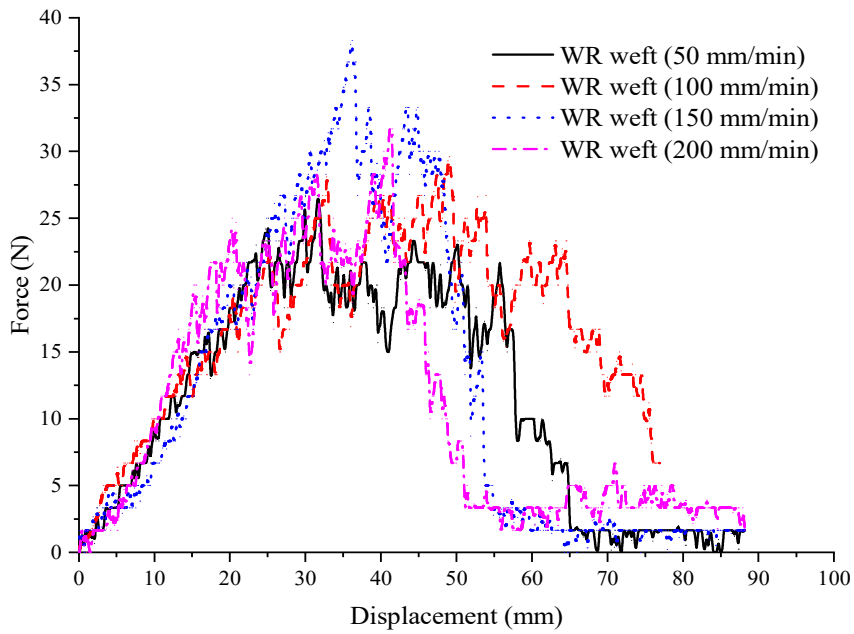


Figure 5.10: Tearing of WR fabric in weft direction

Figures 5.9 and Figure 5.10 shows the tearing load-displacement curves of WR fabric in both warp and weft direction respectively. The nature of the force-displacement curve of WR warp direction is similar to P1 and P2. However, the magnitude of tearing value is significantly high as compared to P1 and P2 fabrics. The significant increase in tearing strength is due to the interlacing of two weft yarns with one warp yarn. The two weft yarns resist the tearing load in warp direction significantly as compared to P2 fabric which is having same GSM as that of WR fabric. During the initial part of the load-displacement curve, as the crosshead speed increases, the rate of resistance decreases. This might be due to the presence of two yarns in warp direction and lesser cover factor in weft direction, which leads to slipping of yarns at slower crosshead speed. Tearing load-displacement curve of WR fabric in weft direction is different from the other cases analyzed. Unlike, the other cases after the initial increase in load and some relatively lesser number of peaks the curve drops to zero rapidly. This indicates that failure of the fabric occurs at a lower tearing length which is around half of the tearing length shown in Figure 5.4 (b). This is due to lesser yarn linear density, number of yarn per unit length. The tearing force is found to be better in weft direction compared to P1 and P2 in weft direction. This signifies that WR pattern exhibit better tearing strength in both warp and weft directions as compared to other two plain woven fabrics.

#### **Analysis of variance (ANOVA)**

It is necessary to consider all points throughout the tearing length of the fabrics to analyze the significance between fabrics and their directions. Table 5.10 shows the average and variance of P1 fabric both in warp and weft directions. Both average and variance values are increasing with loading rate in weft direction. This clearly shows that as the crosshead speed increases the amount of energy absorbed by the material also increases. In warp direction variations on average and variance is observed with increase in the crosshead speed. This might be due to lower crimp value, yarn count and the number of yarns per unit length. These parameters have a significant influence on controlling the gap between maximum and minimum peaks.

ANOVA analysis used to study the significance between fabrics and the rate of loading. The P-value (probability of significance) is then determined from the F-value. The hypothesis is assumed P-value is equal to or smaller than 0.05 (confidence level 95%), then it suggests that the contribution of the factor is significant. Table 5.11 shows the significance test of P1 fabrics between the warp and weft directions for the various loading rates. The P-value is less than 0.05 which indicates that the data is significant. This also indicates that loading direction and rate of loading have significant effect on single rip tearing strength of P1 fabric. Similarly, F-value is greater than F critical which also indicates that the data is significant.

Table 5.10: The variance of P1 fabric between warp and weft groups on static tearing for various crosshead speeds.

<i>Groups</i>	<i>Count</i>	<i>Sum</i>	<i>Average</i>	<i>Variance</i>
P1 weft (50)	499	31198.08	62.5212	236.0039
P1 weft (100)	499	33091.77	66.31618	292.7737
P1 weft (150)	499	33959.85	68.05581	279.3206
P1 weft (200)	499	35415.55	70.97304	329.3858
P1 warp (50)	499	24827.26	49.75404	290.9696
P1 warp (100)	499	22410.38	44.91058	179.4894
P1 warp (150)	499	23773.44	47.64217	239.8766
P1 warp (200)	499	22584.77	45.26006	216.4887

Table 5.11: ANOVA for P1 fabric.

Source of Variation	SS	df	MS	F	P-value	F crit
Between Groups	428523.6	7	61217.66	237.2423	9.3E-296	2.643797
Within Groups	1028026	3984	258.0385			
Total	1456549	3991				

Table 5.12 shows the average and variance of P2 fabric both in warp and weft directions. Both in warp and weft direction, variations in the average value are observed with an increase in the crosshead speed. This may be due to the yarn count and the number of yarns per unit length, yarn count of P2 fabric is higher than P1 fabric and the yarns do not break at a lower force for P1 fabric. These yarn slips from the fabric and leads to variations in maximum and minimum peak values. Table 5.13 shows the significance test

of P2 fabrics between the warp and weft directions for the various loading rates. The P-value is less than 0.05 which indicates that the data is significant. This also indicates that loading direction and rate of loading have significant effect on single rip tearing strength of P2 fabric. Similarly, F-value is greater than F critical which also indicates that the data is significant.

Table 5.12: The variance of P2 fabric in warp and weft groups on tearing for various crosshead speeds

<i>Groups</i>	<i>Count</i>	<i>Sum</i>	<i>Average</i>	<i>Variance</i>
P2 weft (50)	499	6028.275	12.08071	10.89413
P2 weft (100)	499	4403.33	8.824309	7.192844
P2 weft (150)	499	4865.93	9.751363	8.152083
P2 weft (200)	499	4963.94	9.947776	9.535537
P2 warp (50)	499	6294.721	12.61467	12.14682
P2 warp (100)	499	4658.343	9.335358	7.622528
P2 warp (150)	499	5054.14	10.12854	7.309592
P2 warp (200)	499	5019.824	10.05977	8.749436

Table 5.13: ANOVA for P2 fabric

Source of Variation	SS	df	MS	F	P-value	F crit
Between Groups	6055.039	7	865.0056	96.64466	8.9E-131	2.643797
Within Groups	35658.28	3984	8.950372			
Total	41713.32	3991				

Table 5.14 shows the average and variance values of WR fabric over a range of crosshead speed in both warp and weft directions. Table 5.14 clearly indicates that weft direction of the fabrics fails at smaller tearing length due to the presence of fewer number yarns as compared to the other direction. Warp direction of the fabric exhibit better tearing strength than the weft direction. This shows that woven pattern also has a significant effect on the tearing strength of the fabric. Table 5.15 shows the significance test of WR fabrics between the warp and weft directions for the various loading rates. The P-value is less than 0.05 which indicates that the data is significant. This also indicates that loading direction and rate of loading have significant effect on single rip tearing strength of WR fabric. Similarly, F-value is greater than F critical which also indicates that the data is significant.

Table 5.14: The variance of WR fabric between warp and weft groups on static tearing for various crosshead speed

<i>Groups</i>	<i>Count</i>	<i>Sum</i>	<i>Average</i>	<i>Variance</i>
WR weft (50)	499	5751.325	11.5257	70.4992
WR weft (100)	499	7680	15.39078	63.72592
WR weft (150)	499	6163.871	12.35245	135.9861
WR weft (200)	499	5481.971	10.98591	79.80678
WR warp (50)	499	73940.32	148.177	2109.881
WR warp (100)	499	63707.54	127.6704	1739.337
WR warp (150)	499	62524.04	125.2987	1753.408
WR warp (200)	499	63308.95	126.8716	1561.986

Table 5.15: ANOVA for WR fabric.

Source of Variation	SS	df	MS	F	P-value	F crit
Between Groups	14418817	7	2059831	2192.875	0	2.643797
Within Groups	3742286	3984	939.3288			
Total	18161103	3991				

## 5.4 Summary and Conclusion

To summarize the results from this chapter, the influence of textile physical properties on mechanical properties and the deployment of prepared textiles into composite are discussed. It is observed that many of the results are very important in the prediction and interpretation of the properties of sisal fabric reinforced composites.

- P1 type of fabric having fabric density 18 X 20 and yarn count of 80.1 and 85.1 in warp and weft direction, This influenced in the variation of mechanical properties in both warp and weft direction. However, the weft directions possessed the highest tensile properties than the warp direction.
- P2 type fabric possessed similar fabric density in warp and weft direction (12 X 12), even though the tensile properties improved in weft direction.
- WR type of fabric having fabric density (11 warp and 22 weft direction) and yarn count of 65.3 in warp and 182.9 in weft direction and exhibited better tensile

properties in weft direction. This clearly concluded that fabric density and yarn count influenced on textile tensile properties.

- Both P2 and WR having same grams per unit area, but different in textile mechanical properties clearly shown that woven structure also influenced.
- The fabric crimp influenced fabric stretch and recovery behavior, higher the crimp percentages better the fabric stretch and recovery.
- The tearing load of the fabric influenced by woven pattern and GSM of the fabric, but yarn crimp, number of yarns and cover factor influenced on tearing length and cyclic behavior of the tear.

From the above summary of results, it is concluded that all three fabric is a very good cover factor. This enhanced the interfacial adhesion between fiber to matrix surface, this part will be discussed in the next chapter. The GSM and woven patterns are two major properties considered to analyze the influencing of composites mechanical and dynamic mechanical properties.





## CHAPTER-6

### CHARACTERIZATION OF COMPOSITES

The matrix material PVA cross-linked 20% volume fraction GA, exhibit better properties as discussed in Chapter 4. Thus, the composites are prepared by keeping the 20% GA cross-linked PVA as matrix and reinforced with a different type of sisal woven fabric using compression moulding method. In the first phase, the chemical and structural properties of composites are analyzed. Further, the effect of type of weaving pattern, GSM, loading direction (warp and weft) on mechanical (tensile, flexural and impact) and dynamic mechanical properties of the composites are analyzed.

#### 6.1 Structural Components of Composites

##### Fourier transform infrared spectroscopy analysis

The FTIR (Section 3.5) is considered as an important tool for getting information about the specific groups in the compositions as well as the interaction between the PVA, sisal fiber in the composites. The spectra of FTIR for sisal fiber, matrix and composite are shown in Figure 6.1. It exhibits a strong broad peak ranging from 3300  $\text{cm}^{-1}$  to 3500  $\text{cm}^{-1}$  (as noted by Joseph *et al.* 2002) and it demonstrates O-H stretching of the hydroxyl group in the lignin and cellulosic structure. The peak at 1638  $\text{cm}^{-1}$  is due to the characteristic axial vibration of hydroxyl group O-H of cellulose. The small peak around 1590  $\text{cm}^{-1}$  is attributable to the out of plane bending of NH (Ewa *et al.* 2017). The strong peak between 2900  $\text{cm}^{-1}$  to 3950  $\text{cm}^{-1}$  is related to C-H stretching of cellulose component. This is due to the aliphatic saturated C-H stretching vibration in cellulose and hemicelluloses form  $-\text{CH}_2$ . The wavenumber 2920  $\text{cm}^{-1}$  also corresponds to the stretching vibration of  $\text{CH}_2$  groups, while the peak at 1422  $\text{cm}^{-1}$  is interpreted as deformation vibrations of the same group. Also, -C-H stretching at around 2900  $\text{cm}^{-1}$  also observed in sisal fiber spectra (Joseph *et al.* 2002). According

to Namrata *et al.* (2017), the  $1720\text{ cm}^{-1}$  to  $1740\text{ cm}^{-1}$  attributed to C=O unconjugated stretching of the ester linkage of the carboxylic group of the ferulic and *p*-coumaric acids of lignin of the residual hemicelluloses. The small peak  $1638\text{ cm}^{-1}$  assigned to O-H bending due to absorption of water/moisture content in the sisal fiber. The peak at  $1422\text{ cm}^{-1}$  and  $900\text{ cm}^{-1}$  are assigned to  $\text{CH}_2$  symmetric bending of crystalline cellulose and the cellulosic  $\beta$ -glycosidic linkages. The peak  $1372\text{ cm}^{-1}$  attributed to in-the-plane -C-H bending vibration. The peak  $1242\text{ cm}^{-1}$  presence of both lignin and pectin attributed to C-O ring of lignin. The peak  $1242\text{ cm}^{-1}$  indicates lignin assigned to C-O stretching vibration of acyl group present in the lignin. Asha *et al.* (2015) identified the peak line between  $1100\text{-}1160\text{ cm}^{-1}$  assigned to C-O-C stretching vibration and hydrogen-bonded / ether linkage (C-O-C) form lignin or hemicelluloses. The band at  $1088\text{ cm}^{-1}$  is due to the associated hydrogen group and the small band peak also observed at around  $1045\text{ cm}^{-1}$  denotes C-O band of the primary and secondary hydroxyl group in the cellulose, lignin and their glycoside linkages in the sisal fiber. Rajashekarana *et al.* (2017) have reported that the peak around  $1,660\text{ cm}^{-1}$  corresponds to -C=O stretching. This is due to the presence of aliphatic carboxylic acid in the cellulose chain.

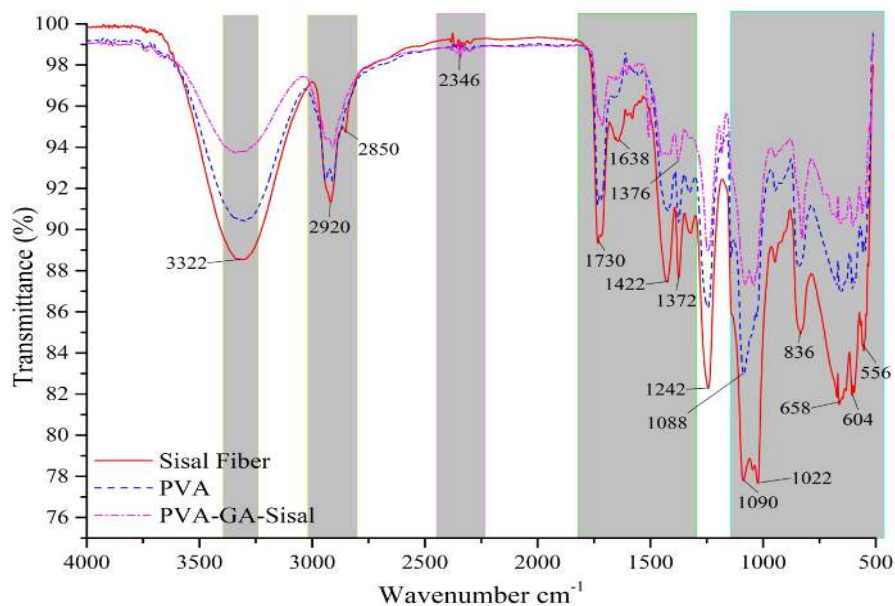


Figure 6.1: FTIR spectra of PVA, sisal fiber and their composites

In the spectrum of PVA a broad peak seen at  $3322\text{ cm}^{-1}$  attributed to the OH group. The peak at  $1645\text{ cm}^{-1}$  corresponds to the carbonyl group, and the peak  $1539\text{ cm}^{-1}$  indicates the OH vibration. The characteristic band seen at  $1732\text{ cm}^{-1}$  indicates the carboxylic (C=O) stretching, and C–O stretching corresponding to alcohol groups were observed at  $1246, 1088, 840\text{ cm}^{-1}$  and  $607\text{ cm}^{-1}$  (Mohan *et al.* 2018). The peaks at  $2910\text{ cm}^{-1}$  indicate the C-H stretching and the peaks at  $1377\text{ cm}^{-1}$  indicate the C-H group (Nasikhudin *et al.* 2017). The broad absorption bands at  $1088\text{ cm}^{-1}$  indicate the C-O stretching. C-H group vibration peaks were observed at  $1240$  and around  $1323\text{ cm}^{-1}$ . Other groups at  $1158, 929,$  and  $835\text{ cm}^{-1}$  attributed, respectively, to C–O–C, C–C, and H–C–H stretching modes. The IR spectra of PVA-GA-sisal composites show the improvement in the peaks. Based on group identifications, the chemical structures of PVA, GA, Sisal fiber (Manindra *et al.* 2013) and its composite were shown in Figure 6.2.

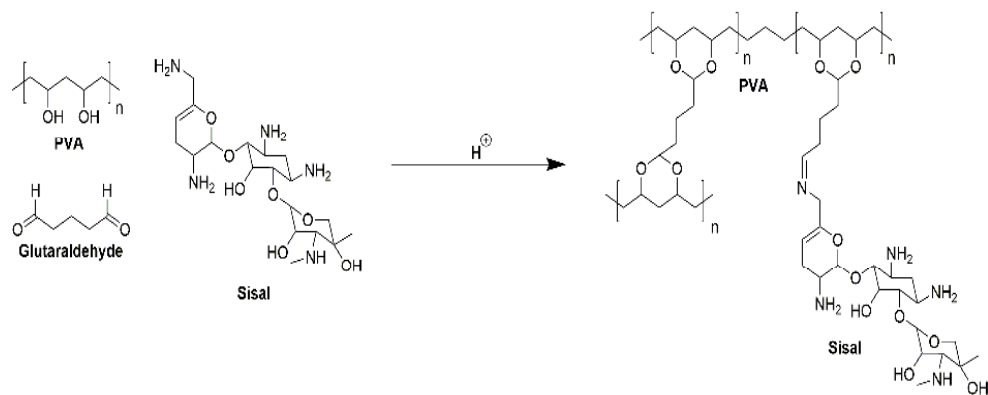


Figure 6.2: Chemical structure of PVA, GA and its composites and reactions

## 6.2 Mechanical Properties of Composites

### 6.2.1 Effect of GSM on mechanical properties

P1 (Plain 1) and P2 (Plain 2) composites have analyzed for the effect of GSM on tensile, flexural and impact properties. This comparison of properties has been made for the fabrics with the same woven pattern.

## Tensile properties

Tensile behaviour of P1 and P2 composites for various weight fractions of sisal fabric in warp and weft directions are analyzed and results are shown in Figure 6.3. From the figure, it is clear that the fiber weight fraction increases the ultimate tensile strength and strain of the composites. The ultimate tensile stress increases by 3.5 and 6.2 times for tensile loading in weft direction for 40 and 60% wt% of fiber. The ultimate stress found to be highest in weft direction as compared to warp directions.

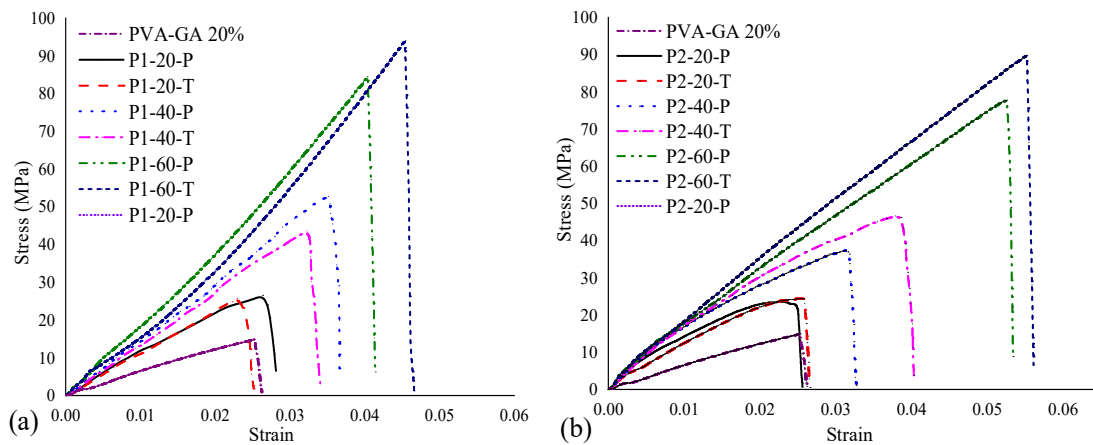


Figure 6.3: Tensile stress-strain curves of (a) P1 and (b) P2 composites for various weight fractions in both warp and weft directions

In P1 type composites, the strain increases with increase in fiber loading; this may be due to the stretching behaviour of fabric material. The tensile strains were found to be less in weft direction even though fabrics having higher strain values, this is due to the cover factor of the fabric. The cover factor of the fabric is lesser in warp direction which leads to resin-rich. This is explained in detail using SEM images in the next section. As yarns are twisted and fibers in yarns are creating crinkles texturing the high degree of interface possesses between matrix to the fabric material. It clearly shows that energy absorption increases with fiber loading. The weft direction of composite exhibit better toughness as compared to warp direction. The increases in ultimate stress could be attributed to the increase in surface area between woven sisal fabric and resin. This also attributed

reference to Figure 5.1, P1 type fabric having a better tensile strength in weft direction as compared to warp direction.

The ultimate tensile stress increased is by 1.58 times in warp and 1.63 times in weft by adding 20% of woven fabric P2 type, which is less than that of P1. The same trend continues at a higher percentage of fiber loadings also. This clearly shows that GSM of fabric is having a significant effect on tensile properties. The strain values of the composites show higher in weft direction as compared to warp direction as already observed in textile tensile properties of the fabric. A comparison of P1 and P2 based composite, P1 based composite shows better ultimate tensile stress. This can be attributed to higher GSM value of P2 fabric compared to the P1 fabric (Krivoshapko 2018). However, in comparison, it is also observed that there is no significant change in the strain at a lower percentage of fiber loading. But, P2 based composites show higher strain value (0.0552) at 60% fiber loading as compared to P1 (0.0454) this may be due to the yarn linear density and yarn twist. This clearly shows that the weft direction of composites possesses more energy absorption as compared to warp direction. It is also observed that strain energy absorption and toughness increases by increasing the fiber percentage in the composites. The nature of the curve was also found to be brittle in both P1 and P2 based composites.

### **Flexural properties**

Stress-strain response of the different types P1 and P2 composites under flexural loading is in Figure 6.4. It is clear that wt% of sisal fabric reinforcement enhances the bending strength of the composite. The same trend has been observed for both warp and weft cases. However, the weft direction of composite exhibit better flexural properties as compared to warp direction. The better load carrying capacity in weft direction is due to the higher yarn count and crimp percentage associated with weft direction as seen in Table 5.1. Influence of sisal fabric loading on strain-strain behaviour of P2 composite under flexural loading is similar to the P1 composites. But, as compared to P1 based composite, P2 based composites have slightly higher load-bearing capacity but fail at a lower amount of strain. This shows that, yarn linear density and yarn count have a

significant impact on flexural properties. The flexural behaviour of P1 based composites are like ductile in nature, but in case of P2 ductile fracture are changed to brittle by reinforcing more amount of fiber to it.

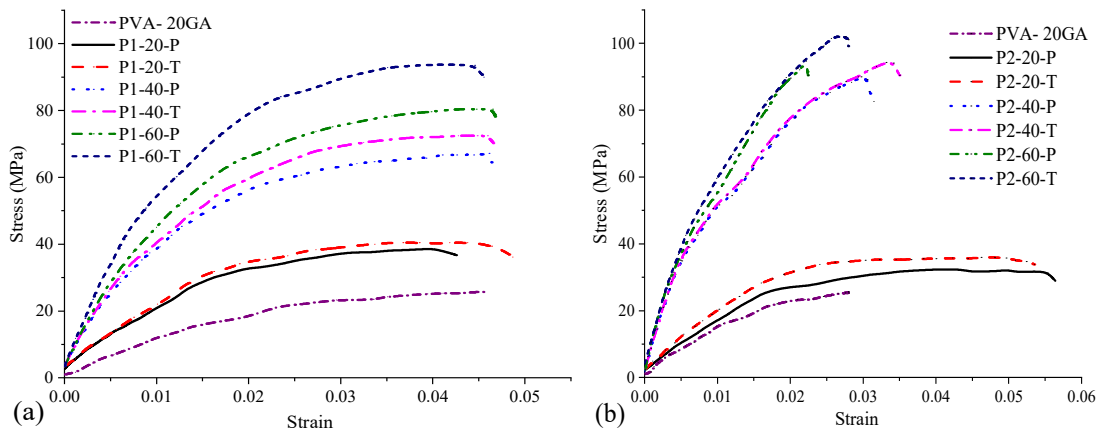


Figure 6.4: Flexural stress-strain curves of (a) P1 and (b) P2 composites

### Impact strength

Influence of fiber loading on the impact strength of the different composite is analyzed and is given in Table 6.1. It is clear that impact strength is influenced by the nature of the fabric. P2 based composites exhibit better impact strength than P1 based composites. This shows that the GSM of the fabric also influences the impact properties. The weft direction of composites exhibits better impact strength both in P1 and P2 based composites compared to warp direction. This may be due to the combined effect of cover factor and crimp.

Table 6.1: Impact strength in  $J/m^2$  by various fiber loading of P1, P2 and WR fabric in warp and weft directions.

Weight %	20 % fiber		40 % fiber		60 % fiber	
	Warp (P)	Weft (T)	Warp (P)	Weft (T)	Warp (P)	Weft (T)
Type of woven						
Plain 1	$0.8 \pm 0.072$	$0.85 \pm 0.053$	$1.11 \pm 0.068$	$1.23 \pm 0.085$	$1.32 \pm 0.070$	$1.35 \pm 0.086$
Plain 2	$0.95 \pm 0.076$	$1.10 \pm 0.080$	$1.23 \pm 0.058$	$1.35 \pm 0.044$	$1.45 \pm 0.070$	$1.54 \pm 0.046$
Weft Rib	$0.94 \pm 0.055$	$0.81 \pm 0.071$	$1.41 \pm 0.147$	$1.12 \pm 0.043$	$1.54 \pm 0.051$	$1.24 \pm 0.086$

Note: ( $\pm$ ) standard deviation for five impact trials

### 6.2.2 Effect of woven structure on mechanical properties

P2 (Plain 2) and WR (Weft Rib) composites have analyzed the effect of weaving pattern on tensile, flexural and impact properties. This comparison is made for the fabrics having the same GSM.

#### Tensile strength

Increase in the fiber weight fraction enhances the tensile properties significantly in both the warp and weft directions. It is observed that tensile properties are better for warp direction compared to the weft direction as seen in Figure 6.5 (a). The ultimate stress increases 9.1 times for warp direction and 7 times for weft direction compared to neat resin case for WR-60 composites. This can be attributed to more number of yarns in warp direction compared to weft direction. Weft yarns are subjected to tearing load and resist more load as compared to deformation. These are two number of yarns in warp direction for every single yarn in the weft direction. Another one important factor is higher yarn count associated with the weft compared to the warp direction.

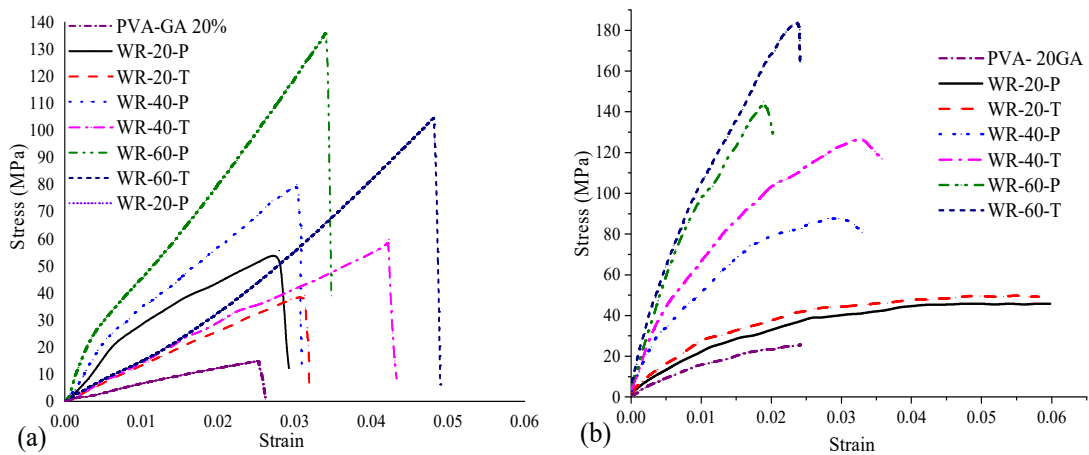


Figure 6.5: Stress-strain diagram of weft rib composites for (a) Tensile and (b) Flexural loading

Warp and weft direction loading also influence the stress-strain variation as shown in Figure 6.5 (a). For warp direction loading increase in stress is significantly higher than the strain in the initial region. Beyond this region, the increase in strain is high compared



to the stress variation. However, there is no such initial region for the weft loading case and stress-strain increases linearly. This clearly indicates that the nature of the weaving pattern significantly influences the tensile properties of fabric reinforced composites. The increase in tensile strength in warp direction attributed to shearing of weft yarns which leads to brittle nature with moderate strain value. The highest strain with moderate tensile load carrying capacity in weft direction attributed to two weft yarns are subjected to axial loading possess maximum strain value which leads to ductile nature.

### **Flexural strength**

P2 and WR composites are analyzed for the effect of weaving pattern on flexural properties as both have the same GSM. Figure 6.5 (b) shows by adding WR fabric, the strain energy absorption decreased, but load carrying capacity increases. This may be attributed that by adding fabric in the composites, the bending resistance increases, leading to an improvement in stress level as compared to strain. For this, it can be clearly shown that matrix material acts as an elastic member and exhibits very good strain rate with moderate loading ability. By adding fabric ductile fracture of composite converted into stiffer in nature. This may be due to the yarn linear density of the fabric and cover factor is higher than P2. As compared to P2 the load-bearing capacity increases drastically in WR based composites even though both fabrics have the same GSM. This shows that woven structure or arrangement of yarn has a significant impact on flexural properties.

### **Impact strength**

P2 and WR composites are analyzed the effect of weaving pattern on impact properties as both fabrics have the same GSM. From Table 6.1 it can be observed that Impact strength increases with fiber loading in both warp and weft directions; this attributed more amount of energy absorption by adding fiber to it. But weft direction of composites exhibits lesser impact strength than the warp direction. This also shows that yarn linear density and cover factor have a significant effect on sudden loading.

### 6.3 Fractured Surface Analysis

Figure 6.6 (a) shows the SEM image of fractured surface of tensile specimen. It is evident that fiber pull out failure is happening for the weft yarns while warp yarns are subjected to shearing failure. This clearly indicates that the weft direction yarns are subjected to axial loading as they are aligned along the loading direction and warp direction yarns are subjected to shear loading as they are under tearing loading. This fiber pullout failure along direction leads to the brittle failure of P1 type composite as discussed in Section 6.1.

The SEM image of fractured surface of P1 based composites under flexural loading is shown in Figure 6.6 (b). It is clear that bottom layers are subjected to tensile loading which leads to pull out of fibers from the matrix material. The pull out of fiber may be due to the crimp and cover factors, as the crimp increases matrix materials occupies the gap between the two yarns hence it increases the resistance against the bending loading. However, the yarns of top layers are subjected to compression and leads to decrease in the space between the fiber yarns until the yarns come into contact with one another. In other words inter yarn friction resist the slippage of yarn to fiber interface due to crinkles like structure with “S” type of twist in yarns of woven composites. Also, it clearly shows that the higher percentage of crimp in weft direction allows more amount matrix in the curvy regions between the yarns which leads to less amount of strain. Finally, sisal fibers breaks like sharp cuts which indicates the brittle nature of sisal fiber. This clearly shows that P1 woven fiber composites are withstanding moderate bending loads with higher strain rate. As the fiber loading increases the pulling capacity increases which results in higher bending strength and higher slipping resistance between the yarns and matrix which results in lesser strain rate.

The SEM image of fractured surface of P2 based composites under tensile loading is shown in Figure 6.6 (c). It shows, pulled-out of yarns, as well as tearing of yarns in many areas, are distinctly observed. Tearing of yarns along the warp direction indicates a good interfacial adhesion between the yarns and matrix. The nature of failure of P2 composites is same as P1 type composites which are brittle failure. The crinkles surface of the yarns

increases the resistance to pull and tear the yarn from the matrix material. The resin-rich regions are also found along warp directions due to the lower cover factor of the sisal fabric.

The SEM image of fractured surface of P2 based composites under flexural loading is shown in Figure 6.6 (d). It clearly shows the adhesion between fiber and matrix material due to crinkles on the surface of yarn and “S” type of yarn twist in a fabric. The top layers of the composites are subjected to tensile loading and both pulling and tearing of yarns are observed at higher magnifications. The matrix penetration between the gaps of two yarns is also observed. This offers more resistance along the surface of the yarns. However, it depends on cover factor and percentage of crimp in both warp and weft directions.

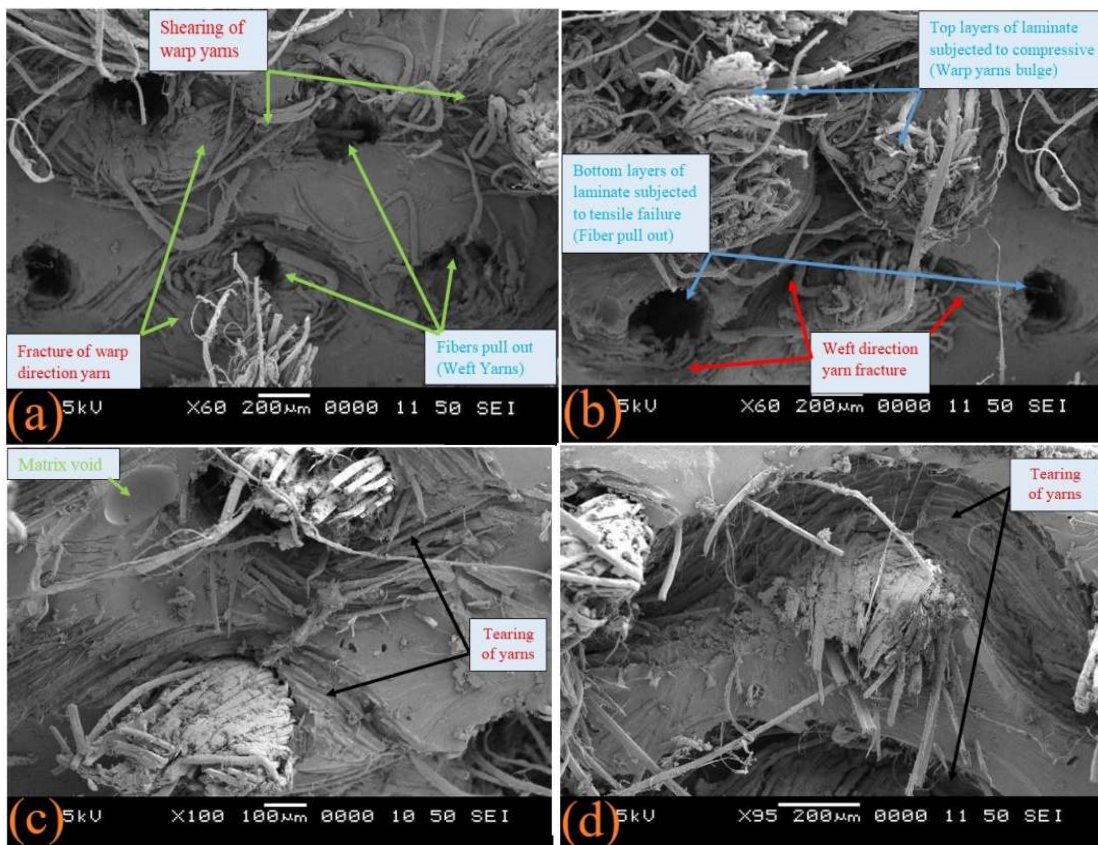


Figure 6.6: SEM image of fractured surface (a) P1 under tensile loading, (b) P1 under flexural loading, (c) P2 under tensile loading, and (d) P2 under flexural loading

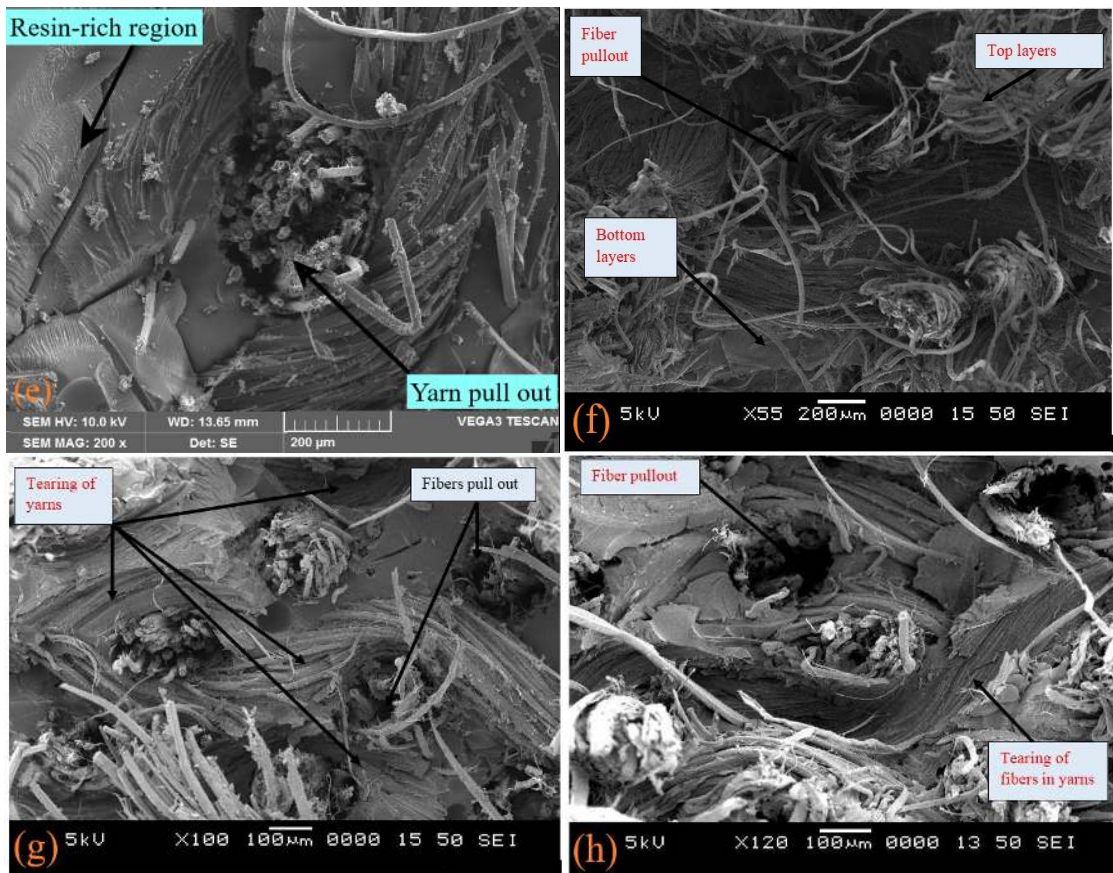


Figure 6.7: (e) WR under tensile loading, (f) WR under flexural loading, (g) P1 under impact loading, and (h) P2 under impact loading

Figure 6.7 (e) shows the fracture surface of WR based composites under tensile loading. Due to higher lower cover factor the resin-rich regions are observed, which leads to matrix failure and pull out of yarns from the matrix material.

The SEM image of fractured surface of WR based composites under bending loading is shown in Figure 6.7 (f). As seen in earlier P1 and P2 composites top layers are subjected to compressive loading and bottom layers are subjected to tensile loading, same was observed in WR based composites also. As each warp yarn is crossed with two weft yarns, the strength in weft direction of fabric higher than warp direction of fabric. Due to the presence of two successive yarns on weft direction with less cover factor in warp direction, the warp direction of composite also exhibits better properties even though yarn linear density and number of yarns are less in warp direction.

The SEM image of fractured surface of P1 based composites under impact loading is shown in Figure 6.7 (g). As yarn linear density is less for warp direction, yarns along warp direction are not transferring the load significantly to the matrix. Figure 6.7 (g) also reveals that there are no resin-rich regions in the fractured surface. It also shows that due to the sudden loading the yarn along the weft direction resists the impact load.

Figure 6.7 (h) shows the SEM image of fractured surface of P2 based composites under impact loading. In case of P2 the yarn linear density is higher than the P1 so impact load transfer from yarns to matrix material and leads to cracks in matrix surface. The fibers in yarns are also pulled out, many holes are seen from fractured surface and cracks have been propagated through the matrix and presence of river patterns near the fiber surface.

#### **6.4 Dynamic Mechanical Analysis**

DMA is one of the most widely used techniques to evaluate the viscoelastic behaviour of polymer composite materials. Among the different types of modes of tests, three-point bending is the best appropriate mode to understand the influence of textile properties on the dynamic composites. The complex modulus ( $G^*$ ) of the specimen is composed of an in-phase component  $G'$  (or storage modulus) and  $G''$  (or loss modulus)  $90^\circ$  out-of-phase component. The surface contact between the fabric and matrix of the composite material depends on the textile properties of the fabric and fabric loading. This in-detail study to analyze the effect of textile physical properties upon composite over a range of temperature is called a micro-finite element.

The GSM and woven pattern are the two major textile physical properties that influence the mechanical properties of composites significantly (Explained in detail in Section 6.1). The effect of these two properties on thermo-mechanical properties of the composite is analyzed. Effect of weight fraction ( $W_{ff}$ ) of all types of fabric-based composite was analyzed and found that 60  $W_{ff}$  of fibre-reinforced composite exhibit better tensile, flexural and impact properties in both warp and weft direction discussed in Section 6.1. In this section storage modulus ( $G'$ ), loss modulus ( $G''$ ),  $\tan \delta$  and deflection were analysed by considering all woven pattern at 60  $W_{ff}$  of fiber.

#### **6.4.1 Effect of GSM on dynamic mechanical properties**

P1 and P2 based woven composites are used to analyze the effect of GSM as both fabrics are the same woven pattern. Figure 6.8 to Figure 6.11 shows the influence of storage modulus, loss modulus,  $\tan \delta$ , deflection and micro finite element analysis of P1 and P2 based woven fabric, similarly like earlier these plots are divided into four different regions.

##### **Storage modulus**

Figure 6.8 (a) shows the variations of storage modulus in linear scale and (b) log scale, it is noticed that by adding fiber the thermo-mechanical stability enhances drastically. But, storage modulus decreases with temperature in all case of woven fiber composite. However, the variation of storage modulus is significantly influenced on gram per unit area of the fabric. To understand these influences of modulus graphs are divided in to four regions. The four regions are (i) glassy region, (ii) transition region, (iii) rubbery plateau region and (iv) very soft region. In region I, storage modulus reduces with increase in temperature, but when compared to other regions, the rate at which the storage modulus decreases with temperature is marginal. This is due to the absence of molecular mobility in the hard plastic state. In the region-I, the storage modulus of P1 warp, P1 weft, P2 warp and P2 weft woven fabric reinforced composites at 30°C are enhanced by 1.8, 2.2, 1.7, and 2.1 times respectively as compared to PVA cross-linked 20% GA. In the case of P1 based composite weft direction exhibit better properties than warp direction. Similarly, in case of P2 based composite weft direction exhibit better storage modulus than the warp direction. As it is a hard plastic region similar behaviour is observed in static tensile and flexural properties (Section 6.1). As compared to P1 and P2 based composite, P1 based composite exhibit (5%) better storage modulus. The variations of storage modulus with respect to temperature in region II is similar to that of region I. However, the rate at which the storage modulus decreases is significant at higher temperature as compared to the region I in general, for all cases. The storage modulus of P1 warp, P1 weft, P2 warp and P2 weft composites is enhanced by 3.9, 5.4, 4.4 and 5.7

times respectively as compared to matrix material at 70°C. The storage modulus of weft direction enhanced by 40% and 30% as compared to warp direction in P1 and P2 based composite respectively. But as compared to P1 and P2, P2 storage modulus is enhanced by 5%.

In middle region II at around 50 to 60°C crossover of storage modulus is observed. It shows that at lower temperature P1 based composite exhibit better properties than the P2 based composite. As the temperature increases the P1 based composite allows flow of polymer phase between to laminates. This slip between fiber to matrix interface is due to many reasons such as (i) the presence resin-rich region between two yarns (x) is higher in P1 based composite, (ii) as thickness of fabric (t) is very less or finer - lesser resistance to flow (molecular movement at higher temperature) may lead to slip between two plies, (iii) due to very poor bonding between fiber and matrix surfaces (iv) diameter of the yarn (y). From the above discussion, it is clear that  $G'$  and  $G''$  are dependent on fiber, matrix and interfaces between fiber and matrix shown in Figure 6.9.

Figure 6.9 shows the micro-finite element model of P1 and P2 based composite. As the fabric is finer, less matrix occupied between interfaces of two laminates starts to flow of molecules at a higher temperature. P1 fabric allows slips as the fabric is finer and matrix occupies less area. But, P2 fabric is rougher than P1 and exhibits more resistance to flow of matrix phase.

The variations of storage modulus in region III is similar to region II, But P2 based composite exhibit better properties than P1 based composite. The storage modulus of P1 warp, P1 weft, P2 warp and P2 weft composites at 100 °C is enhanced by 4.4, 6.2, 5.1 and 7.2 times respectively as compared to the matrix material. At the end of this region storage modulus improved only in P2 weft direction, it is due lower molecular mobility. In region IV, the storage modulus improved drastically in the weft direction of P2 based composite shown in Figure 6.8 (b). The yarn crimp is higher in weft direction as compared warp direction in P1 and P2 based fabrics. For this reason, the weft direction of the composite has more resistance to molecular mobility, this, in turn, improves storage

modulus at a higher temperature. As compared to P1 and P2 based composite, P2 based composite exhibit better storage modulus at a higher temperature. This indicates that both yarn properties and fabric properties significantly on thermo-dynamic properties. Also, PVA contains hydroxyl groups (OH), which have the potential to form hydrogen bonds between molecules, resulting in a significant change in surface bond strength between PVA, sisal and GA matrix.

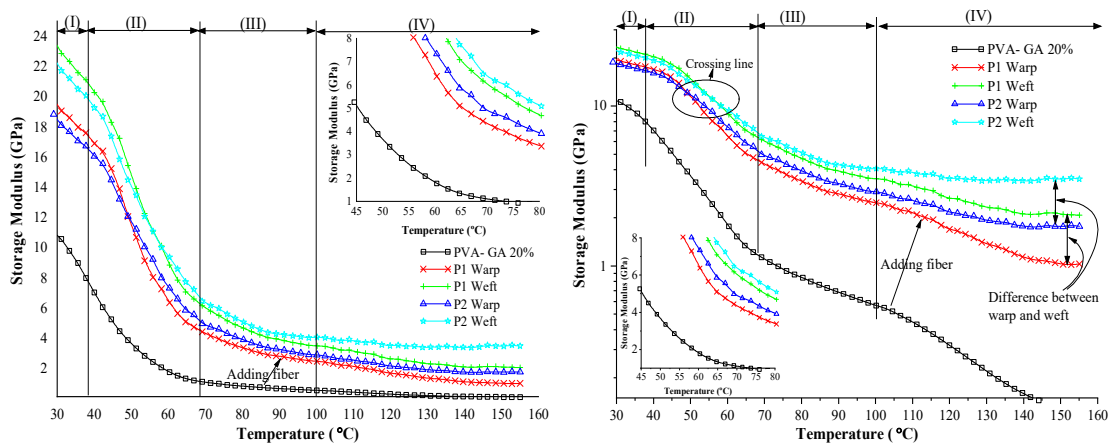


Figure 6.8: Storage modulus of P1 and P2 fabric based composite (a) Linear scale (b) Log scale

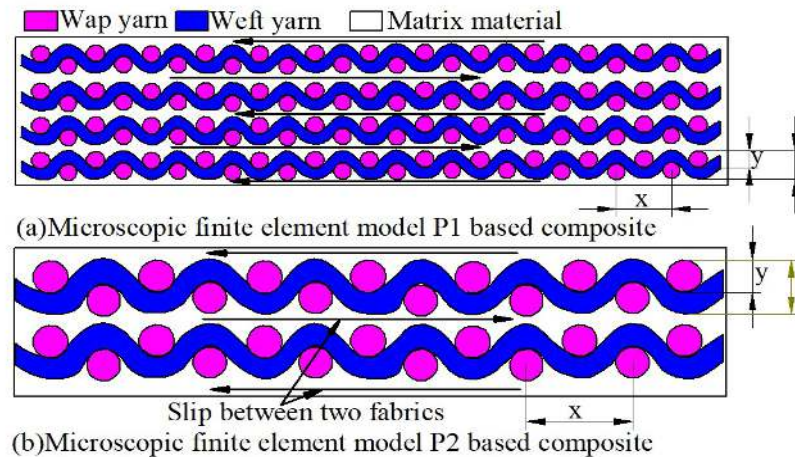


Figure 6.9: Micro-finite element model of P1 and P2 fabric-based composites



## **Loss modulus**

The variations of loss modulus over a range of temperature for P1 and P2 based composites shown in Figure 6.10. Similar to storage modulus plot, the loss modulus plot also divided into four regions for better analysis. In region I, loss modulus improved by adding fiber, in all case of composite. The storage modulus of P1 in the warp and weft direction at 30°C is enhanced by 1.8 times and 2.16 times respectively. But loss modulus is enhanced by 1.08 to 1.32 times. This is attributed to very good bonding between fiber to matrix material at 30°C. Similarly in P2 based composite exhibit better bonding between matrix and fiber interface.

In region II, the storage modulus enhanced by 2.28 to 2.88 times, but loss modulus is 1.26 to 1.4 times at 40°C. This clearly shows that the energy loss in the form of heat due to slip between two fiber phases is very nominal and weft direction shows better modulus. At 70°C storage modulus increased by 3.92 to 5.7 times but loss modulus is 2.28 to 2.88 times, attributed to more energy gained by the material as elastic part. The loss modulus of P1 based composite is higher as compared to P2 based composite, and is attributed to more energy loss in P1 based composite.

In region III, the storage modulus enhanced by 4.4 to 7.2 times but loss modulus enhanced only 1.44 to 1.94 times at 100°C, it is attributed to less energy loss in the form of heat. As compared to P1 and P2 based composite, P1 based composite shows higher loss modulus in the weft direction. This could be due to the finer fabric and lower yarn linear density and number of yarns per unit length in both warp and weft direction.

In region IV, storage modulus enhanced by 8.5 to 28.9 times, but loss modulus is increased from 1.45 to 1.87 times and is attributed to the highest resistance to slip between two laminates. The loss modulus in P1 based composite shows 29% higher than that of P2 based composite, due to this reason P2 based composite exhibit better storage modulus even at higher temperature. This clearly shows that gram per unit area of the fabric influence significantly on the loss modulus.

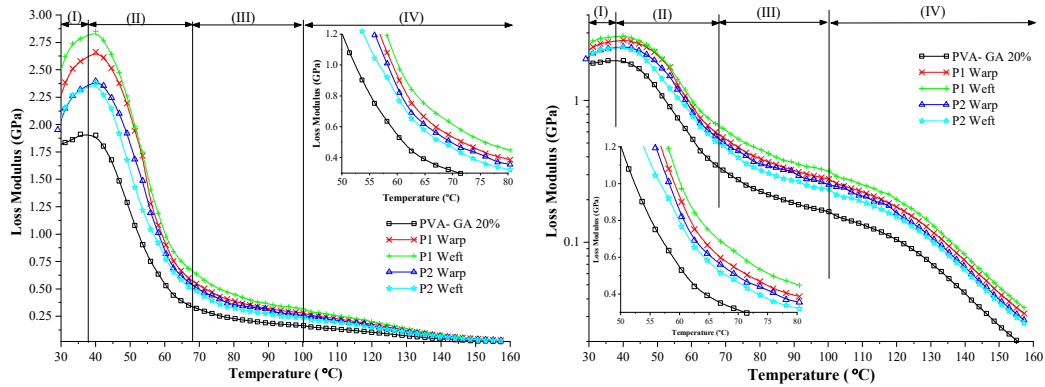


Figure 6.10: Loss modulus of P1 and P2 fabric-based composites (a) Linear scale (b) Log scale

### Tan $\delta$

The variation of  $\tan \delta$  over a range of temperature for P1 and P2 based composite shown in Figure 6.11 (a).  $\tan \delta$  refers damping factor of the composite, which increases with the addition of both P1 and P2 fabric. However, the weft direction of composite exhibit better damping than warp direction both in P1 and P2 based composite. This is due to higher yarn crimp and linear density in weft direction of the fabric while resists the matrix phase. P2 based composite showing better damping factor than the P1 based composite, this clearly shows that GSM has influenced significantly.

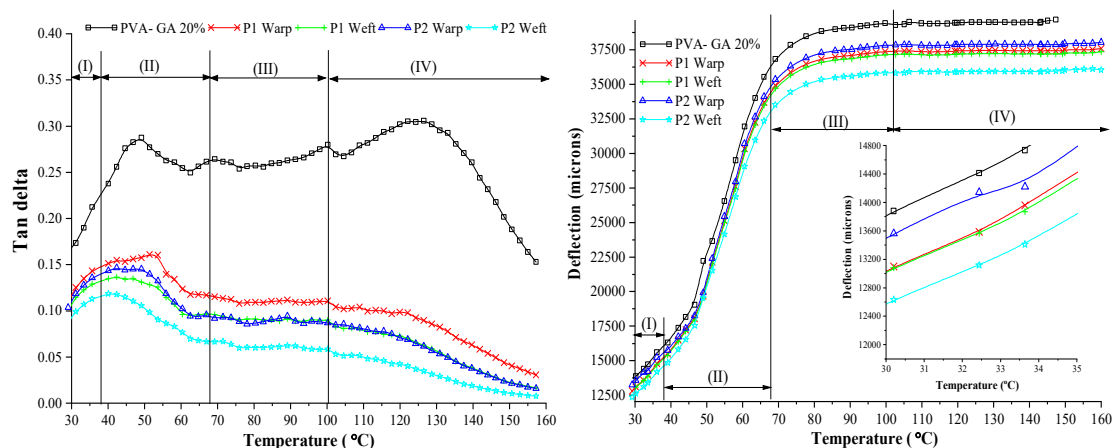


Figure 6.11: (a) Tan  $\delta$  (b) Deflection of P1 and P2 fabric based composite linear scale

## **Deflection**

The deflection of P1 and P2 based composite in warp and weft directions comparing to PVA-GA 20% shown in Figure 6.11 (b). In region I, rate of deflection is very small, as the temperature increases deflection increases. Region II, shows a significant impact on a deflection with temperature, at the end of this region it almost reaches the steady-state region and further constant deflection is observed. As compared PVA-GA 20%, the fibre-reinforced composite exhibited more resistance for bending. Weft direction of the fabric in both P1 and P2 shows lesser deformation than the warp direction. The P2 based composite shows more resistance than P1 based composite, this is due to the effect of GSM.

### **6.4.2 Effect of a woven pattern on dynamic mechanical properties**

P2 and WR based woven composites are used to understand the effect of woven pattern as both fabrics have the same gram per unit area. Figure 6.12 to Figure 6.15 shows the influence of storage modulus, loss modulus,  $\tan \delta$  and micro finite element analysis of P2 and WR based woven fabric, similarly like earlier these plots are divided into four different regions.

#### **Storage modulus**

The influence of woven pattern on storage modulus in both warp and weft directions shown in Figure 6.12. In region I, storage modulus of P2 warp, P2 weft, WR warp, and WR weft direction are enhanced by 1.71, 2.1, 2.46, and 2.63 times respectively compared to PVA-GA20%. From this, it observed that even though P2 and WR based composites have same GSM the woven pattern influenced significantly on storage modulus. WR based woven pattern is enhanced by 2.63 times in warp direction, due to the number yarns and yarn linear density. In region II, as the temperature increases behind 40°C the rate at which storage modulus decreased is very high. Storage modulus of warp and weft directions in WR based composite at 70°C is enhanced by 6.39 and 7.42 times respectively. In region III, the storage modulus of warp and weft direction of WR based

composite is enhanced by 7.28 and 8.94 times respectively. This shows that woven pattern also influenced significantly in higher temperature as compared to a lower temperature. The difference in storage modulus in warp and weft direction of P2 and WR based composites are 1.4 and 1.23 times respectively. This is due to the influence of yarn linear density, cover factor, number of yarn and yarn crimp.

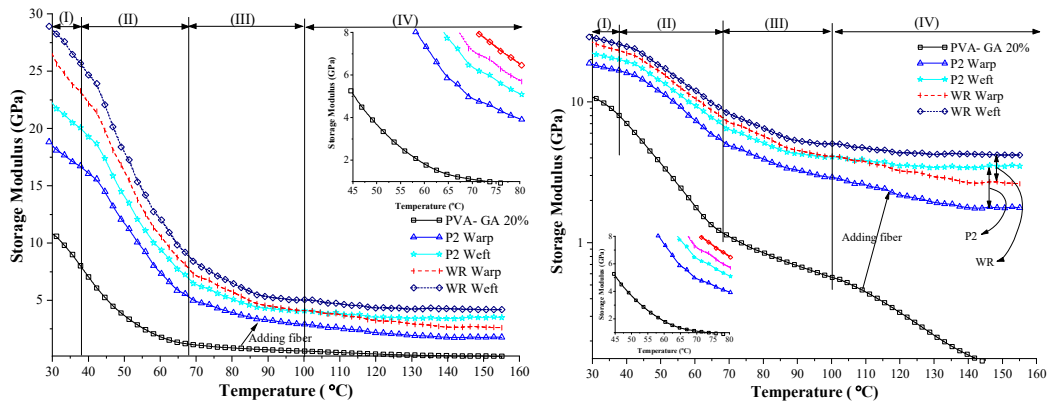


Figure 6.12: Storage modulus of P2 and WR fabric based composite (a) Linear scale (b) Log scale

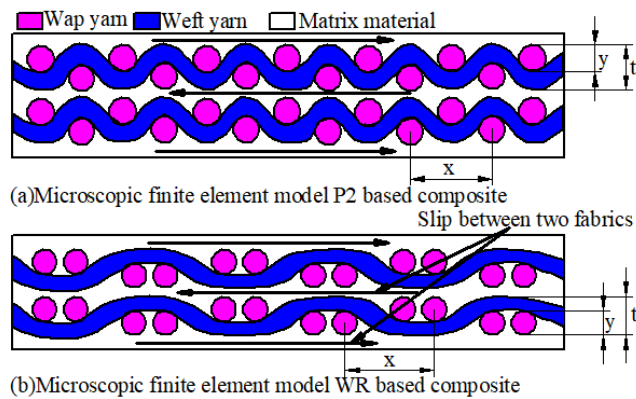


Figure 6.13: Micro-finite element model of P2 and WR fabric-based composite

In case of P2 the yarn linear density and cover factor are almost same in warp and weft direction, while yarn crimp is 6.53 and 11.06 in warp and weft direction respectively. Due to this reason significant change in storage modulus of the P2 based composite in warp and weft directions. But in case of WR based composite, even though crimp is 10.05 in warp and 5.96 in weft direction the difference in storage modulus is lesser. It

may be due to the lesser cover factor in weft and higher yarn linear density in warp direction allows slip molecular moment marginally. In region IV, the weft direction of P2 and WR based composite enhanced by 28.92 and 34.62 times respectively. This is due to the effect of woven pattern, WR based composite stores more energy than P2 based composite. The P2 based composite shows 1.98 times higher storage modulus in weft direction than the warp direction. In the case of P2 weft direction offers more resistance for slip between two layers of fabric, this may be due to higher yarn crimp in the weft direction. The microscopic finite element model of P2 and WR based composite shows in Figure 6.13. This clearly shows woven pattern has also influenced significantly on storage modulus. As there are two yarns in weft direction of WR based composite offers more resistance to flow of molecules and slip between two yarns than P2 based composite.

### **Loss modulus**

The influence of woven pattern on loss modulus in both warp and weft directions shown in Figure 6.14. In the region-I, the loss modulus of P2 warp, P2 weft, WR warp and WR weft direction of the composite is enhanced by 1.08, 1.1, 1.31, and 1.31 times respectively. This shows that material loss modulus enhanced much significantly in WR based composite. However, the difference of loss modulus in warp and weft direction of composites is very marginal so it is negligible. In region II, storage modulus enhanced by 4.39 to 7.4 times, whereas loss modulus enhanced only by 1.48 to 1.68 times. This clearly shows the stored form of energy is enhanced, but the loss of energy in the form of heat is very marginal. In region III, the storage modulus enhanced by 5.15 to 8.94 times at 100°C, but loss modulus from 1.44 to 1.76 times which is marginal. The warp direction of P2 based composite is enhanced 1.07 times than weft direction of P2 composite. Whereas weft direction of WR based composites is enhanced by 1.12 times than the warp direction. This clearly shows material loss factor more is in WR composite, may be due to the influenced of lower yarn linear density in the warp direction and lower cover factor

in weft direction. The similar behaviour is also observed in region IV at 150°C. This clearly shows that woven pattern has a significant effect of loss modulus.

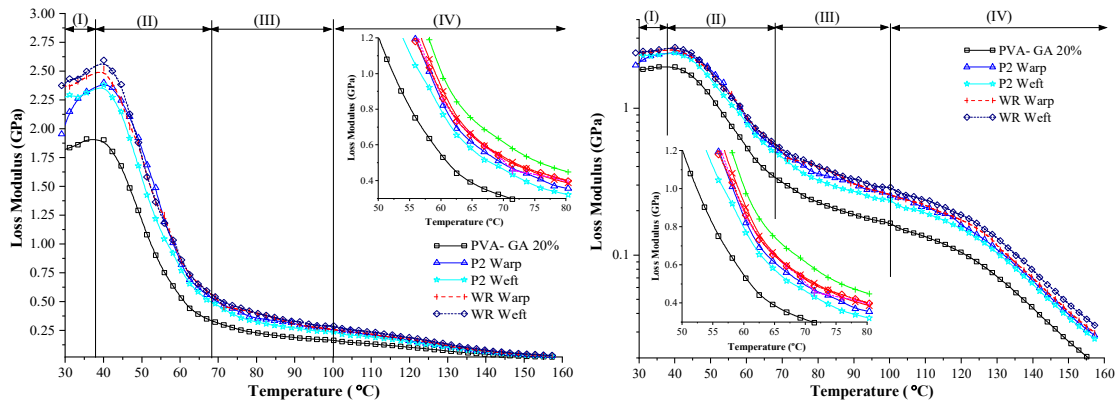


Figure 6.14: Loss modulus of P2 & WR fabric based composite (a) Linear scale (b) Log scale

### Tan $\delta$

Figure 6.15 (a) shows the variation of  $\tan \delta$  over a range of temperature for P2 and WR based composite. The damping factor increases with addition of both P2 and WR fabric. However, the weft direction of composite exhibit better damping than warp direction both in P2 and WR based composite. This is due to higher yarn crimp and cover factor in weft direction of the P2 composite resist the matrix phase and higher yarn linear density in weft direction of the WR composite. WR based composite shows better damping factor than the P2 based composite, this clearly shows that woven pattern has influenced significantly.

### Deflection

Figure 6.15 (b) shows the deflection of P2 and WR based composite in warp and weft directions comparing to PVA-GA 20%. In region I, rate of deflection is very small as the temperature increases deflection increases. In region II, rate of change of deflection is higher, due to glass transition of the materials and also material loss factor is higher in this region. In region III and IV, the change in deflection of the material is neglected. As compared PVA-GA 20%, the fiber reinforced composite exhibited more resistance to

bending. Weft direction of the fabric in both P2 and WR shows lesser deformation than the warp direction. The WR based composite shows more resistance than P2 based composite, this is due to the effect of woven pattern.

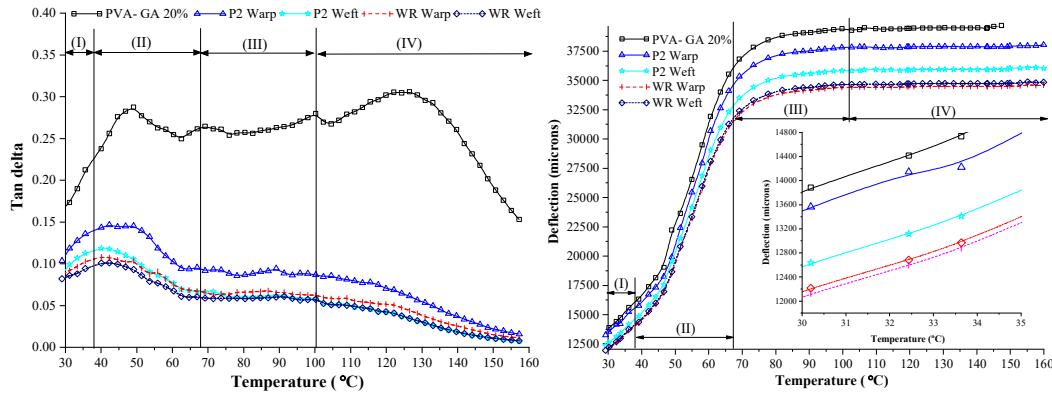


Figure 6.15: (a) Tan  $\delta$  (b) deflection of P2 and WR fabric based composite

### 6.5 Effectiveness

The effectiveness of textile properties on the modulus of the polymer composite can be represented by a coefficient C such as.

$$C = \frac{\left[ \frac{E'_g}{E'_r} \right]_{Composite}}{\left[ \frac{E'_g}{E'_r} \right]_{Matrix}} \dots\dots\dots (6.1)$$

Where

$E'_g$  and  $E'_r$  are the storage modulus values in the glassy and rubbery region, respectively.

Higher the value of constant C, lower the effectiveness of the composite. The values of  $E'_g$  and  $E'_r$  are used for various temperatures to determine the effectiveness as storage and loss modulus is improved at higher temperature. The effectiveness obtained for all types of woven composites in warp and weft directions at 10 Hz are given in Figure 6.16.

**Gram per unit area:** The effectiveness of P1 and P2 based fabric composite enhances at higher temperatures, the same behavior is also noticed in storage and loss modulus plots. The weft direction of the fabric exhibits better performance as compared to warp in both P1 and P2 based composite. It may be due to the influence of yarn crimp, as the yarn crimp increases the effectiveness increases. P2 based composite exhibit better performance than P1 based composite, this clearly indicates that mass per unit area of the fabric influence significantly.

**Woven pattern:** The P2 and WR woven based composite were used to analyze the effect of woven pattern. As the temperature increases the effectiveness increases, this indicates fabric reinforcement enhances the thermal stability of the composite. Weft direction of the P2 and WR based composite shows lowest effectiveness value indicates that P2 and WR show better stability than that of P1 based composite. However, as compared to P2 based composite, WR based composite shows marginal variation in the effectiveness. This indicates that as compared to gram per unit area, the woven pattern of the fabric has a less significant effect on composite properties.

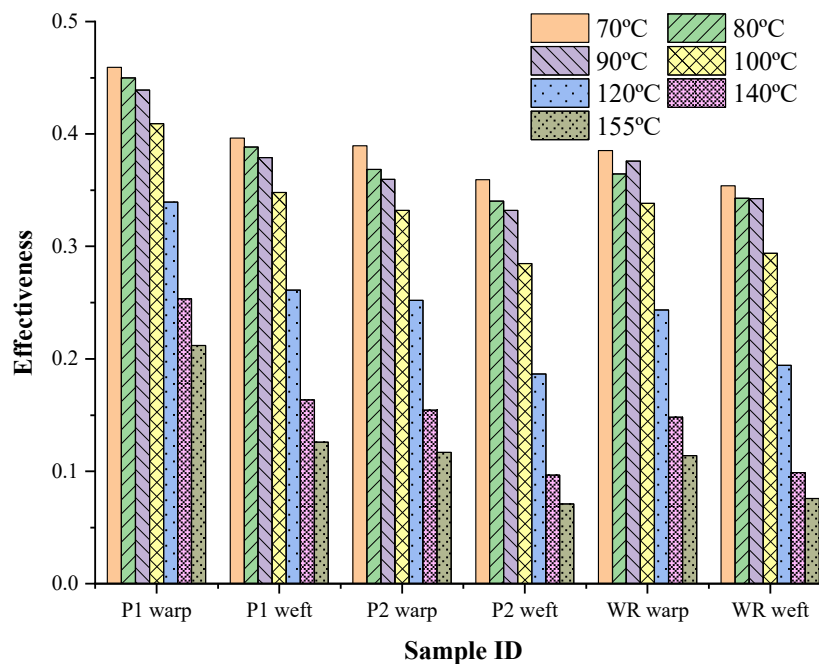


Figure 6.16: Effectiveness of sisal woven composite at various temperatures



## 6.6 Summary and Conclusion

Mechanical properties of fully biodegradable composites developed from PVA and sisal fabric are analyzed. Influence of weaving architecture, GSM, and fiber loading on different mechanical properties under tensile, flexural and impact loadings. It is also observed that all three fabrics are having a good range of cover factor which increases the bonding between matrix and fabric material. It is observed that P1, P2 and WR composites have better mechanical properties for weft direction loading compared to warp direction loading. However, for WR composites the properties are better for the loading under warp direction even though yarn linear density is lesser. Mechanical properties of P1 composites are better than the P2 composites due to lower GSM value associated with P1 composites. Similarly, mechanical properties of WR composites are better than P2 composites (for same GSM) due to the woven pattern shown in Table 6.2.

Table 6.2 Mechanical Properties of various types of composites and its weight fractions

Test	Tensile						Flexural					
	20		40		60		20		40		60	
% of Ga	Strain	Stress MPa	Strain	Stress MPa	Strain	Stress MPa	Strain	Stress MPa	Strain	Stress MPa	Strain	Stress MPa
PVA-GA												
20%	0.0262	14.96					0.0542	26.16				
P1 Warp	0.0281	26.60	0.0366	52.77	0.0414	84.61	0.0426	38.57	0.0464	67.14	0.0467	80.41
P1 Weft	0.0251	25.74	0.0341	43.62	0.0466	94.01	0.0487	40.41	0.0466	72.45	0.0455	93.67
P2 Warp	0.0256	23.61	0.0327	37.40	0.0534	77.83	0.0564	32.34	0.0315	90.01	0.0224	94.68
P2 Weft	0.0266	24.44	0.0403	46.60	0.0561	89.82	0.0535	35.96	0.0351	94.26	0.0279	102.13
WR Warp	0.0293	55.71	0.0309	80.14	0.0348	136.24	0.0598	45.77	0.0330	87.69	0.0201	145.01
WR Weft	0.0319	39.14	0.0433	59.86	0.0491	105.01	0.0581	50.12	0.0357	126.92	0.0240	184.23

The Dynamic Mechanical properties of P1 based composite is better at room temperature, as temperature increases P1 based composites allow to flow of matrix material between interfaces. But P2 based composite lesser dynamic mechanical properties at room temperature; it improved at a higher temperature compared to P1. The dynamic

mechanical properties are better in WR based composite as compared to P1 and P2 composites. However, weft direction of composite exhibits better storage modulus, loss modulus,  $\tan \delta$ , and deflection than the warp direction. The woven pattern of the fabric is influenced significantly on mechanical and dynamic mechanical properties of composite as compared to gram per unit area of the fabric.

## CHAPTER-7

### SUMMARY AND CONCLUSION

In the first phase of the investigation, the cross-linked matrix material is optimized based on mechanical properties and dynamic mechanical properties. The mechanical properties such as tensile and flexural behavior of cross-linked polymer is compared and analyzed with the neat polymer. Similarly, storage modulus, loss modulus, tan delta, deflection and cole-cole behavior are analyzed for various temperatures. Further, adhesion factor, activation energy, life estimation, cross-linking density, and effectiveness are studied. Further, in the next phase the influence of physical properties of fabric with mechanical behavior of fabric is analyzed.

In the third phase, the optimized matrix material is used to prepare the composites using three types of woven fabrics. Further, mechanical behavior like tensile, flexural and impact properties analyzed for the influence of reinforcement materials by considering gram per unit area and woven pattern. Further, dynamic mechanical properties are analyzed over a range of temperatures. Based on the experimental results of the matrix, reinforcement, and composites the following conclusions are drawn,

#### **7.1 Contribution to the Body of Knowledge**

The contribution to knowledge by using biodegradable matrix and reinforcement materials and their influences upon composite. The dynamic mechanical analyzer used to study the effect of cross-linking of various percentages PVA and GA. The shift factor was determined to calculate the testing duration of PVA-GA polymer at various temperatures. Two plain fabrics and one weft rib type of fabrics are prepared using sisal fabric to study the effect of GSM and woven pattern. ANOVA method used to understand the effect of textile structural properties on the mechanical properties of fabrics. The direction of the fabric and textile structural properties are

influencing on mechanical properties and dynamic mechanical properties of composites.

## **7.2 Effect of GA Cross-linking on PVA**

The tensile and flexural property of PVA is enhanced by cross-linking with GA.

The storage and loss modulus enhanced by cross-linking drastically up to 20%, and beyond a marginal improvement is observed. The  $\tan \delta$  peak decreases by adding GA in PVA and concluded that the damping factor of cross-linked polymer is improved.

Similarly, storage and loss modulus enhanced in three-point bending mode dynamic mechanical analysis. The improvement of storage and loss modulus is significant at a higher temperature compared to room temperature of neat specimen. The dynamic mechanical properties are more significant under three-point bending mode as compared to tensile mode. The adhesion factor, cross-linking density and activation energy enhanced by adding GA in PVA. The testing duration is computed to predate the life estimation of PVA-GA polymer and observed that testing duration decreases with temperature.

Further, the influences of fabric physical properties are observed on mechanical strength of fabric in warp and weft directions. The yarn crimp increases the elastic behaviour of the fabric and enhances the elongation during the tensile mode, tearing load and tearing length of the fabric. Similarly, the good cover factor enhanced the tensile strength and tearing of the fabric. Weft direction of the fabric exhibit better tensile properties than warp direction.

## **7.3 Influence Sisal Fabric Properties on Mechanical and Dynamic Mechanical Properties of Composites**

Three fabrics are analyzed and observed that all three fabrics are a good cover factor and enhanced the interfacial adhesion between fabric and matrix.

The tensile, flexural and impact properties are enhanced by fiber loading and found that 60% fiber loading exhibits better mechanical properties. However, weft direction

of the fabric exhibit better mechanical properties than warp direction. The yarn crimp enhances the tensile strain for the composites. Yarn count enhances the tensile stress of the fabric based composites.

The GSM of the fabric influence on mechanical and dynamic mechanical properties of composites. Finer fabric based composites exhibit better mechanical properties and also dynamic mechanical properties at room temperature. As the yarn crimp increases the dynamic mechanical properties enhanced at a higher temperature.

The woven pattern of the fabric influence significantly on the dynamic mechanical properties of the composites than that of GSM of the fabric.

#### **7.4 Scope for Future Work**

This work can be extended to study the influence of textile properties on fatigue and the wear behavior by experimental techniques.



## REFERENCES

- Adewale George Adeniyi, Samson Akorede Adeoye, Damilola Victoria Onifade and Joshua O. Ighalo (2019) “Multi-scale finite element analysis of effective elastic property of sisal fiber-reinforced polystyrene composites”, *Mechanics of Advanced Materials and Structures*, 1-10.
- Aiju Jiang, Xiaowei Chen and Defeng Gao (2019) “Mechanical Properties Comparison of Various Ratios of L-Lactide Grafted Sisal Fibers and Untreated Sisal Fibers Reinforced Poly (lactic acid) Composites”, *Journal of Macromolecular Science, Part B Physics*, 58(1), 161-173.
- Akio Teramoto, Shozaburo Hiratsuka and Yasunori Nishijima (1967) “Studies of micro-brownian motion of a polymer chain by the fluorescence polarization method. II. Segmental motions in concentrated polymer solutions”, *Journal of Polymer Science Part A-2: Polymer Physics*, 5 (1), 37-45.
- Amaresh Gunge, Praveennath G. Koppad, M. Nagamadhu, S. B. Kivade, and K.V. Shivananda Murthy (2019), “Study on mechanical properties of alkali treated plain woven banana fabric reinforced biodegradable composites”, *Composite Communication*, 13: 47-51.
- Amir H Navarchian, Mehdi Jalalian and Majid Pirooz (2015) “Characterization of starch/poly(vinyl alcohol)/clay nanocomposite films prepared in twin-screw extruder for food packaging application”. *Journal of Plastic Film and Sheeting*, 31(3): 309–336.
- A.P. Mouritz (2008), “Tensile fatigue properties of 3D composites with through-thickness reinforcement”, *Composite Science and Technology*, 68, 2503-2510.
- Bajaj P., D.N.Khanna, G.N.Babu (1979) Aromatic-aliphatic copolyesters - I.

Synthesis and characterization, *European Polymer Journal*, 15(12), 1083-1088.

Bernardo Zuccarello and Giuseppe Marannano (2018) “Random short sisal fiber biocomposites: Optimal manufacturing process and reliable theoretical models”, *Materials and Design*, 149, 87-100.

Boon Khoon Tan, Yern Chee Ching, Sin Chew Poh, Luqman Chuah Abdullah and Seng Neon Gan (2015) “A Review of Natural Fiber Reinforced Poly(Vinyl Alcohol) Based Composites: Application and Opportunity”, *Polymers*, 7(11), 2205-2222.

Bridgens, B., and Birchall, M. (2012) “Form and function: The significance of material properties in the design of tensile fabric structures”, *Engineering Structures*, 44, 1–12.

Bhasha Sharma, Parul Malik and Purnima Jain (2019) “To study the effect of processing conditions on structural and mechanical characterization of graphite and grapheme Oxide-reinforced PVA nanocomposite”, *Polymer Bulletin*, 76, 3841–3855.

B. Imre and B. Pukánszky (2013) “Compatibilization in bio-based and biodegradable polymer blends”, *European Polymer Journal*, 49, 1215-1233.

Bing Wang, Kanza Hina, Hantao Zou, Li Cui, Danying Zuo and Changhai Yi, (2019) “Mechanical, Biodegradation and Morphological Properties of Sisal Fiber Reinforced Poly(Lactic Acid) Biocomposites”, *Journal of Macromolecular Science, Part B*, 58(2), 275–289.

Canavan, K. (2015) “Applications of Textile Products”, *Textiles and Fashion, Materials, Design and Technology*, Woodhead Publishing Series in Textiles, 531–545.

Chilton, J., and Velasco, R. (2005) “Applications of textile composites in the construction industry”, *Design and Manufacture of Textile Composites*, Woodhead



Publishing Series in Textiles, 424–435.

Chandramohan, D. and Bharanichandar, J. (2013) “Natural Fiber Reinforced Polymer Composites for Automobile Accessories”, *American Journal of Environmental Science*, 9(6), 494-504.

Ci-jun Shuai, Zhong-zheng Mao, Zi-kai Han and Shu-ping Peng (2014) “Preparation of complex porous scaffolds via selective laser sintering of poly(vinyl alcohol)/calcium silicate”, *Journal of Bioactive and Compatible Polymers*, 29(2), 110–120.

Claire S. Boland, Robb De Kleine, Gregory A. Keoleian, Ellen C. Lee, Hyung Chul Kim and Timothy J. Wallington (2016) “Applications and Implementation Life Cycle Impacts of Natural Fiber Composites for Automotive Applications: Effects of Renewable Energy Content and Lightweighting”, *Journal of industrial ecology*, 20(1), 179-189.

Colman, A. G., Bridgens, B. N., Gosling, P. D., Jou, G., and Hsu, X. (2014) “Composites : Part A Shear behaviour of architectural fabrics subjected to biaxial tensile loads”, *Composites Part A: Applied Science and Manufacturing*, 66, 163–174.

Daehee Choi, M., Hammad Khan and JinyoungJung (2019) “Crosslinking of PVA/alginate carriers by glutaraldehyde with improved mechanical strength and enhanced inhibition of deammonification sludge”, *International Biodeterioration and Biodegradation*, 145, 104788.

Davoodi, M.M., Sapuan, M.M., Ahmad, D., Ali, A., Khalina, A. and Jonoobi, M. (2010) “Mechanical Properties of Hybrid Kenaf/Glass Reinforced Epoxy Composite for Passenger Car Bumper Beam”, *Materials and Design*, 31, 4927- 4932.

Debasish Mondal, May Griffith and Subbu S. Venkatraman (2016) Reviews Polycaprolactone-based biomaterials for tissue engineering and drug delivery: Current

scenario and challenges, *International Journal of Polymeric Materials and Polymeric Biomaterial*, 65(5), 255-265.

D. Puglia, J. Biagiotti and J. M. Kenny (2005) “A Review on Natural Fibre-Based Composites—Part II Application of Natural Reinforcements in Composite Materials for Automotive Industry”, *Journal of Natural Fibers*, 1(3), 23-65.

Elena Butnaru, Catalina Natalia Cheaburu, Onur Yilmaz, Gina Mihaela Pricope and Cornelia Vasile (2016) “Poly (vinyl alcohol)/ chitosan/ montmorillonite nanocomposites for food packaging applications: Influence of montmorillonite content”. *High Performance Polymers*, 28(10), 1124–1138.

Eunsil Lee, Youjung Song and Seungsin Lee (2019) “Crosslinking of lignin/poly(vinyl alcohol) nanocomposite fiber webs and their antimicrobial and ultraviolet-protective properties”, *Textile Research Journal*, 89(1), 3–12.

Faris M., AL Oqla S and M.Sapuan (2014) “Natural fiber reinforced polymer composites in industrial applications: feasibility of date palm fibers for sustainable automotive industry”, *Journal of Cleaner Production*, 66, 347-354.

Florencia Cruces, María Guadalupe García and Nelio Ariel Ochoa, (2019) “Can the maximum volume fraction ensure optimum reinforcement in short-fiber composites?”, *Journal of Applied Polymer Science*, 136(31), 47821.

Furqan Ahmad, Heung Soap Choi and Myung Kyun Park (2015) “A Review: Natural Fiber Composites Selection in View of Mechanical, Light Weight, and Economic Properties”, *Macromolecules Materials and Engineering*, 300(1), 10-24.

Garkhail, S.K., Heijenrath, R.W.H. and Peijs, T. (2000) “Mechanical properties of natural fibre-mat-reinforced thermoplastics based on flax fibres and polypropylene”, *Applied Composite Materials*, 7 (5/6), 351–372.

Ghamsari, A. K., Zegeye, E., and Woldeesenbet, E. (2015) “Viscoelastic properties of syntactic foam reinforced with short sisal fibers”, *Journal of Composite Materials*, 49(1), 27–34.

G Kalaprasad, K Joseph, S Thomas and C Pavithran (1997) “Theoretical modelling of tensile properties of short sisal fibre-reinforced low-density polyethylene composites”, *Journal of Materials Science*, 32(16), 4261–4267.

G. Koronis, A. Silva, and M. Fontul (2013) “Green composites: A review of adequate materials for automotive applications”, *Composite Part B: Engineering*, 44 (1), 120-127.

Goda, Koichi., Nakamura, R., Nakai, A., and Laberge Lebel, L. (2013) “Textile Biocomposites”, *Polymer Composites*, 331–360.

Gurunathan, T., Mohanty, S., and Nayak, S. K. (2016) “A review of the recent developments in biocomposites based on natural fibres and their application perspectives”, *Composites Part A: Applied Science and Manufacturing*, 77, 1-25.

Gupta, M., and Singh, R. (2019) “PLA-coated sisal fibre-reinforced polyester composite: Water absorption, static and dynamic mechanical properties”. *Journal of Composite Materials*, 53(1), 65–72.

Guo R., Hu C., Pan F., Wu H., and Jiang Z., (2006) “PVA–GPTMS/TEOS hybrid pervaporation membrane for dehydration of ethylene glycol aqueous solution”, *Journal of Membrane Science*, 281(1-2), 454-462.

Hari Om Maurya, M.K.Gupta, R.K.Srivastava and H.Singh (2015) “Study on the Mechanical Properties of Epoxy Composite using Short Sisal Fibre”, *Materials Today: Proceedings*, 2(4–5), 1347-1355.

Hagen R. (2016) PLA (Polylactic Acid) in *Reference Module in Materials Science*

*and Materials Engineering*, 10, 231-236.

Hearle, J.W.S., Grosberg, P., and Backer, S. (1969) “Structural Mechanics of Fibers, Yarns and Fabrics”, *John Wiley and Sons, Inc.*, New York, 1.

Horrocks, A. R., and Anand, S. C. (2016) “Handbook of Technical Textiles”, 2nd Edition, Technical textile applications, Woodhead Publishing

H P S Abdul Khalil, Hazwan C Che Mohamad, A R Khairunnisa, F A T Owolabi, M Asniza, Samsu Rizal, M R Nurul Fazita and M T Paridah (2018) “Development and characterization of bamboo fiber reinforced biopolymer films”, *Materials Research Express*, 5, 085309.

Huang X and Netravali A. (2007) “Characterization of flax fiber reinforced soy protein resin based green composites modified with nano-clay particles”. *Composite Science Technology*, 67(10), 2005–2014.

M.S.Huda, L. T.Drzal, D. Ray, A.K. Mohanty, M. Mishra (2008) Natural-fiber composites in the automotive sector in Kim L. Pickering, *Properties and Performance of Natural-Fibre Composites*, Woodhead Publishing Series in Composites Science and Engineering, 221-268.

Icten and B. M., Karakuzu R. (2008) “Effects of weaving density and curing pressure on impact behavior of woven composite plates”, *Journal Reinforced Plastics Composites*, 27(10), 1083-1092.

Idowu David Ibrahim, Tamba Jamiru, Emmanuel R. Sadiku, Williams Kehinde Kupolati, Stephen C. Agwuncha and Gbenga Ekundayo (2015) “Mechanical properties of sisal fibre-reinforced polymer composites: a review”, *Composite Interfaces*, 3(1),15-36.

Ione Cendoya, Danie Lo’ Pez, Ange Alegri’A and Carmen Mijangos (2001)

“Dynamic Mechanical and Dielectrical Properties of Poly(vinyl alcohol) and Poly(vinyl alcohol)-Based Nanocomposites”, *Journal of Polymer Science: Part B: Polymer Physics*, 39(17), 1968–1975.

Jagadish Naik, RF Bhajantri, Sunil G Rathod and Ishwar Naik (2019) “Proton conducting diazanium hydrogen phosphate/poly(vinyl alcohol) electrolytes: Transport, electrical, thermal, structural, and optical properties”, *Journal of Elastomers and Plastics*, 51(5), 390–405.

James Holbery and Dan Houston(2006), “Natural-fiber-reinforced polymer composites in automotive applications”, *The Journal of The Minerals, Metals and Materials Society*, 58(11), 80–86.

J. C. Middleton and A. J. Tipton (2000) “Synthetic biodegradable polymers as orthopedic devices”, *Biomaterials*, 21(23), 2335-2346.

Jiratti Tengsuthiwat, Suchart Siengchin, Richárd Berényi, József Karger-Kocsis (2018) “Ultraviolet nanosecond laser ablation behavior of silver nanoparticle and melamine–formaldehyde resin-coated short sisal fiber-modified PLA composites”, *Journal of Thermal Analysis and Calorimetry*, 132(2), 955–965.

Jiratti Tengsuthiwat, Udom Asawapirom, Suchart Siengchin and József Karger-Kocsis (2018) “Mechanical, thermal, and water absorption properties of melamine–formaldehyde-treated sisal fiber containing poly(lactic acid) composites”, *Journal of Applied Polymer Science*, 135(2), 45681.

Jitendra K., Pandey S. H., Ahn Caroline S. Lee, Amar K., and Mohanty Manjusri Misra (2010) “Recent Advances in the Application of Natural Fiber Based Composites”, *Macromolecular Materials and Engineering*, 295(11), 975-989.

Jibril Al-Hawarin, Ayman S Ayesh and Essam Yasin (2013) “Enhanced physical properties of poly(vinyl alcohol)-based single-walled carbon nanotube

nanocomposites through ozone treatment of single-walled carbon nanotubes”. *Journal of Reinforced Plastics and Composites*, 32(17), 1295–1301.

Jin Jeong and Seungsin Lee (2018) “Electrospun poly(vinyl alcohol) nanofibrous membranes containing *Coptidis Rhizoma* extracts for potential biomedical applications”, *Textile Research Journal*, 89(17), 3506-3518. <https://doi.org/10.1177/0040517518813679>.

John, M.J. and Thomas, S. (2008) “Biofibers and Biocomposites”, *Carbohydrate Polymers*, 71(3), 343-364.

J.P.Carey (2017) “Introduction to braided composites, Handbook of Advances in Braided Composite Materials Theory”, *Production, Testing and Applications*”, 1-21.

J. Richeton, G. Schlatter, K. S. Vecchio, Y. Rémond and S. Ahzi (2005) “A unified model for stiffness modulus of amorphous polymers across transition temperatures and strain rates”, *Polymer*, 46(19), 8194-8201.

Juliana da Luz , Marcelo Andre Losekann , Andressa dos Santos , Jean Halison de Oliveira , Emerson Marcelo Giroto, Murilo Pereira Moises , Eduardo Radovanovic and Silvia Luciana Fa’varo (2019) “Hydrothermal treatment of sisal fiber for composite preparation”, *Journal of Composite Materials*, 53(17), 2337–2347.

Jun-Seo Park, Jang-Woo Park and Eli Ruckenstein (2001) “On the viscoelastic properties of poly(vinyl alcohol) and chemically crosslinked poly(vinyl alcohol)”, *Journal of Applied Polymer Science*, 82, 1816–1823

Karak N. (2012) *Biodegradable polymers in Vegetable Oil-Based Polymers, Properties, Processing and Applications*, Woodhead Publishing, 31-53.

K. Sonker, H. D. Wagner, R. Bajpai, R. Tenne, and X. M. Sui (2016) “Effects of tungsten disulphide nanotubes and glutaric acid on the thermal and mechanical

properties of polyvinyl alcohol”, *Composite Science of Technology*, 127, 47–53.

K. Senthilkumar, N. Saba, N. Rajini, M. Chandrasekar, M. Jawaid, Suchart Siengchin and Othman Y. Alotman (2018) “Mechanical properties evaluation of sisal fibre reinforced polymer composites: A review”, *Construction and Building Materials*, 174, 713-729.

K.C. Manikandan Nair, Sabu Thomas and G. Groeninckx (2001) “Thermal and dynamic mechanical analysis of polystyrene composites reinforced with short sisal fibres”, *Composites Science and Technology*, 61, 2519–2529.

Kátia Moreira deMelo, Thiago Felix dosSantos, Caroliny Minely da SilvaSantos, Rubens Tavares daFonseca, Nestor Dantas deLucena, José Ivan deMedeiros and Marcos Silva deAquino (2019) “Study of the reuse potential of the sisal fibers powder as a particulate material in polymer composites”, *Journal of Materials Research and Technology*, 8(5), 4019-4025.

Khan, T., Hameed Sultan, M. T. B. and Ariffin, A. H. (2018) “The challenges of natural fiber in manufacturing, material selection, and technology application: A review”. *Journal of Reinforced Plastics and Composites*, 37(11): 770-779.

Kin-tak Lau, Pui-yan Hung, Min-Hao Zhu and David Hui (2018) “Properties of natural fibre composites for structural engineering applications”, *Composites Part B Engineering*, 136, 222–233.

Kumbar S. G., A. R. Kulkarni and T. M. Aminabhavi (2008) Crosslinked chitosan microspheres for encapsulation of diclofenac sodium: effect of crosslinking agent, *Journal of Microencapsulation*, 19(2), 173-180.

Koichi Goda, M.S.Sreekala, Alexandre Gomes, Takeshi Kaji and Junji Ohgia (2006) “Improvement of plant based natural fibers for toughening green composites—Effect of load application during mercerization of ramie fibers”, *Composites Part A: Applied*

*Science and Manufacturing*, 37(12), 2213-2220.

Krivoshapko S. N. ( 2018) “The perspectives of application of thin-walled plastic and composite polymer shells in civil and industrial architecture”, *Journal of Reinforced Plastics and Composites*, 37(4), 217-229.

Kuruvilla Joseph, Sabu Thomas and C. Pavithran (1993) “Dynamic Mechanical Properties of Short Sisal Fiber Reinforced Low Density Polyethylene Composites”, *Journal of Reinforced Plastics and Composites*, 12(2), 139-155.

Kuruvilla Joseph, Sabu Thomas, C. Pavithran and M. Brahmakumar (1993) “Tensile properties of short sisal fiber-reinforced polyethylene composites”, *Journal of Applied Polymer Science*, 47(10), 1731-1739.

M. A. Dweib, B. Hu, H. W. Shenton, and R. P. Wool (2006) “Bio-based composite roof structure: Manufacturing and processing issues”, *Composite Structures*, 74, 379-388.

M. A. Dweib, B.Hu, A. O'Donnell, H.W.Shenton and R.P.Wool (2004) “All natural composite sandwich beams for structural applications”, *Composite Structures*, 63(2) , Pages 147-157.

M Asem, W M F W Nawawi and D N Jimat. (2018) “Evaluation of water absorption of polyvinyl alcohol-starch biocomposite reinforced with sugarcane bagasse nanofiber : Optimization using Two-Level Factorial Design”, *The Wood and Biofiber International Conference*, IOP Conference Series, Materials Science and Engineering, 368, 012005.

Magalhães, M. D. S., Toledo Filho, R. D., and Fairbairn, E. D. M. R. (2015) “Thermal stability of PVA fiber strain hardening cement-based composites”, *Construction and Building Materials*, 94, 437-447.



Maria Ernestina Alves Fidelis, Thatiana Vitorino Castro Pereira, Otávio da Fonseca Martins Gomes, Flávio de Andrade Silva and Romildo Dias Toledo Filho (2013) “The effect of fiber morphology on the tensile strength of natural fibers”, *Journal of Materials Research and Technology*, 2(2), 149–157.

Gy. Marosi, B. Szolnoki, K. Bocz, and A. Toldy (2016) Fire-retardant recyclable and biobased polymer composites in De-Yi Wang, *Novel Fire Retardant Polymers and Composite Materials*, Woodhead publishing, 117-140.

Maya, M. G., George, S. C., Jose, T., Sreekala, M. S., and Thomas, S. (2017) “Mechanical Properties of Short Sisal Fibre Reinforced Phenol Formaldehyde Eco-Friendly Composites”, *Polymers from Renewable Resources*, 8(1), 27–42.

M. J. John and S. Thomas (2008) “Biofibres and biocomposites”, *Carbohydrate Polymers*, 71, 343-364.

M. Krumova, D. Lopez, R. Benavente, C. Mijangos and J.M.Perena (2000) “Effect of crosslinking on the mechanical and thermal properties of poly(vinyl alcohol)”, *Polymer*, 41(26), 9265–9272.

M. T. Ramesan, P. Jayakrishnan, T. K. Manojkumar and G. Mathew, (2018) “Structural, mechanical and electrical properties biopolymer blend nanocomposites derived from poly (vinyl alcohol)/cashew gum/magnetite”, *Materials Research Express*, 5, 015308-11.

Mengyuan Dun, Jianxiu Hao, Weihong Wang, Ge Wang and Haitao Cheng (2019) “Sisal fiber reinforced high density polyethylene pre-preg for potential application in filament winding”, *Composites Part B: Engineering*, 159, 369-377.

M. R. Sanjay, G. R. Arpitha, L. Laxmana Naik, K. Gopalakrishna, and B. Yogesha (2016) “Applications of Natural Fibers and Its Composites: An Overview”, *Natural Resources*, 7, 108-114.

M Rajesh and Jeyaraj Pitchaimani (2017) “Mechanical characterization of natural fiber intra-ply fabric polymer composites: Influence of chemical modifications”, *Journal of Reinforced Plastics and Composites*, 36(22), 1651-1664.

M. T. Ramesan, P. Jayakrishnan, T. K. Manojkumar and G. Mathew (2018) “Structural, mechanical and electrical properties biopolymer blend nanocomposites derived from poly (vinyl alcohol)/cashew gum/magnetite”, *Materials Research Express*, 5, 015308-11.

Mishra, S., Tripathy, S. S., Misra, M., Mohanty, A. K., and Nayak, S. K. (2002) “Novel Eco-Friendly Biocomposites: Biofiber Reinforced Biodegradable Polyester Amide Composites—Fabrication and Properties Evaluation”, *Journal of Reinforced Plastics and Composites*, 21(1), 55–70.

Misonon, M. I., Islam, M. M., Epaarachchi, J. A., and Lau, K. tak (2014) “Potentiality of utilising natural textile materials for engineering composites applications”, *Materials and Design*, 59, 359-368.

Mohini Saxena, Asokan Pappu, Ruhi Haque and Anusha Sharma, “Sisal Fiber Based Polymer Composites and Their Applications”, *Springer Berlin Heidelberg*, chapter 22.

Muhammad Pervaiz and Mohini M. Sain (2003) “Sheet-Molded Polyolefin Natural Fiber Composites for Automotive Applications, macromolecules materials and engineering”, *Macromolecular Materials and Engineering*, 288(7), 553-557.

Nadir Ayrilmis, Songklod Jarusombuti, Vallayuth Fueangvivat, Piyawade Bauchongkol and Robert H (2011) “Coir fiber reinforced polypropylene composite panel for automotive interior applications”, *Fibers and Polymers*, 12, 919.

Naik, N. K., Borade, S. V., Arya, H., Sailendra, M. and Prabhu, S. V. ( 2002) “Experimental studies on impact behaviour of woven fabric composites: Effect of

impact parameters”, *Journal of Reinforced Plastics and Composites*, 21, 1347-1362.

Nakamura, R., Goda, K., Noda, J., and Netravali, A.N. (2010) “Elastic Properties of Green Composites Reinforced with Ramie Twisted Yarn”, *Journal of Solid Mechanics and Materials Engineering*, 4(11), 1605–1614.

Namrata V. Patil, Muhammad M. Rahman and Anil N. Netravali (2019) “Green composites using bioresins from agro-wastes and modified sisal fibers”, *Polymer Composite*, 40(1), 99-108.

Naushad, M., Nayak, S. K., Mohanty, S., and Panda, B. P. (2017) “Mechanical and damage tolerance behavior of short sisal fiber reinforced recycled polypropylene biocomposites”, *Journal of Composite Materials*, 51(8), 1087–1097.

Netravali, A. N., Huang, X., and Mizuta, K. (2007) “Advanced green composites”, *Advanced Composite Materials*, 16(4), 269–282.

Nishino, T., Hirao, K., and Kotera, M. (2003) “Kenaf reinforced biodegradable composite”, *Composites Science and Technology*, 63 (9), 1281–1286.

Nor Hasrul Akhmal Ngadima, Noordin Mohd Yusof, Ani Idris, Denni Kurniawan and Ehsan Fallahiarezoudar (2017) “Fabricating high mechanical strength  $\gamma$ -Fe<sub>2</sub>O<sub>3</sub> nanoparticles filled poly(vinyl alcohol) nanofiber using electrospinning process potentially for tissue engineering scaffold”, *Journal of Bioactive and Compatible Polymers*, 32(4), 411– 428.

Noushini, A., Samali, B., and Vessalas, K. (2013) “Effect of polyvinyl alcohol (PVA) fibre on dynamic and material properties of fibre reinforced concrete”, *Construction and Building Materials*, 49, 374-383.

O.A. Cevallos and R.S. Olivito (2015) “Effects of fabric parameters on the tensile behaviour of sustainable cementitious composites”, *Composites Materials: Part B*

*Engineering*, 69, 256-266.

Özdemir, H. and Mert, E. (2013) “The effects of fabric structural parameters on the tensile, bursting and impact strengths of cellular woven fabrics”, *The Journal of The Textile Institute*, 104 (3), 330-338.

Parinaz Sabourian, Masoud Frounchi and Susan Dadbin (2017) “Polyvinyl alcohol and polyvinyl alcohol/polyvinyl pyrrolidone biomedical foams crosslinked by gamma irradiation”, *Journal of Cellular Plastics*, 53(4), 359–372.

Phillips, S., and Lessard, L. (2012) “Application of natural fiber composites to musical instrument top plates”, *Journal of Composite Materials*, 46(2), 145–154.

Ping Tan, Liyong Tong, G.P. Steven and Takashi Ishikawa (2000) “Behavior of 3D orthogonal woven CFRP composites. Part I”, Experimental investigation” *Composites Part A: Applied Science and Manufacturing*, 31 (3): 259-271.

Pothan, L. A., Mai, Y. W., Thomas, S., Li and R. K. Y. (2008) “Tensile and flexural behavior of sisal fabric/polyester textile composites prepared by resin transfer molding technique”, *Journal of Reinforced Plastics and Composites*, 27, 1847-1866.

P. V. Joseph, Kuruvilla Joseph and Sabu Thomas (2002) “Short sisal fiber reinforced polypropylene composites: the role of interface modification on ultimate properties”, *Journal Composite Interfaces*, 9(2), 171-205.

Qi Xie, Fangyi Li, Jianfeng Li, Liming Wang, Yanle Li, Chuanwei Zhang, Jie Xu and Shuai Chen (2018) “A new biodegradable sisal fiber–starch packing composite with nest structure”, *Carbohydrate Polymers*, 189, 56–64.

Qiu, X. Lim, and E. Yang (2016) “Fatigue-induced deterioration of the interface between micro-polyvinyl alcohol (PVA) fiber and cement matrix”, *Cement and Concrete Research*, 90, 127–136.

Rajesh M., and Pitchaimani Jeyaraj (2016) “Dynamic mechanical analysis and free vibration behavior of intra-ply woven natural fiber hybrid polymer composite”. *Journal of Reinforced Plastics and Composites*, 35 (3), 228-242.

Rajashekar Karthikeyan, Jimi Tjong, Sanjay K. Nayak, and Mohini M. Sain (2017) “Mechanical Properties and Cross-Linking Density of Short Sisal Fiber Reinforced Silicone Composites”, *BioResources*, 12(1), 211-227.

Rajesh, G., Prasad, A. R., and Gupta, A. (2015) “Mechanical and degradation properties of successive alkali treated completely biodegradable sisal fiber reinforced poly lactic acid composites”, *Journal of Reinforced Plastics and Composites*, 34(12), 951–961.

Ravindra V. Gadhave, Prakash A. Mahanwar and Pradeep T. Gadekar (2019) “Effect of glutaraldehyde on thermal and mechanical properties of starch and polyvinyl alcohol blends”, *Designed Monomers and Polymers*, 22(1), 164-170.

Ren-De Chen, Chih-Feng, Huang, and Shan-hui Hsu (2019) “Composites of waterborne polyurethane and cellulose nanofibers for 3D printing and bioapplications”, *Carbohydrate Polymers*, 212, 75-88.

Renbo Zhang, Liu Jin, Yudong Tian, Guoqin Dou and Xiuli Du (2019) “Static and dynamic mechanical properties of eco-friendly polyvinyl alcohol fiber-reinforced ultra-high-strength concrete”, *Structural Concrete*, 20(3), 1–13.

Rudra R., V. Kumar, and P. P. Kundu (2015) “Acid catalysed cross-linking of poly vinyl alcohol (PVA) by glutaraldehyde: effect of crosslink density on the characteristics of PVA membranes used in single chambered microbial fuel cells” *RSC Advances*, 5(101), 83436–83447.

Rodrigues, J. and Fujiyama, R. (2010) "Mechanical Behavior of Polyester and Sisal Fibers," *SAE Technical Paper*, 36, 0409.

Saba, N., Jawaid, M., Allothman, O. Y., Paridah, M., and Hassan, A. (2016) “Recent advances in epoxy resin, natural fiber-reinforced epoxy composites and their applications”, *Journal of Reinforced Plastics and Composites*, 35(6), 447–470.

Sahoo S.K., Khandelwal V. and Manik G. (2019) “Sisal Fibers Reinforced Epoxidized Nonedible Oils Based Epoxy Green Composites and Its Potential Applications”, *Green Composites, Textile Science and Clothing Technology*, 73-102.

Sahu, P. and Gupta, M. (2017) “Sisal (*Agave sisalana*) fibre and its polymer-based composites: A review on current developments”, *Journal of Reinforced Plastics and Composites*, 36(24): 1759-1780.

Samal, S.K., Mohanty, S. and Nayak, S.K. (2009) “Banana/Glass Fiber-Reinforced Polypropylene Hybrid Composites: Fabrication and Performance Evaluation”. *Polymer-Plastics Technology and Engineering*, 48(4), 397-414.

Satyanarayana, K.G., Arizaga, G.G.C. and Wypych, F. (2009) “Biodegradable Composites Based on Lignocellulosic Fibers An Overview”, *Progress in Polymer Science*, 34(9), 982-1021.

Saurabh Chaitanya, Inderdeep Singh and Jung Il Song (2019) “Recyclability analysis of PLA/Sisal fiber biocomposites”, *Composites Part B: Engineering*, 173, 106895

Saurabh Chaitanya and Inderdeep Singh (2017) “Processing of PLA/sisal fiber biocomposites using direct- and extrusion-injection molding”, *Materials and Manufacturing Processes*, 32(5), 468–474.

Shadpour Mallakpour and Mohammad Dinari (2013) “Enhancement in thermal properties of poly(vinyl alcohol) nanocomposites reinforced with Al<sub>2</sub>O<sub>3</sub> nanoparticles”, *Journal of Reinforced Plastics and Composites*, 32(4), 217–224.

Shamima Eaysmine, Papia Haque, Taslima Ferdous, Md Abdul Gafur and

Mohammed M Rahman (2016) “Potato starch-reinforced poly(vinyl alcohol) and poly(lactic acid) composites for biomedical applications”, *Journal of Thermoplastic Composite Materials*, 29(11), 1536–1553.

Shankar Adhikari and Barbara Ozarska (2018) “Minimizing environmental impacts of timber products through the production process “From Sawmill to Final Products””, *Environmental Systems Research*, 7 (6), 1-15.

Shanshan Liu, Heyi Ge, Yu Zou and Juan Chen (2019) “Glutaraldehyde/Polyvinyl Alcohol Crosslinked Nanosphere Modified Corn Stalk Reinforced Polypropylene Composite”, *IOP Conference Series: Materials Science and Engineering*, 472(1), 012064.

Siby Varghese, Baby Kuriakose and Sabu Thomas (1994) “Short sisal fibre reinforced natural rubber composites: high-energy radiation, thermal and ozone degradation”, *Polymer Degradation and Stability*, 44(1), 55-61.

Stéphane Guilbert, Nathalie Gontard (2005) Agro-polymers for edible and biodegradable films: Review of agricultural polymeric materials, physical and mechanical characteristics in Jung H. Han, *Innovations in Food Packaging, A volume in Food Science and Technology*, Academic Press, 263-276.

Subhakanta Nayak and Jyoti Ranjan Mohanty (2019) “Study of Mechanical, Thermal, and Rheological Properties of Areca Fiber-Reinforced Polyvinyl Alcohol Composite”, *Journal of Natural Fibers*, 16(5), 688–701.

Sushanta K. Sahoo, Smita Mohanty and Sanjay K. Nayak (2017) “Mechanical, Thermal, and Interfacial Characterization of Randomly Oriented Short Sisal Fibers Reinforced Epoxy Composite Modified with Epoxidized Soybean Oil”, *Journal of Natural Fibers*, 14(3), 357-367.

Susheel Kalia, B.S. Kaith and Inderjeet Kaur (2009) “Pretreatments of natural fibers

and their application as reinforcing material in polymer composites—A review”, *Polymer Engineering Science*, 49(7), 1253-1272.

Sunil Kumar Ramamoorthy, Mikael Skrifvars and Anders Persson (2015) “A Review of Natural Fibers Used in Biocomposites: Plant, Animal and Regenerated Cellulose Fibers”, *Polymer Reviews*, 55 (1), 107-162.

Takasu A., Itou H., Takada M., Inai Y., Hirabayashi T. (2002) “Accelerated biodegradation of poly (vinyl alcohol) by a glycosidation of the hydroxyl groups”, *Polymer*, 43 (1): 227-231.

T. Gurunathan, S. Mohanty, and S. K. Nayak (2015) “A review of the recent developments in biocomposites based on natural fibres and their application perspectives”, *Composites: Part A Applied Science and Manufacturing*, 77, 1–25.

Teresa M Pique, Claudio J Pe´rez, Vera A Alvarez and Anali´a Va´zquez (2014) “Water soluble nanocomposite films based on poly(vinyl alcohol) and chemically modified montmorillonites”, *Journal of Composite Materials*, 48(5), 545–553.

Ting Hou . Kechun Guo . Zhongguo Wang . Xiong-Fei Zhang . Yi Feng . Ming He . and Jianfeng Yao (2019) “Glutaraldehyde and polyvinyl alcohol crosslinked cellulose membranes for efficient methyl orange and Congo red removal”, *Cellulose*, 26(8), 5065–5074.

Tosun-felekog, K., and Keskinates, M. (2016) “A comparative study on the compatibility of PVA and HTPP fibers with various cementitious matrices under flexural loads”, *Construction and Building Materials*, 121, 423–428.

Uma Thanganathan and Masayuki Nogami (2014) “Influence of glutaraldehyde cross-linking with polymer/heteropolyacid membranes”, *Emerging Materials Research*, 3(2), 85-90.



Witt U., T Einig, M. Yamamoto, I. Kleeberg, W. D Deckwer, R. J. Müller (2001) Biodegradation of aliphatic–aromatic copolyesters: evaluation of the final biodegradability and ecotoxicological impact of degradation intermediates, *Chemosphere*, 44(2), 289-299.

Xiaohua Deng, Yun Huang, Amin Song, Bo Liu, Zhengli Yin, Yuanpeng Wu, Yuanhua Lin, Mingshan Wang, Xing Li, Haijun Cao (2019) Gel polymer electrolyte with high performances based on biodegradable polymer polyvinyl alcohol composite lignocellulose, *Materials Chemistry and Physics*, 229, 232-241.

Xiaohong Qin, Guanxian Dou, Guojun Jiang and Sai Zhang (2013) “Characterization of poly (vinyl alcohol) nanofiber mats cross-linked with Glutaraldehyde”, *Journal of Industrial Textiles*, 43(1), 34-44.

Yang H, Yan R, Chen H, Lee DH and Zheng C. (2007) “Characteristics of hemicellulose, cellulose and lignin pyrolysis”, *Fuel*, 86, 1781–8.

Yashwant S Munde, Ravindra B Ingle and I Siva (2019) “Effect of sisal fiber loading on mechanical, morphological and thermal properties of extruded polypropylene composites”, *Materials Research Express*, 6(8), 085307.

Yujiang Fan, Masami Kobayashi and Hideo Kise (2000) Synthesis and Biodegradability of New Polyesteramides Containing Peptide Linkages, *Polymer Journal*, 32, 817-822.

Yuansen Liu, Qi Wang and Li Li (2016) “Reuse of leather shavings as a reinforcing filler for poly (vinyl alcohol)”, *Journal of Thermoplastic Composite Materials*, 29(3), 327–343.

Y. Wang and Y. Lo Hsieh (2010) “Crosslinking of polyvinyl alcohol (PVA) fibrous membranes with glutaraldehyde and peg diacylchloride”, *Journal of Applied Polymer Science*, 116, 3249-3255.

Zheng, Zhang, Ophir Ortiz, Ritu Goyal and Joachim Kohn (2014) Biodegradable Polymers in Kayvon Modjarrad and Sina Ebnesajjad, *Handbook of Polymer Applications in Medicine and Medical Devices*, Plastics Design Library, 303-335.

Zulfiqar Ali Raza, Sharjeel Abid, Ibrahim M.Banat (2018) Review Polyhydroxyalkanoates: Characteristics, production, recent developments and applications, *International Biodeterioration & Biodegradation*, 126, 45-56.

## PUBLICATIONS

1. Nagamadhu M., Jeyaraj P., G. C. Mohan Kumar (2019) “Characterization and Mechanical Properties of Sisal Fabric Reinforced Polyvinyl Alcohol Green Composites: Effect of Composition and Loading Direction”, *Material Research Express*, (SCIE), 6 (12), 125320.  
<https://doi.org/10.1088/2053-1591/ab56b3>.
2. Nagamadhu M., Jeyaraj P., G. C. Mohan Kumar (2020) “Influence of Textile Properties on Dynamic Mechanical Behavior of Epoxy Composite Reinforced with Woven Sisal Fabrics”, *Sadhana Publications*, (SCIE), 45 (1), 1-10..  
<https://doi.org/10.1007/s12046-019-1249-z>
3. G. C. Mohan Kumar, Jeyaraj P., Nagamadhu M. (2020) “Influence of Glutaraldehyde Cross-linker on Dynamic Properties of Polyvinyl Alcohol polymer”, *Emerging Materials Research*, (SCIE), 9 (1), 168-179.  
<https://doi.org/10.1680/jemmr.18.00059>
4. Nagamadhu M., Jeyaraj P., G. C. Mohan Kumar (2019) “Mechanical and Tribological Behavior of Woven Sisal Fabric”, *Tribology in Industry*, (SCOPUS), 41 (4), pp 622-633.  
<https://doi.org/10.24874/ti.2019.41.04.14>
5. G.C. Mohan Kumar, Jeyaraj P., Nagamadhu M. (2019) “Dynamic Mechanical Analysis of Glutaraldehyde Cross linked Polyvinyl Alcohol under Tensile Mode”, *AIP Conference Proceedings*, (SCOPUS), 2057, 020017.  
<https://doi.org/10.1063/1.5085588>.



## CURRICULUM VITAE

Name of Student : **Nagamadhu M.**

Address for Communications : S/O Mahadevappa M,  
Kiragasuru Village, Madapura Post  
Chamarajanagara, Karnataka, India 571313.  
**Email:** nagamadhu74@gmail.com  
Phone No : 9611338626

Date of Birth : 10<sup>th</sup> September 1985

Organization : Acharya Institute of Technology, Bengaluru.

### Academic Qualifications

Degree	Institution	University	Year	Specialization
B.E (Mech)	National Institute of Technology, Mysuru.	Visvesvaraya Technological University (VTU)	2007	Industrial and Production Engineering
M Tech.	R.V. College of Engineering, Bengaluru.	Visvesvaraya Technological University (VTU)	2010	Machine Design
Ph.D.	N.I.T.K. Surathkal		Viva voce Completed 03/06/2020	

### Work Experience

Sr. No	Institution/Industry	Period of service	Designation
1	Dyna Vac Systems, Bengaluru.	August 2007 to July 2008	Designer
2	Vacuum Systems and Products, Bengaluru.	January 2010 to July 2010	Research Engineer
3	R.V. College of Engineering, Bengaluru.	July 2010 to March 2011	Research Assistant
4	T. John institute of Technology, Bengaluru.	April 2011 to August 2013	Assistant Professor
5	Acharya Institute of Technology, Bengaluru.	August 2013 to till date	Assistant Professor

Date :

Place : NITK Surathkal, India

Nagamadhu M